

Improving the predictions of ship speed and fuel consumption for Heavy Lift vessels

MSC. THESIS R. BURGER

MARINE TECHNOLOGY

March 7, 2017

Delft University of Technology
Supervisor - Prof. dr. ir. T.C.J.van Terwisga
Commission member - Dr. ir. H.J. de Koning Gans
Commission member - Dr. ir. A. Vrijdag

Hosting company BigLift Shipping B.V.
Supervisor - Drs. ir. R. Verwey
Supervisor - Ing. P. Ganzeveld

In collaboration with MARIN
Supervisor - Ir. R. Grin



Abstract

The current ship speed prediction at a given fuel consumption shows large differences with the actual operational values for the Happy Star. This can result in schedule fines, unexpected fuel expenditures and difficulties in bunker schedules. The first goal of this research is to improve these predictions for the expected range of weather conditions and expand it for cargo or no-cargo condition in good or bad weather. A second goal of this research is to gain insight in the uncertainty of predicting fuel consumption.

A prediction model is built which takes into account the calm water, added resistance due to wind- and swell waves and added resistance due to wind. The total resistance follows from the sum of these separate components. The total resistance is translated to a value for daily fuel consumption. Using hind-casting a validation is performed with daily fuel consumption from noon reports. The uncertainties accompanied with these calculations are reported as well as the uncertainty propagation in the translation of resistance to consumed fuel.

From the results of the simulations it seems justified to conclude that;

1. The separation of cargo/no-cargo conditions and good/bad weather gives an improved estimation the relation between vessel speed and daily fuel consumption, as expressed by the prediction error;
 - For no-cargo condition from 79% to 60%/55% in good/bad weather respectively
 - For cargo condition from 79% to 56%/60% in good/bad weather respectively
2. The goodness of the fit for no-cargo conditions is 63% while this is 32% for cargo conditions. This difference results from overhanging and high deck cargoes.
3. Wind resistance is the dominant resistance component after calm water resistance in all sailing conditions. In cargo condition during bad weather this contribution gets up to 32% of the total resistance comparing to 9% for wave resistance.
4. Following from the previous statement, the most important calculation parameters including highest uncertainty are the true wind angle, the wind load coefficient and true wind speed.

Recommendations

- In case of a long voyage with a large deck-cargo, BigLift should consider to perform a more extensive research on the wind resistance.
- The used methodology allows BigLift to calculate the fuel consumption ship speed relation for other vessels in the fleet.
- Monitoring of the following parameters would decrease the uncertainty in the calculations for fuel consumption;
 - PTO enabled and how many power produced
 - Combinator or fixed shaft frequency mode enabled
 - A flow meter for the main engine only
 - Automated measurements of shaft and break power
 - The actual power setting provided by the captain

Contents

Abstract	ii
Introduction	v
Definitions and Nomenclature	vii
1 Definition Study	9
1.1 Problem definition	9
1.1.1 Research question and hypothesis	10
1.1.2 Scope	10
1.1.3 Relevance	12
1.2 Approach	13
1.3 Calm water Resistance	13
1.3.1 Available methods	13
1.3.2 Available data	17
1.4 Added Resistance due to Wind	18
1.4.1 Available methods	18
1.4.2 Available data	20
1.5 Added Resistance due to Waves	21
1.5.1 Available methods	21
1.5.2 Available data	22
1.6 Total resistance	23
1.7 Translation resistance to fuel consumption	24
1.8 Sources of Uncertainty	27
1.8.1 Calm water resistance	27
1.8.2 Wind resistance	28
1.8.3 Wave resistance	29
1.8.4 Translation to fuel consumption	29
2 Calm water resistance	30
2.1 Calculation procedure	30
2.2 Calculations and results	30
2.2.1 Calm Water Resistance from Sea Trials	32
2.2.2 Comparing with model tests	33
2.2.3 Calm water resistance during operations	34
2.3 Discussion on Calm Water Resistance	35
2.4 Conclusions and recommendations	35

3	Added Resistance due to Wind	37
3.1	Calculation procedure	37
3.2	Calculations and results	37
3.2.1	Construct a hull model	37
3.2.2	Cargoes	38
3.2.3	Calculate wind loading	38
3.3	Discussion	39
3.4	Conclusion and recommendations	41
4	Added Resistance due to Waves	42
4.1	Calculation procedure	42
4.2	Calculations and results	42
4.2.1	Transfer function	42
4.2.2	Wave loading	42
4.3	Discussion	43
4.4	Conclusions and recommendations	45
5	Total Resistance and Fuel Consumption	46
5.1	Calculation procedure	46
5.2	Calculations and results	46
5.3	Discussion	47
5.4	Sensitivity analysis	53
5.5	Conclusion and recommendations	55
6	Conclusion and Recommendations	56
	List of Figures	58
	List of Tables	59
	Appendices	60
A	Specifications Happy Star	61
B	BigLift way of working	64
C	Voyage data - Cargo conditions	66
D	Sensitivity Analysis	79
E	Uncertainty Analysis	81
E.1	Calculation Procedure	81
E.2	Calculation and results	83
E.3	Discussion	85

Introduction

BigLift is a heavy lift shipping company which currently experiences differences in designed and actual vessel speed for the largest vessels in the fleet. A good ship design will realize or outperform its design requirements. In order to predict the performance of the vessel more accurately during its design phase, extensive calculation methods and model tests can be performed. However, not all operational situations can be accurately calculated or tested by numerical methods or model tests, within a limited budget. This limits the range of operational conditions which can be predicted.

Sea trials are performed after launch of the vessel. This is for the shipyard to prove the vessel meets its design requirements. Sea trials are performed in calm weather and mainly ballast conditions and are therefore not representative for operational conditions. Changes in the design during the construction process are also common, for which the realized performance deviate even further from the predictions on model scale.

A shipping company depends on accurately predicted vessel speed and fuel consumption for a wide range of operational conditions. Especially the vessel speed at a certain fuel consumption is important for scheduling and costs calculations, this parameter is a direct result of the resistance a vessel encounters. Heavy lift vessels are designed to lift and transport a wide range of cargo volumes which can weigh up to several thousand tonnes. In many cases these cargoes are restricted by volume and not mass. This results only in small changes in the ships' displacement, but drastically influences the projected wind areas. This may indicate a significant influence of the wind loading on the total resistance of a ship. The uniqueness of every cargo might also explain the scatter BigLift currently experiences in operational data

The current predictions of ship speed at a given daily fuel consumption are mainly based on scaled model tests and sea trial data in idealised conditions. The first goal of this research is to improve these predictions for the expected range of weather conditions and expand it for cargo or no-cargo condition in good or bad weather. A second goal of this research is to gain insight in the uncertainty of predicting fuel consumption.

This report starts with a definition study which includes a problem definition, the research question, the scope and a review on the methods and data available. The second chapter, third and fourth chapter are used to calculate the resistance components. In the fifth chapter the total resistance is discussed. The conclusions on this research are stated in the final chapter.

Company Profile

This graduation thesis is performed at both BigLift Shipping as the Marine Research Institute Netherlands, MARIN. BigLift shipping hosts the project whereas MARIN provides additional knowledge and software, leading to a different approach than a 100% BigLift approach.

A short description of both companies is given.

BigLift Shipping

BigLift operates in the heavy lift industry since 1973, starting as Mammoet Shipping. Since 2000 the company is full subsidiary of the Spliethoff group, a Dutch shipping company based in Amsterdam. BigLift operates a fleet of 15 vessels specialised in worldwide ocean transportation of heavy lift and project cargoes. The lifting capacities of the vessels range from $2 * 275[mt]$ to $2 * 900[mt]$ and also have roll-on roll-off capabilities. Most customers operate in the shipping, offshore, mining and power industry, Shipping [2008].

Most cargoes require dedicated engineering, planning and execution, leading to diverse group of employees of around 70 people at the Amsterdam office. More employees work in satellite offices around the world and the crew on board of the vessels must be included as well.

Maritime Research Institute Netherlands

The Maritime Research Institute Netherlands was founded in 1929 in collaboration with the Dutch government and the maritime industry. MARIN's purpose was to fulfill the large demand for research in the maritime industry. Over the years, facilities were built to perform research in the fields of powering performance, sea-keeping and manoeuvring, cavitation, vibration and more. With the development of computing power the services of MARIN expanded to training of seafarers and providing computer models to simulate reality.

MARIN is located in Wageningen and employs around 350 people in the Netherlands

Definitions and Nomenclature

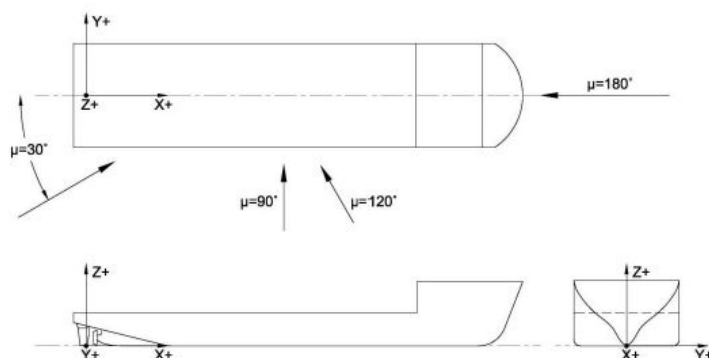


Figure 1: Sign convention used throughout the report, BigLift [2017]

- α is the difference between the true wind speed and the course of the vessel
- μ_{wind} is direction of apparent wind angle.
- $\mu_{current}$ is defined as going to, not coming from as with μ_{wind} and μ_{wave}

The terms uses in uncertainty analysis are explained

- Verification is the process of checking if the calculations are in line with what is expected, W.C. Lin [1990].
- Validation is the process comparing calculations with actual data in order to determine that the model works properly , W.C. Lin [1990].
- Uncertainty is related to accuracy, an accurate model indicates a small uncertainty. The level of uncertainty is determined by the amount, type and distribution of errors. Uncertainty is often calculated for a certain level of confidence. 95% confidence means that 95% of the calculated values lie within the uncertainty limits.
- An error is the absolute difference between a calculated or measured variable and the true value of that variable.
- Systematic errors are also known as bias errors indicate an offset between the mean of a sample and the true value.
- Precision errors are random or repeatability errors which lead to a different answer each time the test is repeated. The calculated value then follows certain distribution of the calculated answer. See Figure 2 for a representation of both systematic and precision error, the precision error influences the wideness of the probability distribution function.

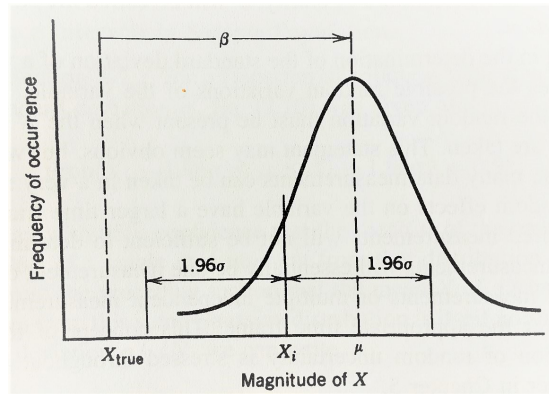


Figure 2: Illustration of error types , H.W. Coleman [2009]

Nomenclature and Abbreviations

Symbol	Unit	Description	Symbol	Unit	Description
α	[degrees]	True wind angle	μ	[degrees]	Relative wave/current/wind direction
Δ	[tonne] or [-]	Displacement or difference	λ	[m]	Wave length
η	[-]	Efficiency	ρ	[kg/m ³]	mass density
AHR	[μm]	Average Hull Roughness	MCM		Monte Carlo Method
A_{proj}	[m ²]	Projected Wind Area	MDO		Marine Diesel Oil
BF		Beaufort	M_z	[kNm]	Yaw moment
CAD		Computer Aided Design	P_b	[kW]	(break) Power
CFD		Computational Fluid Dynamics	PTO	[kW]	Power Take Off
C_{fr}	[-]	Friction coefficient	Q_f	[MJ/kg]	Fuel heating value
C_{wp}	[-]	Waterplane coefficient	R	[kN]	Resistance
COG		Center Of Gravity	RAW_{nd}	[-]	Wave Added Resistance
C_x	[-]	Wind coefficient in x	SF		Sensitivity Factor
F_n	[-]	Froude Number	T_p	[s]	(wave) Peak period
FC	[t/day]	Fuel Consumption	TAW	[-]	Wave Added Thrust
H_{wave}	[m]	(significant) Wave Height	V_{stw}	[m/s]	Speed Through Water
HFO		Heavy Fuel Oil	V_{sog}	[m/s]	Speed Over Ground
L_{pp}	[m]	Length between perpendiculars			

Table 1: Used symbols and abbreviations

Chapter 1

Definition Study

This chapter elaborates on the problem description, the approach to the main phase and the theoretical background and data available for the calculations to be made.

1.1 Problem definition

The current ship speed prediction at a given fuel consumption show large differences with the actual operational values. This is the case for the newest and largest vessels in the BigLift fleet, the Happy S-type. The design process together with the sea trial normally gives a fair estimate of the expected speed of the vessel at a certain daily fuel consumption [t/day] during calm weather. This is used to calculate the expected fuel costs of the voyage and to make the schedule. The currently used prediction are displayed in Table 1.1 and do not suffice in accuracy.

The discrepancy between predicted and realised vessel speed and fuel consumption have two undesired consequences. The first is schedule fines due to delayed arrival times. A first estimation of sailing schedule is made when a cargo request enters the enquiry department. This estimation is based on distance between ports and the speed-power relation of the suitable vessels. Inaccurate predictions in ship speed can lead to delays which in turn can lead to schedule fines. Secondly, the unpredictable fuel consumption. Leading to unexpected fuel expenditures and troubles in the bunker schedules.

It is more likely that a vessel experiences unexpected fuel costs than schedule fines, as the commercial department plan the vessels with a certain time buffer. In addition, schedule fines can also be the result of a delayed departure when for example the previous cargo was not ready.

Furthermore, the introduction mentioned large differences in wind projected areas due to voluminous cargoes. Wind loads are calculated for each voyage, using DNV [2007] regulations . These calculations are used to determine the desired strength of sea fastening and can be used to calculate added resistance due to wind. This method is however only useful for more generic cargo shapes, for example cylinders or closed square blocks. The method is less suitable for more complex cargoes that are shipped in the heavy lift industry. The unreliable wind loading predictions are expected to pay a significant contribution to the inaccuracy of ship speed and fuel consumption prediction.

The goal of this research is to improve these predictions and expand it for cargo or no-cargo conditions in good or bad weather.

Sailing mode name	Ship speed [kn]	Fuel consumption [t/day]
Slow	13.6	25
Eco	14.3	30
Speed	15.3	37

Table 1.1: Currently used speed prediction at given fuel consumption

1.1.1 Research question and hypothesis

The research question defines the core of this thesis and should be answered in the concluding chapter. The sub questions used throughout the report should contribute to answering the main research question.

In order to improve scheduling and cost calculations the prediction of operational ship speed and fuel consumption must be increased in accuracy. These considerations lead to the following main question that this research aims to answer is:

How much can the ship speed prediction be improved at a given fuel consumption?

Before answering the main question, first the following sub-questions must be clarified:

1. How can the main resistance components be calculated with the available data?
2. What is the contribution of these components with respect to the total resistance?
3. What is the uncertainty of the predictions of these components?
4. What are the most important sources of these uncertainties

The most dominant and uncertain resistance components will be further investigated since these will have the largest influence on the total accuracy of the resistance prediction.

1.1.2 Scope

This section discusses the scope of this research which are shortly stated:

- The vessel in consideration is the Happy Star
- Deviations due to commercial or weather rerouting are not taken into account
- The final solution should be of low complexity and short calculation time.
- Focus on resistance due to environmental loading.

Although BigLift Shipping owns a diverse fleet of heavy lift vessels, the problem description currently fits the most to the Happy S-type vessels. This class consists of the Happy Star and the Happy Sky, with a third vessel on its way, the Happy Sun. The Happy Sky entered service in 2013, where the maiden voyage of the Happy Star was in 2014, the Happy Sun is expected in 2018.

The Happy Star is the vessel of scope in this research since the problem description fits this vessel the most. In a late stage of the design process the hull is widened while propulsion configuration is unchanged. Furthermore larger crane jibs are installed than on its sister vessel Happy Sky. Although the Happy Star and the Happy Sky are within the same class, they are still somewhat different in main dimensions and consequently, performance. Appendix A shows the specifications of the Happy Star.

Since the end of 2015 the masters of the Happy Sky and Happy Star started to actively log ship performance and send the data ashore. The values for fuel consumption, shaft torque, shaft frequency and trim are not automatically logged as is the case with weather and motion data. Therefore, a more accurate validation of the model can only be performed using the voyages from November 2015 on.

Weather rerouting and commercial decisions to sail at lower speeds than is possible are not taken into account in this research. Weather rerouting is the avoidance of weather conditions that reach limiting accelerations. Other reasons for reducing speed can be commercial, for example when port or berthing contributions are too high compared with sailing at a lower speed and arriving just in time. These commercial decisions and weather rerouting are challenging to include in a calculation method. Figures 1.1 and 1.2 show an example of weather rerouting due to a hurricane. Extra time and distance due to weather rerouting or commercial reasons are not in the scope of this research since this can not be known a long time in advance.



Figure 1.1: Route as planned



Figure 1.2: Actual route

Appendix B elaborates on the process how a cargo is booked within BigLift shipping. A solution to the problem described earlier will have the most positive contribution during the inquiry phase and shortly after the cargo is booked.

Simplifications are made in the translation of calculated resistance to fuel consumption, such as constant heat losses in gearbox and shaft. Fuel quality inconsistency and auxiliary system losses are also not investigated in-depth. The focus of this research is mainly on the environmental loading as it is expected that this will be most varied between voyages.

1.1.3 Relevance

The current prediction methods for ship resistance are mostly based on databases of the most dominant ship types, i.e. tankers, bulk carriers and container vessels. These methods do not suit the heavy lift ships due to the wide range of operational profiles. The large voluminous deck cargoes can lead to large wind loading. The drastic changes in projected wind areas are not covered in current methods.

Container vessels also change in projected area regularly, but less drastically since a container vessel is almost never completely empty. For high speed container vessels, 20 – 24[kn], the aerodynamic resistance can get up to 10% of the total resistance. K. Hassan [2015]) found that an optimal container stack arrangement can reduce the total wind resistance by 30%. Although heavy lift vessels operate in lower speeds in the range 10 – 15[kn]. The projected area of a heavy lift vessel including cargo can easily double or triple the projected area in no-cargo conditions. These drastic changes in projected wind area are expected to influence wind loads significantly.

Deck cargo has the disadvantage that the Centre Of Gravity(COG) is higher than cargo stowed below deck. When the vessel is rolling and pitching due to the environmental loading, the high moments lead to high reaction forces in the sea fastening. The limits of the sea fastening strength are to be avoided at all costs and therefore heavy lift vessels are harsh weather elusive. Ship motions as a result of waves are provide the largest contribution to loading on the sea fastening. Extreme wave conditions are therefore avoided which limits the relative contribution of wave resistance and increases the relative contribution of wind resistance to the total resistance.

The calculation of ship resistance includes many parameters each with their own uncertainty. Uncertainty is also introduced in the used calculation method and the propagation of uncertainties will lead to a certain band width in which the calculated value could lie. A secondary goal of this research is to gain insight in these uncertainties and their importance with respect to the results.

1.2 Approach

The main resistance components can be divided in the calm water resistance, added resistance due to wind and the added resistance due to waves. The level of residual resistance will indicate if there is a large unknown resistance component. This section elaborates on the approach to calculate these separate components.

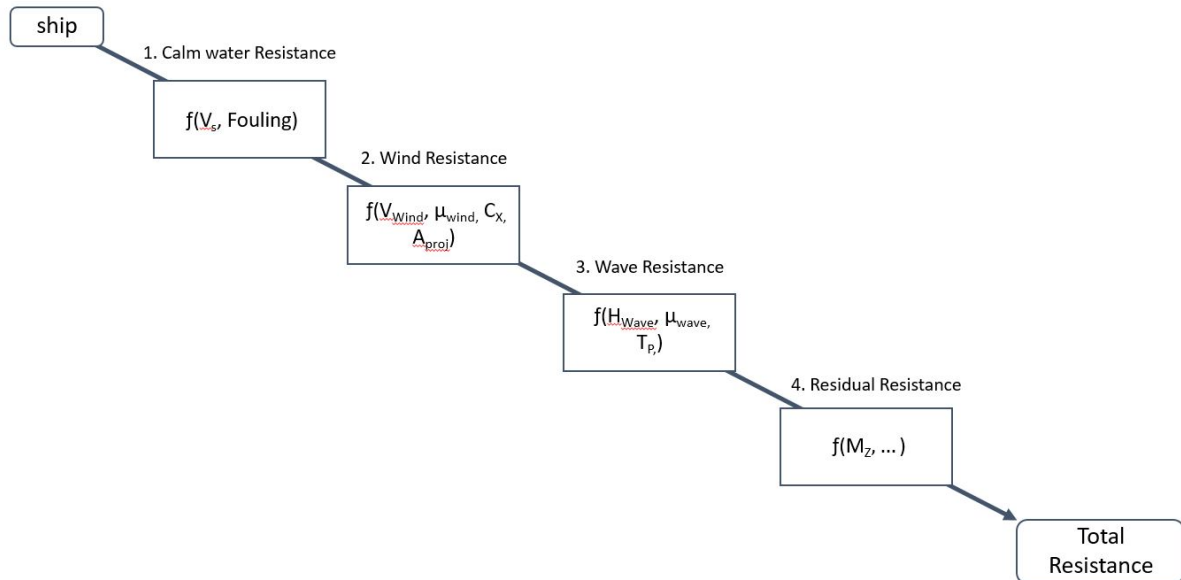


Figure 1.3: Approach to calculate the total resistance

Figure 1.3 shows an overview on how to calculate the total resistance. The components are separately discussed in the following sections. Within these sections the available methods, available data and known sources of uncertainties are discussed. Once the total resistance is calculated the translation towards consumed fuel is made, this will be discussed in Section 1.7. The final section provides some context in the theory used in uncertainty analysis, see Section 1.8

1.3 Calm water Resistance

This section elaborates on the methods and data available to calculate the calm water resistance. The theory and methods to determine the uncertainty of these components will be discussed in Appendix E.

1.3.1 Available methods

Frictional and pressure losses are the main sources of resistance at lower speeds. Pressure losses are a result of the shape of the vessel and its appendages. The frictional resistance is mainly influenced by the hull surface roughness. For speeds higher than Froude Number $F_n = 0.2[-]$

wave making resistance becomes a large component of energy loss. For the Happy Star this means a speed of around $V_s = 15[kn]$, which is already at the top of the operational speed range. The wind resistance as a result of the wind generated by the vessel speed is also considered part of the calm water resistance. Model tests are the most common method to predict the calm water resistance and is also performed for the Happy Star and sister ships.

Model tests

Model tests are widely used to validate calculations and predict sea keeping behaviour. The International Towing Tank Conference (ITTC) aims to standardize towing tank procedures in order to create a level playing field, Murdey [2014]. Although the ITTC regulations are adopted worldwide, there are still differences in results between towing tank facilities. Uncertainties in model tests are:

- Extrapolating uncertainty
The measured values on model scale are calculated to full size conditions using the scaling equations. An important parameter in these equations is the scaling factor which is the full size length divided by the length of the model.
- Measurement uncertainty
Errors in the calibration procedure of sensors, damages, temperature differences affecting sensors etc.
- Calculation uncertainty
ITTC prescribes procedures and regulations for scaled model tests and how to process the test results. Some corrections need to be made based on experience, which is for example the correlation allowance.

More well-known institutes have similar quality in extrapolating and measurement errors. The correlation allowance is however the main source of discrepancy between institutes.

Sea trials

Most of the sea trials are performed by the shipyard that builds the ship. Weather conditions are never completely ideal which require correction methods in order to know the calm water performance. Ship yards are fined when design criteria are not met, which gives them an incentive to perform and influence the sea trial. Therefore the shipyards generally adopt the correction methods which are most beneficial to them, which are chosen as yard standards.

Sea state higher than 3 (Beaufort scale) should be avoided, while the direction and magnitude of wind, waves and current should be monitored during the tests, SNAME [2015]. The surface current together with the speed over ground determine the speed through water, to which calm water resistance is related. The effect of surface current is canceled out by averaging the speed over the measured distance in two opposite directions. This will also average out wind loading if the wind speed and direction is steady.

The International Maritime Organizations acknowledges that different yard standards lead to biased results and developed a code to standardize correction methods of sea trial results. This creates a level playing field for all corrections on sea trial results. The Sea Trial Analysis (STA) project is a Joint Industry Project (JIP) in which MARIN is involved. The program STAIMO is developed by MARIN and certified by IMO, it combines the results of the STA JIP in one easy-to-use program. The wave loading is calculated using the STAWAVE-2 method, H. van den Boom [2013], this method takes into account added resistance due to wave reflection and wave radiation for head waves only. Head waves are defined as waves incoming at the bow with a

bandwidth of 45 degrees, $\mu = 180 \pm 45 [deg]$. Outside this interval the added resistance due to waves is assumed zero. The STAWAVE-1 method only takes into account wave reflection which is only valid for very large vessels which are not subjected to ship motions. Therefore STAWAVE-2 will be used in STAIMO rather than STAWAVE-1.

Another methods are Jinkine and Ferdinande [1974] which only takes into account wave resistance due to wave radiation. This method can also include the influence of the loading conditions on the peak value of RAW. The method of Fuji and Takahashi [1975] only features the wave resistance due to wave reflection. Both the Jinkine and Fuji method are included in STAWAVE-2 method , Grin [2014].

The wind resistance is calculated using a wind coefficient from comparable ship types. The user is also able to add wind coefficients from wind tunnel tests or from calculations. The wind resistance due to the forward speed of the vessel is the still air resistance and should be included in calm water resistance.

Fouling

The increase in frictional resistance due to marine growth is part of the calm water resistance as it does not depends on environmental loading. The increase in resistance can get up to 10% , ITTC [2008] of the total calm water resistance. Equation 1.1 is used to calculate the resistance due to hull friction. The friction coefficient C_{fr} depends on the type of fouling as well as the increase in hull roughness. Townsin [1983] developed an empirical Equation 1.2 to calculate this increase in frictional resistance based on average hull roughness(AHR). Equation 1.3 is developed by HSVA and shows comparable values when using the same average hull roughness. Figure 1.4 shows both methods. Although the offset between the curves is significant, the f_r is almost equal. The Townsin equation is used as this is based on operational conditions rather than scaling of model tests results.

$$\Delta R_{fric} = \frac{1}{2} \cdot \rho_w \cdot V_s \cdot S_{wetted} \cdot \Delta C_{fr} \quad (1.1)$$

where $\rho_w [kg/m^3]$ is the water density, $V_s [m/s]$ the speed through water, $S_{wetted} [m^2]$ the wetted surface of the underwater body and $\Delta C_{fr} [-]$ the change in friction coefficient

$$C_{fr} = 0.044 \left(\frac{AHR^{\frac{1}{3}}}{L_{pp}} - 10 \cdot \left(\frac{1}{Rn_{L_{pp}}} \right)^{\frac{1}{3}} \right) + 0.000125 \quad (1.2)$$

where $AHR [\mu \cdot m]$ is the average hull roughness, $R_n [-]$ the Reynolds number and L_{pp} the length between perpendiculars

$$C_{fr} = \frac{0.075}{\log_{10}(Rn_{L_{pp}} / (1 + 0.0011 \cdot (AHR/L_{pp}) \cdot Rn_{L_{pp}}) - 2)^2} \quad (1.3)$$

Rate of marine growth depends on water conditions, ship speed, periods of idleness and anti-fouling system used. The thickness of a fouling layer on moving marine structures can get up to 1000 [μm] , G. Swain [2016]. Classification requires intermediate main class survey at least every five years for a complete hull inspection , DNV [2003] and fouling removal. Other options in removing marine growth is brushing of the hull and/or propeller by divers. The contribution of frictional resistance of the propeller on the total frictional resistance is relatively large as the water speed over the propeller is higher than along the hull. Brushing the propeller by divers

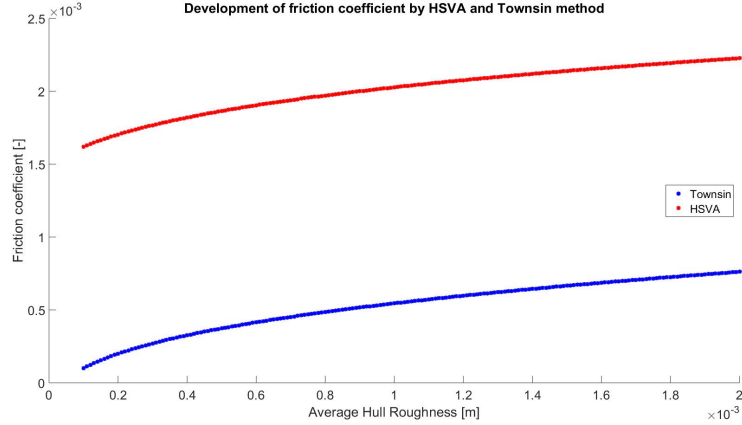


Figure 1.4: Townsin and HSVA method to determine the increase in friction coefficient

quickly proves profitable as the surface area is small with respect to the hull. It can decrease the required propulsion power up to 5% , Townsin [1983]. The following reasons make it challenging to include the effect of marine growth in a calculation model:

- The vessel in consideration does not sail in line service, so water conditions often change
- The vessel has intermediate periods of idleness, which increases marine growth
- The vessel sails through ice almost every year, which removes fouling around the waterline
- The vessel only sails since 2014, so no docking has yet been performed. The actual condition of marine growth on the underwater body is therefore unknown

Using the aforementioned literature, the average hull roughness of the Happy Star is estimated $AHR = 300[\mu m]$. Some footage from the crew of the Happy Star showed fouling of more than $1000[\mu m]$.

Ship speed

The calm water resistance is related to the speed through water, which is measured using a speed-log. In many cases the speed-log data is of low accuracy due to several error sources , Hasselaar [2014]:

- Changes in boundary layer due to speed variations, draft and hull roughness
- Drift induced swirls beneath the ship
- Ship motions
- Distance from the hull

The speed through water(V_{stw}) data is not stored and the uncertainty is high. Therefore the V_{stw} is calculated using navigational and weather data. From navigational data the speed over ground(V_{sog}) is known. Equation 1.4 is used to calculate V_{stw} . The longitudinal component of the current influences V_{stw} while the transverse component of the current does not impose extra resistance.

$$V_{stw} = V_{sog} - V_{currentx} = V_{sog} - V_{current} \cdot \cos(\mu_{current}) \quad (1.4)$$

where $\mu_{current}[deg]$ is the angle of the current relative to the ship. Other than waves, this indicates where the c

1.3.2 Available data

Model tests data

Model test results are available for the Happy Star and sister ships Happy Sky and Happy Sun. The Happy Sky has a different hull shape and will not be used for further calculations. The Happy Sun has similar hull shape but features a ducted propeller. The model tests of the Happy Star are performed at SVA Potsdam at 7[m] draft while the Happy Sun is tested at HSVA Hamburg for 7.5[m] draft. Chapter 2 will further discuss how the both model test results are used for further calculations.

Sea Trial data

The sea trials of the Happy Star are performed without the crane masts and jibs installed. This underestimates the value for air resistance and increases the uncertainty of the actual required power. The sea trial test results show that the weather conditions at the time of testing were a maximum of 3 BF. Wave height - wave period, $H_s - T_p$, combination at a certain Beaufort scale is different per region. Since wave conditions in open ocean differ from wave conditions in more confined areas. Figure 1.5 shows the most probable $H_s - T_p$ scatter diagram for the location of the sea trial.

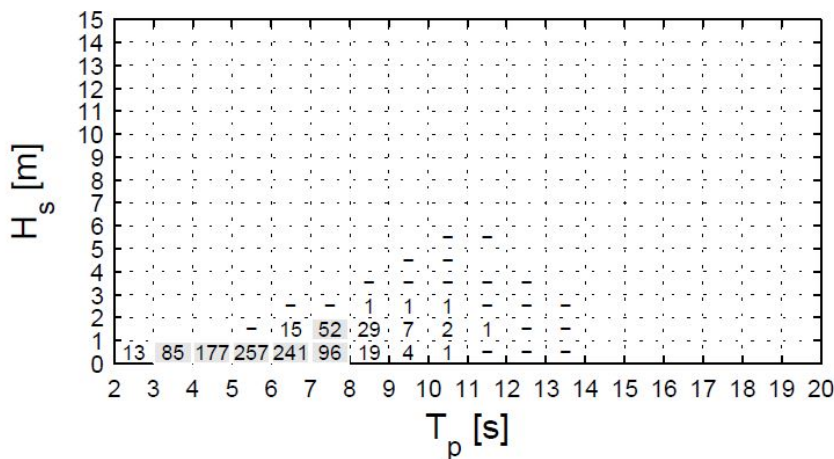


Figure 1.5: Most probable $H_s - T_p$ combinations for 3 Beaufort in the Chinese sea

During sea trial tests it is unclear if the PTO is enabled during trials. A perfectly constant transmission coefficient and constant shaft frequency indicates it is enabled. From a shipowner perspective it could be a requirement that the vessel should reach its trial speed with PTO enabled.

1.4 Added Resistance due to Wind

This section elaborates on the methods and data available to calculate the added resistance due to wind. It is expected that this component plays a more important role for heavy lift vessels as the projected wind areas can become very large drastically changes between different voyages. It is expected to be more important than wave loading, which will be discussed in the next section.

1.4.1 Available methods

Added resistance due to wind is the result of viscous drag, pressure difference and a component of lift in the undesired direction. The general formula for wind resistance is Equation 1.5. The wind coefficient is influenced by the location, surface roughness, shape and shielding effects of wind exposed structures.

Steady or averaged wind is important in wind loads, while gusts may induce undesired effects like resonance, Faltinsen [1990]. Gusts are generally very local effects, so it is less likely to affect large superstructures with respect to resonance. This report focuses on the steady wind loads as this has continuous influence on the total resistance. The unsteadiness of wind is included in the uncertainty and sensitivity analysis further in the report.

$$R_{wind} = \frac{1}{2} \cdot \rho_{air} \cdot V_{wind}^2 \cdot A_{proj} \cdot C_R \quad (1.5)$$

At BigLift Shipping wind loads are also calculated for the design of sea fastening strength and configuration. Using rules and regulations by DNV [2007], the wind loads can be calculated using the environmental conditions, the geometry, shielding effects and solidification of both the ship and cargo combined. Solidification can be explained as the inverse permeability of a structure, where a lattice structure is less solid than a closed block structure. Although the DNV method can properly model the wind loads on basic geometries, the manual effort and knowledge required to reach sufficient accuracy increases for more complex structures.

Accuracy can be increased using computational fluid dynamics (CFD). There is a rapid development in CFD but it still requires some complex proceedings to reach a relative good uncertainty of 10% compared to reality. The level of detail and desired accuracy determine the amount of grid cells. The Reynolds number is in the order of millions for large scale, high wind speeds and low viscosity of air. Both the many grid cells and high Reynolds number requires many computational hours.

Wind tunnel tests can also be performed but these are very expensive. Comparable with model tests in a towing tank, wind tunnel results are also subjected to extrapolation uncertainties and an experience based correlation allowance. Blendermann [1996] performed many wind tunnel tests with typical ship types in his research. Blendermann did not perform tests on heavy lifting vessels.

The final method is a comparison with the DNV method but then included in a program which uses a building block approach. A marine structure is build from multiple simple geometries. The loads on all individual components are summed with shielding and wake effects taken into account. The program WINDOS developed at MARIN works using this method. A small database of shape coefficients for typical ship types is included in the WINDOS database.

Figure 1.6 shows a comparison of the C_x values for no-cargo condition used by BigLift, a comparable ship type in Blendermann and calculated in WINDOS. The Blendermann curve is estimated most uncertain as the general cargo ship used is significantly different than the Happy Star. Since this research aims to deliver an easy to use tool which provides solutions in a short amount of time, CFD and/or wind-tunnel tests are not practical. WINDOS limits the amount of knowledge and manual input required with respect to the DNV approach, while keeping sufficient accuracy. This method is used in this research and will be compared to the DNV method currently used.

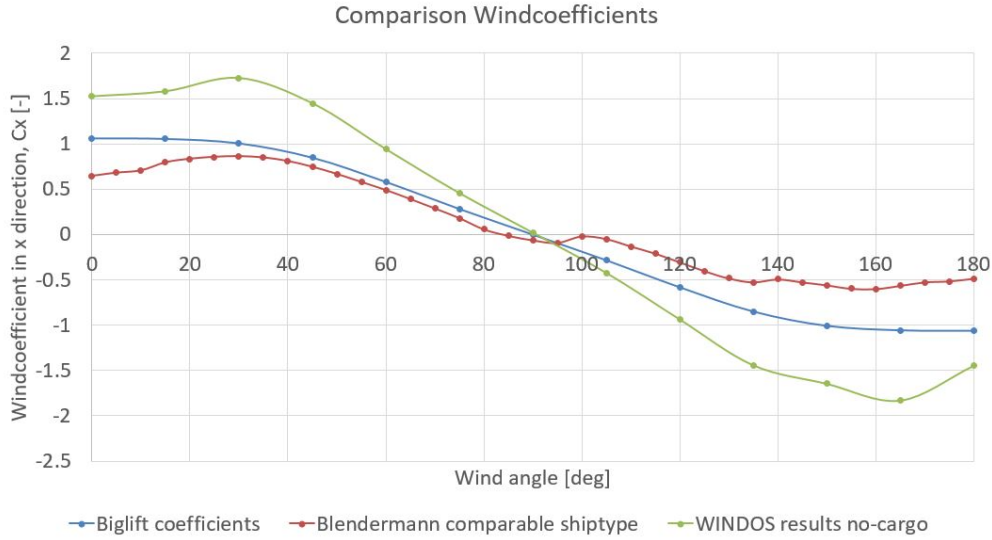


Figure 1.6: Comparison of wind coefficients by BigLift, Blendermann and WINDOS

Wind prediction

Wind velocities are generally expressed in U_{10} , which is the wind velocity 10[m] above the surface, time averaged over 10 minutes, DNV [2007]. This way, close to surface effects such as small discontinuities are not accounted for. When the known wind velocity is not measured at 10[m] height, Equation 1.6 is used to correct to the desired height. This calculation method assumes a logarithmic gradient of the wind velocity from the surface up, Simiu and Scanlan [1978]. The gradient is influenced by the roughness of the sea.

Alternatives for the log-law are the power law and the *Frøya* wind profile. Where the log-law is favorable above the power law as it provides more detailed constants for surface roughness and drag coefficients. The *Frøya* wind profile well applicable for extreme wind speed prediction, DNV [2007]. Since heavy lift vessels generally avoid extreme weather conditions the *Frøya* wind profile is disregarded.

$$U(z) = \frac{u_*}{k} \cdot \ln \frac{z}{z_0} \quad (1.6)$$

where u_* is the wind speed at reference height, k a roughness value and z_0 the reference height

1.4.2 Available data

SPOS(Ship Performance Optimisation System) is the weather forecast source for all BigLift Shipping vessels and is mainly used for weather rerouting and accelerations prediction, in this thesis SPOS will be used to calculate the resistance during a voyage. SPOS is a product of Meteogroup [2015] and combines several weather forecast models. All the data is automatically logged and stored for each BigLift vessel every fifteen minutes in an on-line database. There is no human interaction needed and the data can be retrieved any desired moment. On some vessels the system is expanded using extra sensors like an anemometer to measure wind direction and speed.

The Happy Star makes use of this anemometer which is located at the right top corner of the bridge, at a height of approximately 22.5[m] above the water. The anemometer is able to measure both apparent wind speed [m/s] and direction [deg]. The apparent wind speed is a result of the true environmental wind and the sailing wind generated by the vessel. Equations 1.7a and 1.7b are used to calculate the apparent wind from known weather data in order to make a comparison between the anemometer and weather data. The influence of the rolling motion on the wind speed measured by the anemometer is negligible. Figure 1.7 shows that the location of the sensor is also not optimal as it is not located in the undisturbed wind field. The variation in speed and direction is considered too large and this data will not be used in further calculations. Instead, the calculated apparent wind speeds and direction from SPOS is used.

$$V_{apparent} = \sqrt{V_{ship}^2 + V_{wind}^2 + 2 \cdot V_{ship} \cdot V_{wind} \cdot \cos(\alpha)} \quad (1.7a)$$

where α is the true wind angle relative to the ship

$$\mu_{wind} = \arccos\left(\frac{V_{wind} \cdot \cos(\alpha) + V_{ship}}{V_{apparent}}\right) \quad (1.7b)$$



Figure 1.7: Windsensor on top of the wheelhouse - Happy star

1.5 Added Resistance due to Waves

This section elaborates on the methods and data available to calculate the added resistance due to waves. The contribution of waves to the total resistance is expected to be low as large waves are avoided to secure the safety of the ship, cargo and crew.

1.5.1 Available methods

Added resistance due to waves (RAW) is induced by radiated waves as a result of ship motions and reflected waves as a result of incoming waves reflecting against the ships' hull. The effects of both the radiated waves and the reflected waves are shown in Figure 1.8.

- Short waves do not influence the motion of the vessel as the wave height of short waves is limited. Wind waves are generally short waves and give the largest contribution to wave reflection.
- Long waves or swell waves provide the largest contribution to wave radiation. For wave radiation calculations it is important to take into account the loading condition as this determines the motion response.

The STAWAVE-2 method mentioned in Section 1.3 is suitable for head waves only, this method is extended to all wave directions and developed into the SPAWAVE method. Figure 1.8 shows the parameters that influence the function of wave added thrust(TAW) against the relative wave length, these parameters are shortly discussed based the paper of Grin [2014];

- The peak value at L_{pp}/λ increases with F_n , width(B) and μ and decreases with L_{pp}
- The peak value shifts left with increasing F_n , L_{pp} , and μ .
- The height of the tail is increased with the waterline coefficient (C_{wp}), B, F_n and μ
- The height of the tail is decreased with L_{pp}

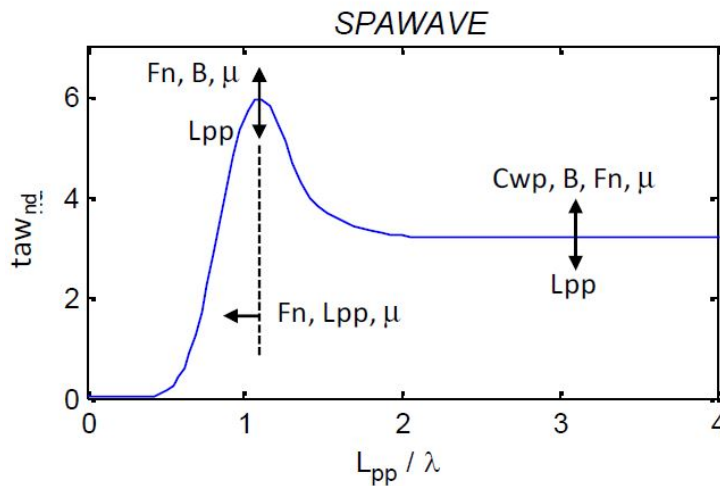


Figure 1.8: Parameters that influence SPAWAVE , Grin [2014]

Wave predictions

The development of waves is directly linked to wind. Waves develop as winds travel over a certain distance or fetch of water. A long fetch leads to higher waves. Waves are commonly expressed as wind waves or swell. Wind waves are the direct result of wind input and are considered young waves. Wind waves have short wave periods and multiple wave heights. The direction of wind waves generally follow the direction of the wind. Swell is the result of a storm or active wind area at a large distance from the observer. Characteristics of swell are long wave periods and constant wave height. The direction of swell wave do not need to agree with the wind direction.

The development of waves is directly linked to the presence of wind. Conditions at sea are often expressed in Beaufort scale, which is related to the wind force. The position of the ship and direction of the wind determines the fetch and thus the wave height. A certain Beaufort scale sea condition therefore does not always mean the same wave conditions.

1.5.2 Available data

Weather data in the SPOS database is separated in wind waves, swell waves and combined waves. The resistance due to wind and swell waves is calculated separately as the characteristics of the combined wave does not lead to the same resistance. This is mainly due to the fact that waves from two different angles give different resistance value than the combined wave.

Appendix C shows an overview of the voyages including summarized weather conditions.

1.6 Total resistance

This section discusses the known or expected remaining components that influence fuel consumption such as the added resistance due to induced drag, propulsion efficiency and fuel quality. A summary is given about the voyages used to validate the total resistance.

Induced drag

Wind and wave loading can result in a yawing moment when wind and/or wave directions are oblique or projected area's are asymmetrical. A yawing moment leads to a drift angle, which has to be compensated by the rudder resulting in undesired rudder forces. The induced drag due to a drift angle is composed of the lift induced drag on the bare hull and the reduced propulsion efficiency due to asymmetric inflow. A drift angle of 5[deg] can increase the required power up to 30% , Hasselaar [2016]. It is however not possible to measure induced drag directly. It can be related to the rudder position during a constant course, but this data is not available.

Voyage data

Since the Happy Star's maiden voyage in November 2014 the vessel performed 11 voyages with cargo and multiple voyages without cargo. The data of these voyages is used to validate the calculations. Some voyages are excluded from validation as the data is not complete. Table 1.2 shows a summary of the voyages used for validation. A more detailed description of the voyages including cargo is given in Appendix C The sailing mode(slow, eco or speed) is not always known, but the default mode is eco.

#	Voyage code	Port from-to	Duration [d]	Arrival date	Cargo type
1	-	Balboa - Dalian	30	April '15	-
2	-	Port Hedland - Singapore	6	May '15	-
3	Voy004	Batam - Onslow	8	Jun '15	Topside
4	-	Onslow - Manila	8	Jul '15	no-cargo
5	Voy006(1)	Shanghai - Haiphong	6	Sep '15	Tugs
6	Voy006(2)	Haiphong - Da Nang	1	Sep '15	Tugs
7	Voy006(3)	Da Nang - Singapore	4	Sep '15	Tugs
8	Voy006(4)	Singapore - Rotterdam	26	Oct '15	Tugs
9	-	Rotterdam - Freetown	9	Nov '15	-
10	-	Freetown - Maceio	5	Nov '15	-
11	Voy007(1)	Maceio - Itajai	5	Nov '15	Warf deck
12	Voy007(2)	Itajai - Durban	15	Jan '16	Chem. plant
13	Voy007(3)	Durban - Qingdao	26	Feb '16	Chem. plant
14	-	Pyeongtaek - Ulsan	1	May '16	-
15	Voy010(1)	Ulsan - Singapore	8	Jun '16	Coke drum
16	Voy010(2)	Singapore - Shuaiba	12	Jun '16	Coke drum
17	-	Shuaiba - Singapore	13	Jul '16	-
18	-	Singapore - Nantong	8	Jul '16	-
19	Voy011	Nantong - Vancouver	19	Sep '16	Crane
20	-	Port Angeles - Masan	16	Oct'16	-

Table 1.2: Summary of voyages used for validation C

1.7 Translation resistance to fuel consumption

This section elaborates on the translation of calculated resistance to fuel consumption, this calculated fuel consumption can then be compared with the reported fuel consumption. Simplifications such as constant efficiencies and fuel quality introduces uncertainties which will be explained in this section as well.

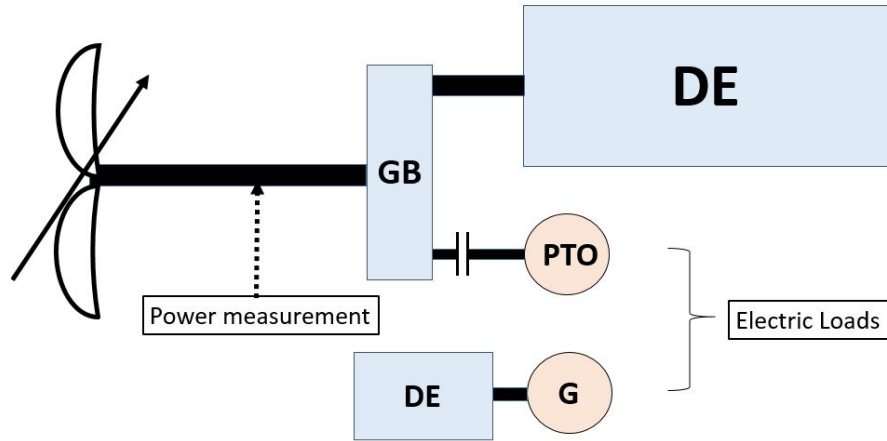


Figure 1.9: System diagram of the engine configuration

Figure 1.9 shows the propulsion configuration of the Happy Star.

- The main engine's MCR is $8775[kW]$ at an engine speed of $500[RPM]$
- The rotational frequency of the shaft for the PTO to be enabled is $138[RPM]$
- The nominal electric load is $450[kW]$
- The Happy Star features a controllable pitch propeller
- The vessel also has the possibility to sail under combinator mode

Figure 1.10 shows the calculation procedure from a sailing ship to fuel consumption. This procedure is based on the book H. Klein Woud [2002], but adjusted to fit this research. The detailed description in the book would require exact knowledge about the thrust, torque and other parameters, these are however unknown in this research.

1. Effective power

In case of a constant vessel speed, the resistance of the ship balances the effective power produces by the propeller. The vessels speed is the speed through water.

2. Delivered power

The delivered power is calculated using the delivered efficiency consisting of the relative rotative, hull and open water efficiency. The rotative efficiency, η_R , is influenced by rudder behind the propeller which reduces the losses of fluid velocities in y-direction of the ship fixed system. The hull efficiency, η_H , is calculated using the thrust deduction and wake factor which depend on the shape of the vessel. The values of η_R and η_H efficiencies are determined in model tests. The open water efficiency, η_O , depends on the mode in which the ship sails. The combinator mode

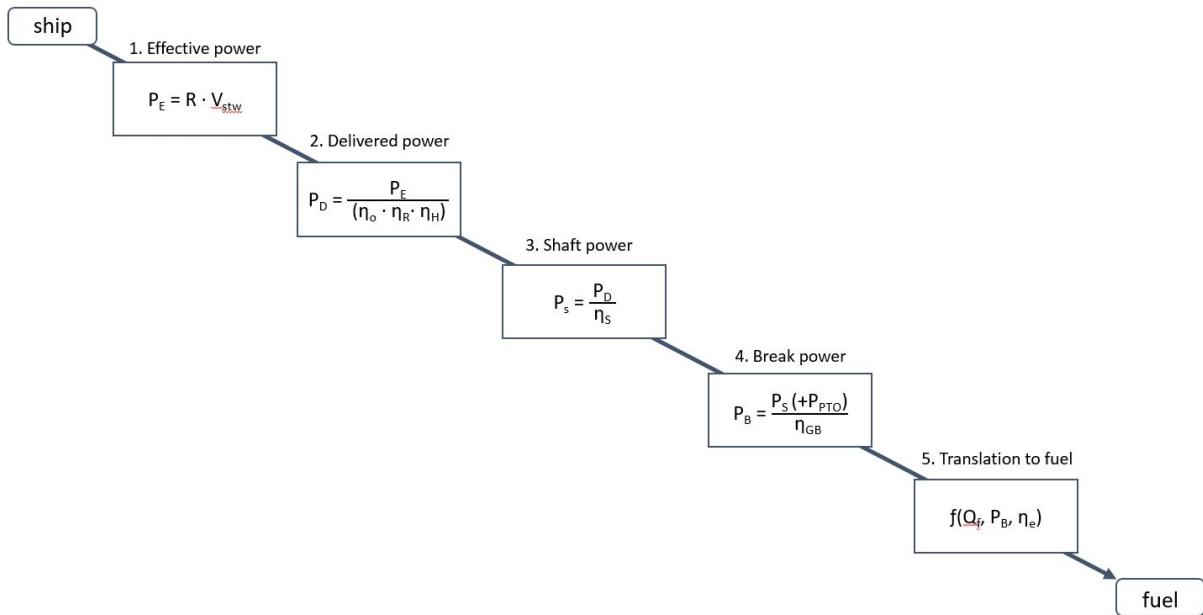


Figure 1.10: Calculation process of resistance to fuel, based on H. Klein Woud [2002]

is expected to have a higher efficiency than fixed shaft frequency mode. It is not known which mode is enabled from data. It is also not known what η_O is in case of speeds outside the tested range. Following a typical open water diagram the efficiency reduces for lower velocities over the propeller.

3. Shaft power

The losses in the shaft originate from friction losses in bearings that support the shaft. These losses are generally estimated at 0.5 or 1% , H. Klein Woud [2002]. A shaft efficiency of $\eta_S = 0.99$ is used throughout this research. The Happy Star is able to measure the shaft power using strain gauges on the shaft. The amount of strain in the shaft is related to the stresses together with the Young's modulus. The stresses are related to the power onto the shaft. The accuracy of the measured shaft power depends on the quality of the strain gauges, their calibration and the uncertainty Young's modulus used for the shaft. These uncertainties are taken into account in the uncertainty analysis in Appendix E.

4. Break power

The gearbox efficiency of $\eta_{GB} = 0.97$ and the power consumed by the PTO determine the break power. Frictional resistance in the gearbox generally lead to a 3 to 5% for medium speed diesels , H. Klein Woud [2002]. The nominal speed of Happy Star's engine is in the lower range of medium speed diesels, therefore a 3% loss is taken. It is not known from data when the PTO is enabled or in other words, in which mode the vessel sails.

5. Translation to fuel consumption

The translation of break power to fuel consumption is a function of fuel quality, break power en engine efficiency. Figure 1.11 shows the relation of daily fuel consumption and break power

based on manufacturer and operational data. The manufacturer takes into account a certain tolerance and uses high calorific Marine Diesel Oil(MDO) while the Happy Star uses Heavy Fuel Oil(HFO). Both corrections are made to the data provided by the manufacturer. The quality of marine fuels is not consistent over the world. K.E. Nielsen [2008] found a standard deviation of $\sigma = 0.51[MJ/kg]$ for MDO with a mean value of $\mu = 42.7[MJ/kg]$ for over 83 worldwide samples. The blue dotted line in 1.11 shows this standard deviation applied to HFO.

The operational data used to validate the manufacturer data includes several uncertainties.

1. The shaft power is measured rather than the break power, a translation to break power need to be made. The uncertainty of an enabled PTO is eliminated for the data set used. This is a data set actively logged on the ship for a certain period of time.
2. The condition of the engine is unknown.
3. The fuel consumption reported is measured by a flow meter which measures fuel to both the main engine and the diesel generators. The chief engineer reports the fuel for the main engine based on experience. This introduces an input or human error in the data.
4. The quality of the fuel is unknown.

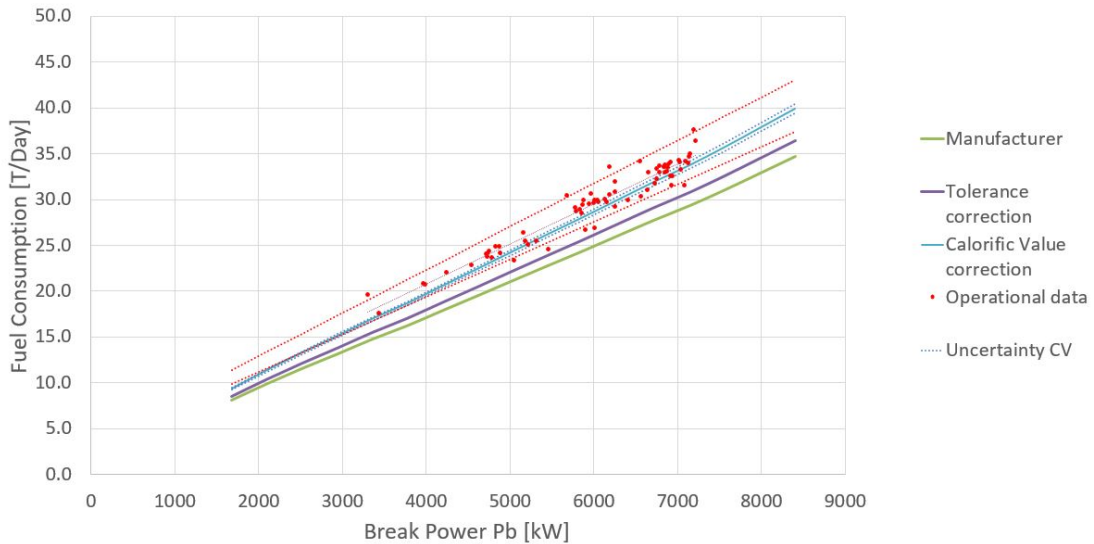


Figure 1.11: Relation of fuel consumption against break power

Captain's decision

The speed of the vessel influenced by the captain is not measured nor logged. The captain determines the amount of power to meet the planning, manage the daily fuel consumption and more importantly, to reduce vessel motions. This change in power by human interaction is challenging to quantify and can therefore lead to unexpected values in the daily noon reports. The vessel speed is assumed not to be influence by the captain in case of fairly constant weather conditions and a standard deviation of less $0.25[kn]$ over one day.

Based on information from several seafarers, a criteria of Beaufort 6 sea conditions is set for bad weather conditions. The seafarers however pointed out that wave slamming and motions due to swell at $2.5[m]$ gave the captain reason to reduce power. Since wave slamming is related

to wind waves heave/roll motions mainly due to swell, this criteria is set for both wind- and swell waves. As wind is an important part of this research, the limiting criteria of 2.5[m] is converted to a Beaufort scale 6 condition. This limiting criteria is used to define good or bad weather.

1.8 Sources of Uncertainty

Uncertainties are grouped by H.W. Coleman [2009] into three groups input, methods and model uncertainty. Within an uncertainty source two types of errors are distinguished, precision and bias errors. Uncertainties will propagate through the calculations to an uncertainty in the final answer. An overview of the known uncertainty sources and, if possible, their magnitude is given. Appendix E elaborates on the calculations to determine the magnitude of uncertainty.

1.8.1 Calm water resistance

Input uncertainty Correction to the calm water resistance are made after the calculations in STAIMO to construct the final calm water resistance. The input parameters for these corrections are discussed.

- Speed over ground, $U_{V_{sog}} < 1\%$
Speed over ground can be accurately measured using GPS with an uncertainty less than 1%. One data point is generated every 15 minutes, in which the ship typically covers 5[km] while the GPS is accurate up to tens of meters.
- Speed over ground, $U_{V_{stw}} = 5\%$
The main source of uncertainty is the direction and magnitude of the current.
- Sea trial data, $U_{Seatrial_{data}} = 10\%$
The trials are performed with a independent third party on board, this decreases uncertainty. Taking into account measurement errors the total uncertainty of the sea trial data is estimated by an expert opinion at 5% (Hasselaar, MARIN, 2017).
- Weather conditions during trial, $U_{Seatrial_{weather}} = 4\%$
These are estimated as the most probable conditions for that area, the possibility exists that there were worse conditions during trials. The worse weather conditions are taken as a bandwidth around the calculated sea trial data to indicate the uncertainty.
- Model test data, $U_{Model_{test}} = ?$
The uncertainty in model test data is mainly introduced in the extrapolation of model data to full scale predictions.
- Average Hull Roughness, $U_{AHR} = 100\%$
Section 1.3 already mentioned the many parameters that influence the amount of hull fouling. The uncertainty is estimated respect to the nominal value of $AHR = 300[\mu m]$ as periods of idleness increases fouling significantly while sailing through ice completely removes the growth.

Method uncertainty The program STAIMO is used to calculate the calm water resistance. The fouling resistance is calculated using Townsin and the wind coefficients are calculated in WINDOS.

- STAIMO, $U_{STAIMO} = 30\%$
The uncertainty of this program is estimated at 30%. The bias or systematic error is estimated zero since this program is acknowledged by the IMO to create a level playing

field for sea trial corrections. The yard standard correction methods are generally biased since the yard chooses the method that suits them best.

- Townsin friction coefficient equation, $U_{Townsin} = ?$
The uncertainty of this method is unknown. It is expected that the uncertainty of the input, the average hull roughness will be dominant.
- WINDOS, $U_{WINDOS} = 40\%$
The main source of uncertainty is that the program does not correctly include detailed construction elements.
- Extrapolation, $U_{extrapolation} = ?\%$ per knot vessel speed
Model test data is known for a range of $Vs = 12 - 17[kn]$ while only the four highest speeds of the sea trial data are used. Extrapolated data increases the uncertainty significantly as it is based on the gradient of the last known data points.

1.8.2 Wind resistance

Input uncertainty

- Apparent wind speed, $U_{V_{appwind}} = 21\%$
Dominant factor in this uncertainty is the wind speed and wind direction, as the V_{sog} and course of the vessel are accurately known.
- Apparent wind angle, $U_{\alpha} = 20\%$, $U_{\mu_{wind}} = 20\%$
 U_{α} is based on a SPOS accuracy study explained in the next paragraph. The course and V_{stw} of the vessel is accurately known, this leaves the uncertainty of α as the main source of uncertainty for μ_{wind}
- Wind gusts, $U_{gusts} = ?\%$
The measured frequency of SPOS is 15 minutes and in between two measured values wind gusts can temporarily lead to a higher wind loading.
- Projected wind area, $U_A = 0\%$
CAD drawings are used to construct the model. The level of detail increases the accuracy of the projected area, but this is a limit of the method, not the input.
- Air mass density, $U_{\rho_a} = < 5\%$
The vessel can sail in arctic areas as well as more warmer areas, this influences the air mass density. Faltinsen [1990] showed this for the range $0 - 20[degCelsius]$ which leads to the mentioned uncertainty. The nominal value is considered at $10[degCelsius]$ and is ρ_a .

Method uncertainty

- SPOS, $U_{SPOS_{wind}} = 26\%$
The data used in this research is the real-time forecasting for the location of the vessel, stored in SPOS(NOW). The Spliethoff Group studied the accuracy of SPOS forecasting for wave height, wind speed and wind direction, D. Wouters [2016]. The uncertainties are determined for a 90% confidence level. The data in SPOS(NOW) is not fore-casted but real-time data. The translation from weather buoy to ship specific location also introduces uncertainties. It is expected that the increase in accuracy for real-time data balances the decrease in accuracy due to location translation.
- WINDOS, $U_{WINDOS} = 40\%$
Walree [2010] mentioned that WINDOS' accuracy is sufficient for use in the design stage. Based on an expert opinion (J. de Wilde, MARIN, 2017), the uncertainty of WINDOS with respect to CFD is 30%. The uncertainty of CFD with actual wind loading is order of magnitude 25%, based on a comparison study of wind loads on a FPSO calculated in CFD and wind tunnel tests, de Wilde [2016].

- Data reduction, $U_{reduction} = -\%$.
Data reduction or interpolating introduces uncertainties as calculated values are not based on data, but on a fitted curve. It is expected that interpolating uncertainties are not a dominant uncertainty in this research. Regression uncertainty is discussed in Appendix E

1.8.3 Wave resistance

Input uncertainty

- Wind wave characteristics, $U_{H_s} = 7.5\%$, $U_{T_p} = 7.5\%$, $U_{\mu_{windwave}} = 20\%$.
The uncertainty of wave height is from the research by D. Wouters [2016] mentioned earlier. The uncertainty of wave period is estimated equal to wave height as these parameters both depend on wind speed and fetch. The wave direction is estimated equal to the wind direction as wind waves and wind are strongly related.
- Swell wave characteristics, $U_{H_s} = 4\%$, $U_{T_p} = 4\%$, $U_{\mu_{windwave}} = 10\%$.
These uncertainties are considered roughly half of the wind wave characteristics since swell waves are better predictable, as mentioned in Section 1.5

Method uncertainty

- SPAWAVE, $U_{SPAWAVE} = 30\%$
Based on an expert opinion (Grin, MARIN, 2017). The main source of uncertainty is the fact that the data from SPAWAVE is from comparable ship types and not based on model tests of the Happy Star itself.

1.8.4 Translation to fuel consumption

Input uncertainty

- Delivered efficiency, $U_{\eta_d} = -\%$
The uncertainty of the delivered efficiency is speed dependent due to the speed dependency of η_o . The uncertainty increases for lower speeds as there is no data for vessels speeds below 12 knots. In addition, it is not known from data in which mode the vessel sails; combinator or fixed frequency mode.
- Shaft efficiency, $U_{\eta_s} = 0.25\%$, Gearbox efficiency, $U_{\eta_{gb}} = 1\%$
The transmission efficiency is the shaft and gearbox efficiency combined. This indicates the losses from break- to shaft power. Sources of uncertainty in this value is the actual value of the shaft Young's modulus and the uncertainty in the strain gauges which measure the power.
- Reported fuel consumption, $U_{FC_{noon}} = 1.5[t/day]$
The main sources of uncertainty is the human error in determining the fuel consumed by the main engine measured by a single flow meter. Additionally it is not known from noon reports when the PTO is enabled.
- Fuel quality, $U_{Q_f} = 2.5\%$.
Two times the standard deviation of MDO as found by K.E. Nielsen [2008]. HFO contains more pollution than MDO which increases the uncertainty

Method uncertainty

- Regression function, $U_{regression} = 7.1\%$
The calculation procedure for the regression uncertainty is explained in Appendix E

Chapter 2

Calm water resistance

The aim of this chapter is to predict the calm water resistance, R_{calm} . The chapter starts with the calculation procedure and is followed by the calculations itself. The discussion of the results includes a verification and validation. The chapter is concluded with the calm water curve which is used to calculate the total resistance.

2.1 Calculation procedure

1. Model tests of the same hull at two different institutes are compared in order increase accuracy of the predictions at model scale
2. The sea trial results to be corrected for wind and waves, as no fully calm weather conditions were present during trials.
3. The model tests are validated with the corrected sea trial results.
4. Fouling and still air resistance are part of the calm water resistance during operations. Therefore corrections need to be made.
5. The calm water resistance is validated using operational calm weather conditions. Calm weather is defined by the user as $H_{wind} = H_{swell} < 0.5[m]$ and $V_{wind} < 5[kn]$, in no-cargo conditions

2.2 Calculations and results

The first step in the calculation procedure is to compare the model tests from the same hull at two different institutes, this is to increase the accuracy of the model tests.

	Happy Star	Happy Sun
Institute	SVA - Potsdam	HSVA - Hamburg
Draft	7.0 [m]	7.5 [m]
Speed range	13 - 17 [kn]	12 - 17 [kn]
measured speeds	7	11
Remarks	-	Ducted propeller

Table 2.1: Model test specifications

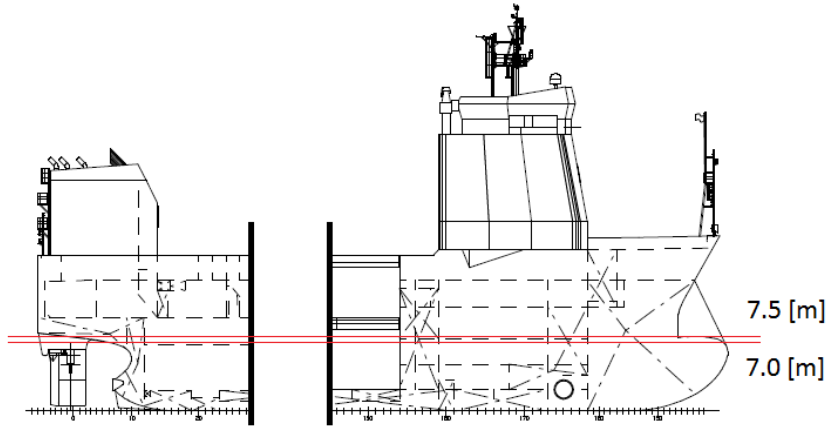


Figure 2.1: 7.0 and 7.5 [m] draft visualized

Table 2.1 shows an overview of the two model tests. Figure 2.1 shows the difference in draft. In order to compare both model test results some corrections need to be made;

- Draft. A draft correction can be made using the Admiralty function, Equation 2.2. This equation is only valid for small changes draft. The change from 7.5 to 7.0 meter draft is the moment when the bulbous bow emerges. The admiralty equation does not takes this into account so this increases the uncertainty of the draft corrected HSVA results.
- Ducted propeller. A different propulsion configuration results in a different delivered efficiency. Equation 2.1 is used to compare the model tests results. The efficiency of the propeller and duct is included in the open water efficiency, η_o . While the hull and relative rotative efficiency, η_h and η_r respectively, are in theory equal for both vessels. By taking the η_o from SVA, both model tests can be compared.

The results of these corrections are shown in Figure 2.2. The gradient of both curves is different, where gradient of the SVA results seems to lead to a non-zero shaft power at zero ship speed. This is not correct. It is even more preferred to continue with the HSVA corrected results as this model test features more tested speeds which decreases uncertainty of the gradient.

$$P_{dHSVA-corr} = P_{dHSVA-uncorr} \cdot \frac{\eta_{dHSVA}}{(\eta_{hHSVA} \cdot \eta_{rHSVA} \cdot \eta_{oSVA})} \quad (2.1)$$

where $\eta_d = \eta_h \cdot \eta_r \cdot \eta_o$,

$$C_{adm} = \frac{\Delta^{\frac{2}{3}} \cdot V_s^3}{P_d} \quad (2.2)$$

Δ is the displacement, V_s the ship speed and P_d the delivered power

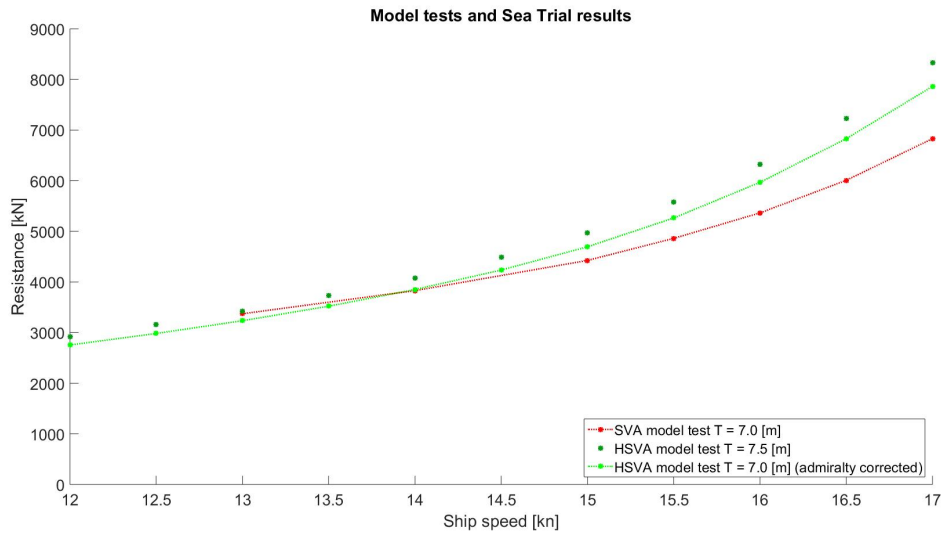


Figure 2.2: Comparison of scaled model tests including the corrected curve

2.2.1 Calm Water Resistance from Sea Trials

The second step in the calculation procedure is to correct the sea trial results for wind and waves which were (presumably) present during trials.

Sea trial data

Figure 2.3 shows the measured shaft power during sea trials and the calculated shaft power from the modified model tests. The difference between both curves is significant and can possibly be explained by the PTO being enabled. Although this is not reported, it is likely due to the following reasons;

- The transmission efficiency remains equal for each power setting. This is highly unlikely as heat losses due to for example gearbox friction have a larger relative contribution at lower power settings. It is likely that the break power is measured and the shaft power calculated with a fixed transmission efficiency.
- The shaft frequency remains equal for each power setting at the frequency for which the PTO can be enabled
- It seems logical from the owner's perspective that the vessel should be able to reach it's trial speed while the PTO is enabled. This is can not be confirmed.

The statements above lead to the assumption that the PTO was enabled during sea trials, therefore corrections to shaft power are made and are shown in the graph by the green dots.

Wind and wave resistance

The sea trial is performed under non-ideal weather conditions. Wind and waves are categorized in Beaufort 3. Using STAIMO, corrections are applied in order to achieve the calm water resistance in ideal conditions. The user is also able to include wind coefficients other than from typical ships which are included in the WINDOS database. As mentioned in 1.4 the wind coefficients in this research are calculated in WINDOS. The calculations are made for the Happy Star in no-cargo conditions without cane masts and jibs. It is not known what the exact conditions

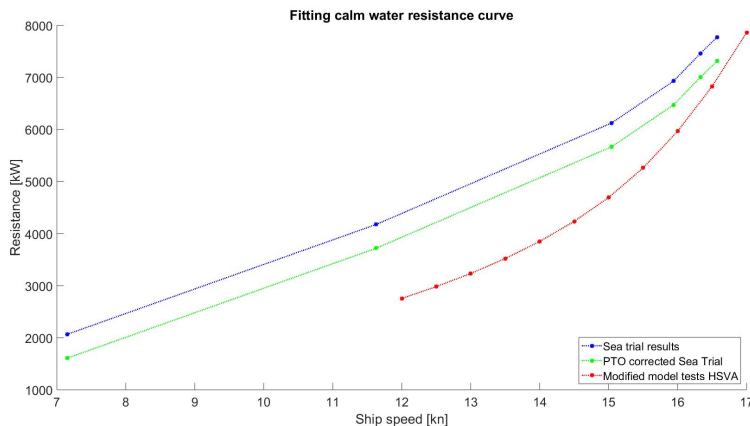


Figure 2.3: Sea Trial Power Take Off correction

were at the time, but using a wave database the most probable conditions can be estimated at Beaufort 3, this is shown in Figure 1.5 in Appendix E. The sea trial results are corrected for these most probable wave data.

Figure 2.4 shows the speed-power relation by STAIMO, for a clean hull and no-crane condition. The most probable weather condition is a wave height of $H_s = 1[m]$ with a peak period of $T_p = 5.0[s]$. It is also possible higher wave heights or longer peak periods were present. The wave loading at $H_s = 1.5[m]$ and $T_p = 8.0[s]$ is also calculated as this is a typical swell wave condition which results in a significant contribution of wave resistance. The calculated resistance value in STAIMO and taken as an uncertainty around the curve, shown as the black dotted line.

2.2.2 Comparing with model tests

The PTO and wind/wave corrected sea trial results are compared with the corrected model test results, see Figure 2.4. The difference between both curves at lower speeds is still significant, while at higher speeds a better fit is visible. H. Klein Woud [2002] stated that power is cubically related to the speed. It is not possible to fit a cubical relation through all the points of the sea trial, while still crossing the origin of the graph. Instead a cubical relation is fitted through the model test results which is shown in the same figure by the dark green line. Extrapolated data points have an increased uncertainty.

Translation of power to resistance

The power in calm water conditions is translated to resistance for further calculations. This translation is done using the shaft and delivered efficiency. The shaft efficiency is assumed constant but the delivered efficiency need to be extrapolated to zero ship speed. While the hull and relative rotative efficiency remain fairly equal over the whole speed range, $V_s = 0-17[kn]$, the open water efficiency does not. Figure 2.5 shows the known open water efficiency from model tests. A cubical relation is fitted through these points. Although this procedure introduces significant uncertainties, it is expected to have a lower uncertainty than a linear extrapolation. The open water curves for this controllable pitch propeller are not available.

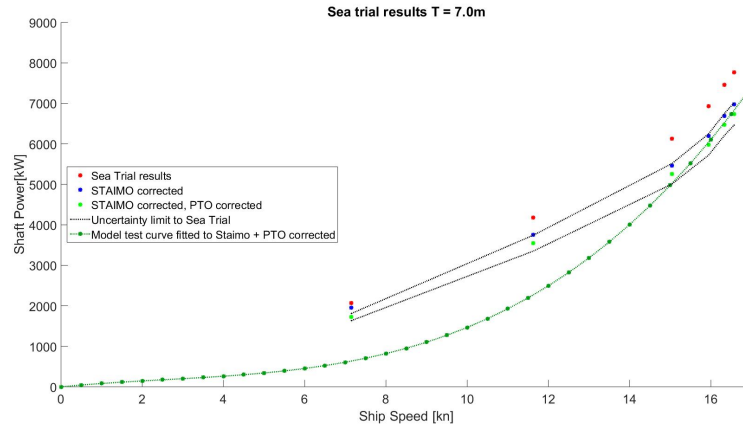


Figure 2.4: Sea Trial corrections

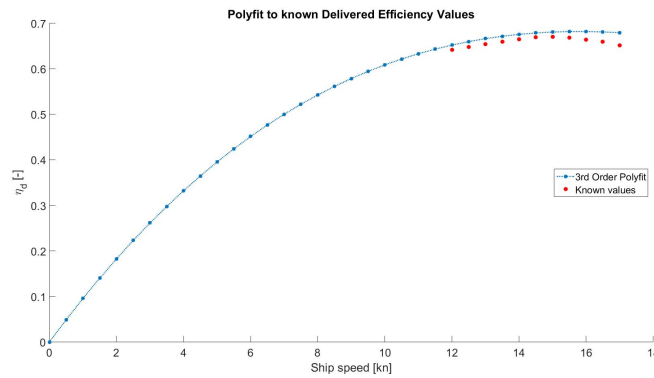


Figure 2.5: Polynomial fit to known delivered efficiency values

2.2.3 Calm water resistance during operations

Still air resistance

Also the mast and jib of both cranes were not yet installed during sea trials. STAIMO calculates the wind loading using the wind coefficients from WINDOS for no-cargo conditions without cranes installed. When the ship enters service cranes will be installed so the added resistance due to the cranes need to be taken into account. No-cargo condition with and without cranes and resulted in $C_{x0} = 1.45[-]$ and $C_{x0} = 1.22[-]$ respectively. The difference between these coefficients is used to correct the sea trial results and is shown by the red dots in Figure 2.6.

Fouling resistance

Corrections for fouling need to be made as the hull will not be so clean in operations as during sea trials. The correction for marine fouling is calculated by the Townsin method described in 1.3. The averaged hull roughness for the ship in service is estimated at $AHR = 300[\mu \cdot m]$ and leads to an increase in resistance as shown in Figure 2.6.

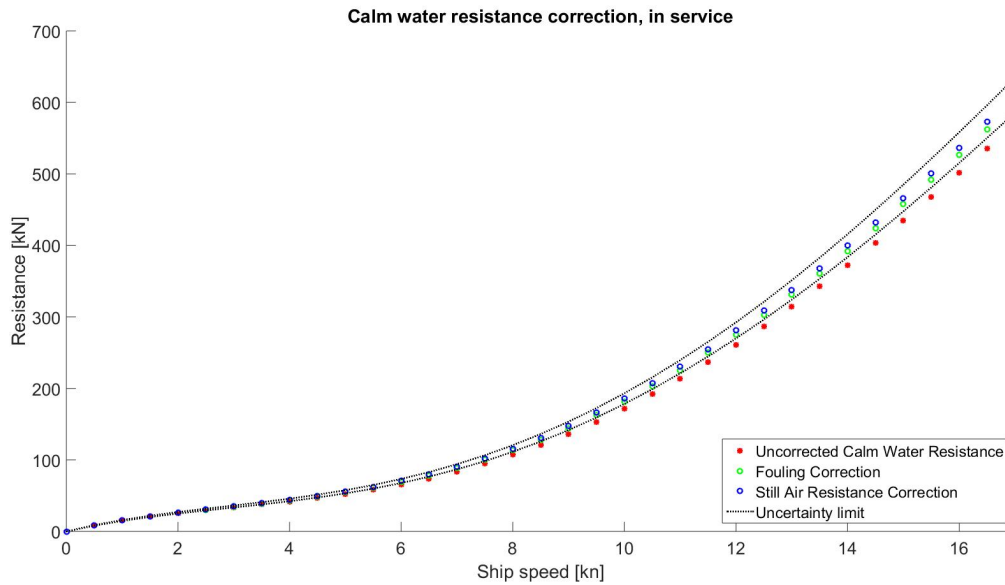


Figure 2.6: Sea Trial results translated to resistance and corrected for fouling and cranes

2.3 Discussion on Calm Water Resistance

Verification

Due to the third order polynomial fit the curve shows an unphysical course for lower vessel speeds. It is possible to force this point down, but this leads to larger deviations from the modified model test curve. Since the lower vessel speeds, range 0 - 6 knots, are of lower importance, this error is accepted.

Validation

Figure 2.7 shows the calculated calm water resistance curve including the uncertainty limits. The figure also shows several data points of calm water conditions defined as no swell waves, wind waves smaller than $0.5[m]$ and no cargo on board. These individual data points have their own uncertainty in vessel speed and reported fuel consumption, this is visualized by the green patches. Based on this figure the calm water resistance seems to be under predicted.

2.4 Conclusions and recommendations

The calm water resistance curve is constructed using the model tests and sea trial results. Both the model tests and sea trial are corrected for the known errors in the data. Corrections to the model tests are made for draft and delivered efficiency. The sea trials are corrected for increased power due to wind and waves present during the trial. After extrapolation to zero ship speed the translation is made from power to resistance. Finally, corrections for fouling and still air resistance are made. The calm water curve is validated using calm water operational conditions in the typical range of $V_s = 10 - 14[kn]$.

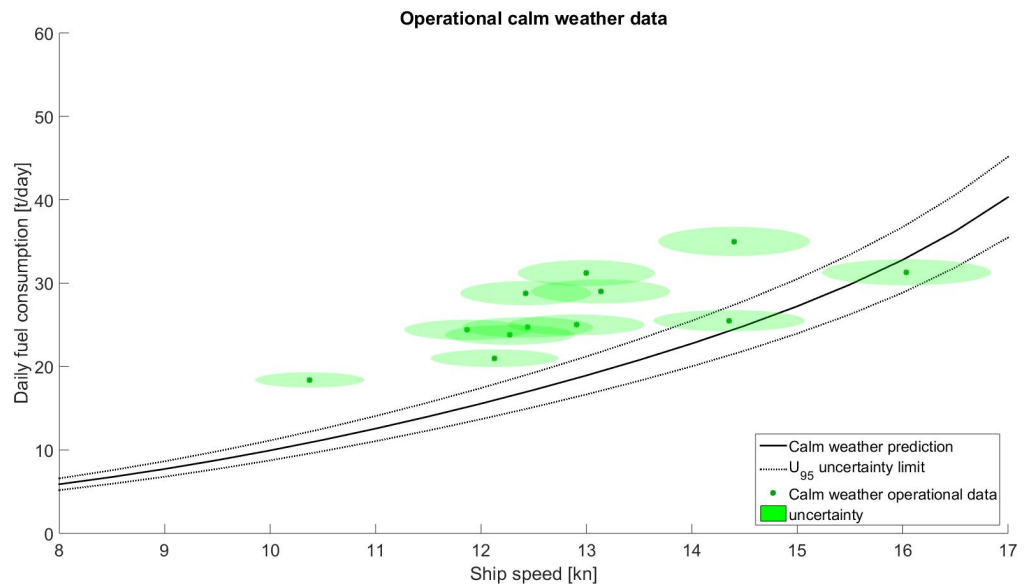


Figure 2.7: Fuel Consumption in calm weather conditions including operational data points

Recommendations

- Future model tests should be extended to lower speeds to provide better insight in the resistance at lower speeds. Different loading or trim conditions would also provide better insight on the influence of trim and loading on resistance.
- Knowing when the PTO is enabled provides better insight in the performance of the vessel.

Chapter 3

Added Resistance due to Wind

This chapter will explain the calculation procedure for wind loading. The calculations and their results are shown and discussed. Using the program WINDOS the calculated wind coefficients show up to a 60% increase with respect to the wind coefficients used by BigLift.

3.1 Calculation procedure

1. Construct a hull model
2. Model the cargoes onto the hull
3. Calculate wind loading

The calculations of the wind coefficients are done in the program WINDOS. WINDOS is a program designed to calculate wind induced loadings on marine structures. It is based on a building block approach and can quickly provide insight on separate objects on a marine vessel or offshore structure. WINDOS is also used to calculate the wind induced moments. Using environmental data from SPOS the wind loading can be calculated.

3.2 Calculations and results

3.2.1 Construct a hull model

A WINDOS model consists of a hull element to which other basic rectangular, circular and lattice type elements can be added. The user is free to adjust the size and location of each element in order to construct the desired model. The hull element can be given a user defined set of wind coefficients, or a selection from the WINDOS database of general ship types can be made. Due to the vertical velocity profile of wind and the shielding effect, it is important to find a comparable vessel with the accommodation in front. Such a vessel is not in the WINDOS database. For the most comparable ship an accommodation is modelled as a cargo to construct a hull comparable to the Happy Star.

Due to aforementioned reasons, the model of the Happy Star is constructed using as few elements as possible. Figure 3.1 shows the result of the no-cargo condition compared with the

CAD drawing.

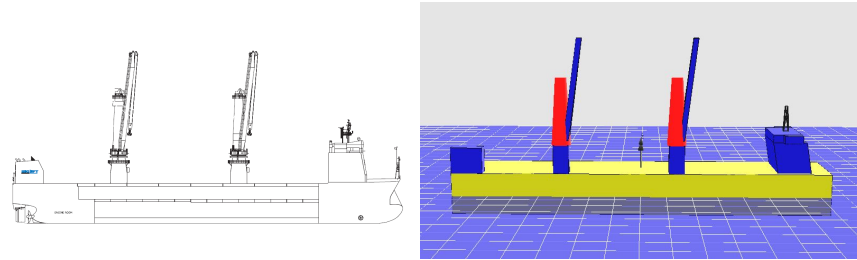


Figure 3.1: Happy Star and the simplified model in WINDOS

3.2.2 Cargoes

The voyages with deck cargo used throughout this research are also modelled in WINDOS. Using the Computer Aided Design (CAD) drawings the cargoes size, shape and location is modelled with as few elements as possible. Figure 3.2 shows a comparison between a CAD drawing, the WINDOS simplified model and the actual sailed condition for voyage 007, for details of this voyage see Appendix C.

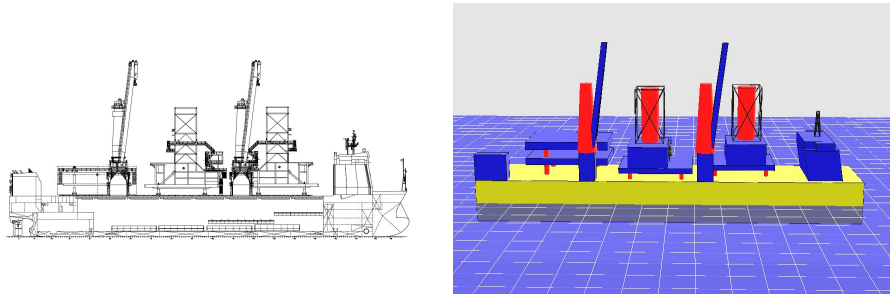


Figure 3.2: Cargo voyage 7 as in the shipping manual and the simplified model in WINDOS

3.2.3 Calculate wind loading

Equation 3.1a is used to calculate the air resistance. This is the wind resistance a vessel encounters when there is no true wind but only the wind generated by the forward speed of the vessel. This component of the wind resistance is included in the calm weather resistance calculations as mentioned in Chapter 2.2.1. The added wind loading due to the presence of the cargo can be calculated using Equation 3.1b. The results presented only features the wind coefficients in longitudinal direction, C_x . The effect of wind loading in transverse direction, C_y and the yawing moment will be discussed in Chapter 5.

$$R_{air} = \frac{1}{2} \cdot \rho_a \cdot V_{sog}^2 \cdot C_{no-cargo} \cdot A_{no-cargo} \quad (3.1a)$$

$$R_{wind} = R_{windcargo} - R_{air} \quad (3.1b)$$

Important to note is the method to calculate the non-dimensional wind coefficients. This normally done using Equation 3.2a. The projected area of each cargo is different. When using the mentioned equation, the effect of the change in shape and size is combined in the wind coefficient. Equation 3.2b shows that the coefficients are made non-dimensional using the same projected area as no-cargo condition, to provide a clear insight when comparing cargoes.

$$C_x = \frac{F_{WINDOS}}{\frac{1}{2}\rho V^2 A_{total}} \quad (3.2a)$$

$$C_x = \frac{F_{WINDOS}}{\frac{1}{2}\rho V^2 A_{hullonly}} \quad (3.2b)$$

A comparison between the wind loading calculated by WINDOS and BigLift for a voyage including cargo can only be made based on the wind force. A comparison of wind coefficients does not provide a clear image as the coefficients by WINDOS are made non-dimensional with the projected area of no-cargo conditions. Figure 1.6 shows that the relative difference between the BigLift used coefficients and those calculated in WINDOS differ up to 60% for C_x at an apparent wind angle of $\mu_{wind} = 30[deg]$. This apparent wind angle leads to the highest C_x values since the shielding effect is lower than pure frontal conditions but the project area increases. When the apparent wind angle increases even more, the component of the force in longitudinal direction decreases fast as the function behaves like a cosine.

Figure 3.3 shows a time series of the wind loading over twenty voyages, cargo and no-cargo conditions. It is shown that the voyages including cargo provide higher wind resistance than without. Wind loading can lead to a decrease in resistance when the apparent wind angle is within $\pm 90[deg]$ of aft incoming wind, $\mu_{wind} = 0[deg]$. That is why the time series shows negative values.

3.3 Discussion

The results presented only features the wind coefficients in longitudinal direction, C_x . Wind loading in longitudinal direction directly influences the required propulsive power. Wind loading in longitudinal and transverse direction also influence the yaw moment, possibly resulting in a leeway drift angle. This yaw moment can be calculated, but not validated in this chapter. The influence the yaw moment is investigated in Chapter 5

WINDOS Method

The accuracy of the wind coefficients used from the WINDOS database is increased by manually adjusting the wind coefficients of a comparable ship. Size and location are taken from CAD drawings and it is certain that this is the actual location during the voyage. The cargo is placed on the vessel exactly as planned, since ballast condition, rigging, deck layout and more depend on the location of the cargo. The vessel and cargo geometry is modeled in a simplified manner. This is to reduce near by effects of elements close to each other.

The wind coefficients are calculated from $0 - 360[deg]$ with steps of $15[deg]$. Some uncertainties arise when these data points are linearly interpolated to a continuous function. These uncertainties are expected to be very low as the function does not include sudden sign changes or large gradients.

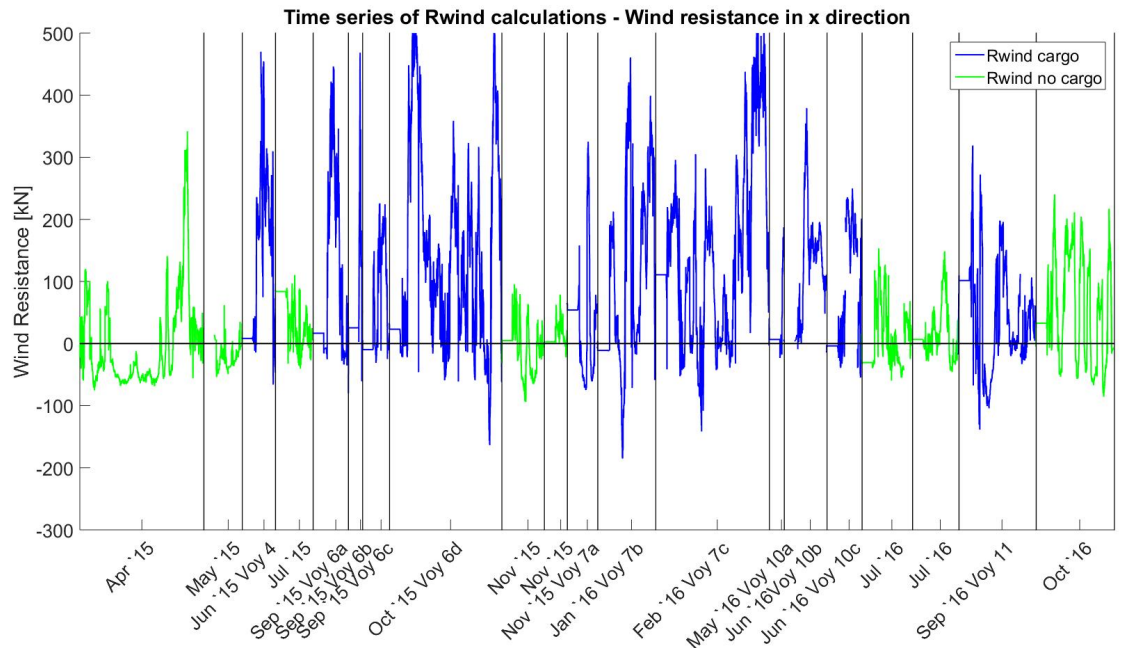


Figure 3.3: Time series of the wind resistance over several voyages

Verification

Blendermann [1996] used wind tunnel tests in his research for wind coefficients of the most dominant ship types. The most comparable ship type is a general cargo ship with cranes on deck. BigLift uses wind coefficients which are probably based on Blendermann but adjusted to the Happy Star specific, this is a common procedure in ship design. Figure 3.4 is repeated shows a comparison between the wind coefficients by Blendermann, BigLift and WINDOS. There are large differences between the three curves.

A verification study for WINDOS is performed from which it can be concluded that the change in results are in line with the expectations. It is however challenging to determine if the magnitude of the results is in line with the expectations due to the lack of reference material.

Uncertainties

Another important uncertainty due to the quadratically relation to wind loading is the apparent wind speed, $U_{V_{wind}} = 21\%$. The uncertainty in the apparent wind angle, $U_{\mu_{wind}} = 20\%$ can not be disregarded as well. 15 degrees change in μ_{wind} can lead to a 50% change in wind coefficient. Which is directly related to magnitude of wind loading.

Validation The wind loading results can be verified according to what is expected, but validation is not possible as wind and waves are dependent. The validation of calculated wind resistance with actual wind resistance is therefore combined with the wave resistance in Chapter 5.

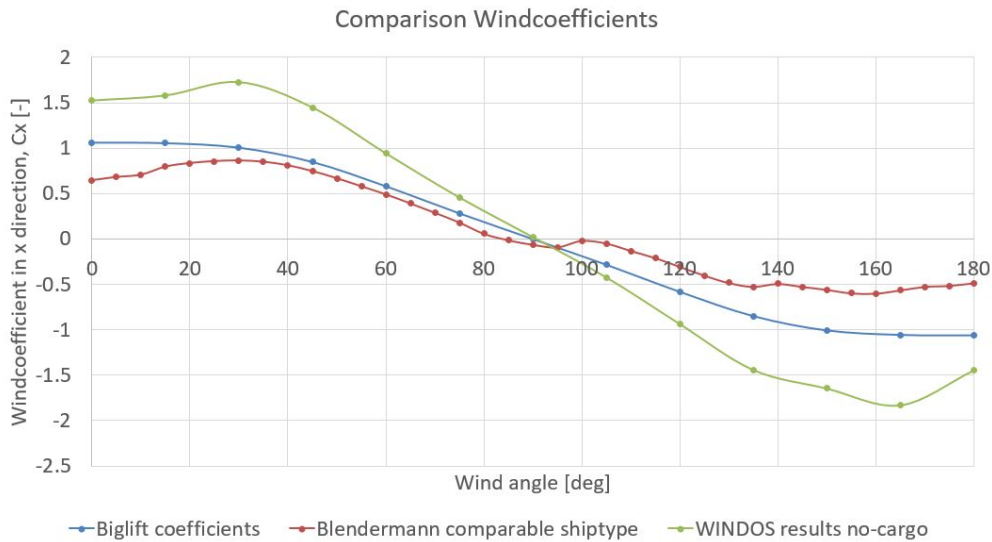


Figure 3.4: Comparison of C_x by three different methods

3.4 Conclusion and recommendations

The added resistance due to wind is of importance due to the large differences in projected wind areas for heavy lift vessels carrying voluminous cargoes on deck. WINDOS is a program based on a building block approach which includes the shielding effect and other interactions between structural elements with respect to wind loading. Using STAIMO the wind coefficients of the vessel in no-cargo and cargo conditions are calculated which resulted in higher coefficients than BigLift currently uses.

Recommendations

- The difference magnitude and course of the wind coefficients calculated in WINDOS are reasons for BigLift to revise the currently used ones.
- For both MARIN and Biglift WINDOS can be used to investigate the effect of ship and cargo geometries on the wind resistance, while saving time and resources due to the easy to use program.
- A comparison study between WINDOS and a more advanced method as for example CFD will provide better insight in the accuracy of WINDOS and its usability in predicting wind loads

Chapter 4

Added Resistance due to Waves

The added resistance of a ship in waves (RAW) is determined by radiated waves and wave reflection, due to wind- and swell waves respectively. In this chapter the added resistance is calculated using the operational data available.

4.1 Calculation procedure

1. The transfer function is determined using SPAWAVE
2. The wave loads are calculated separately for wind- and swell waves

Equation 4.1 shows that the added resistance in waves is determined by a function of wave height, wave period and wave direction, for both swell and wind waves. This transfer function is determined at one meter significant wave height.

$$RAW = f(H_s^2, T_p, \mu)_{swell/wind} \quad (4.1)$$

4.2 Calculations and results

4.2.1 Transfer function

Section 1.5 explained the working principle of the SPAWAVE method. The parameters of the Happy Star are used to construct the TAW transfer function. This function is verified with comparable ship types in the database of SPAWAVE. The TAW is translated to RAW by multiplying it with one minus the thrust deduction.

4.2.2 Wave loading

The resistance due to wind waves is calculated separately from swell waves and then summed. The parameters are also provided as one parameter in a combined wind- and swell waves. Figure 4.3 shows that the period of the swell waves are dominant, where the wave height can be summed. This may lead to incorrect values since the wave height has quadratic influence on the added wave resistance, using Equation 4.1.

Figure 4.1 shows a time series of the total wave resistance over twenty voyages, cargo and no-cargo conditions. The figure shows the sum of the added wave resistance due to wind waves and swell waves.

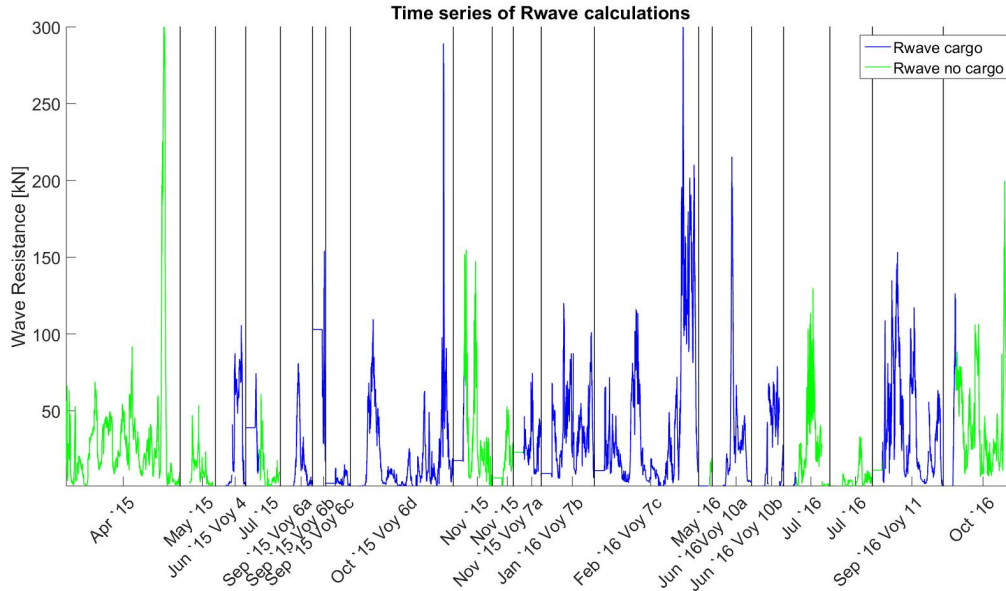


Figure 4.1: Time series of the calculated added resistance due to waves

4.3 Discussion

Verification

Figure 4.1 shows a time series of the wave resistance over twenty voyages, cargo and no-cargo conditions. The resistance generated by wind and swell waves are added to form the total added resistance due to waves. The contribution of wave resistance in cargo and no-cargo condition does not change, which is expected. SPAWAVE uses ship speed, wave height, wave period and wave direction as input, which do not change in cargo/no-cargo condition. Although the method works as expected, the change in loading condition does have influence on the added resistance due to ship motions, radiated waves. This is not included in this method and is therefore included in the uncertainty of SPAWAVE

Figure 4.2 shows one day of calculated wave resistance split into wind and swell waves. One data point is calculated for every 15 minutes, explaining the stepwise curve. Figure 4.3 shows the wave conditions for that specific day. The gradual increase of R_{sea} is related to the constant relative wave direction and a proportionally growth of wave height. Around the 10th data point there is a sudden jump in R_{swell} , this is due to a sudden change in relative wave direction due to course change of the vessel. The swell wave height is relatively constant which is also shown in Figure 4.2

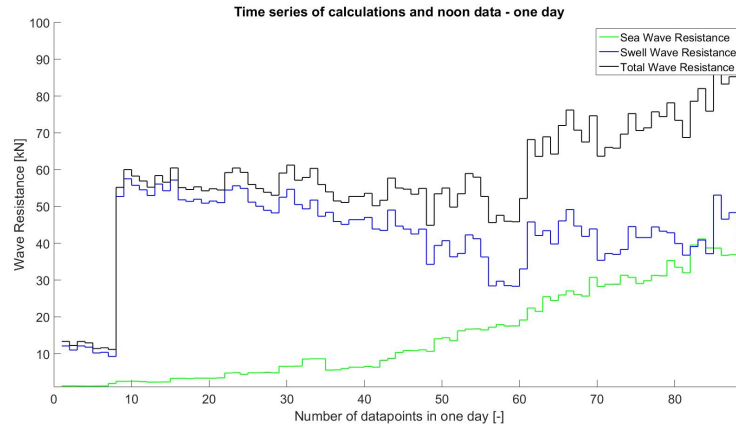


Figure 4.2: One Day Time series of the Wave Resistance - 29 March 2015

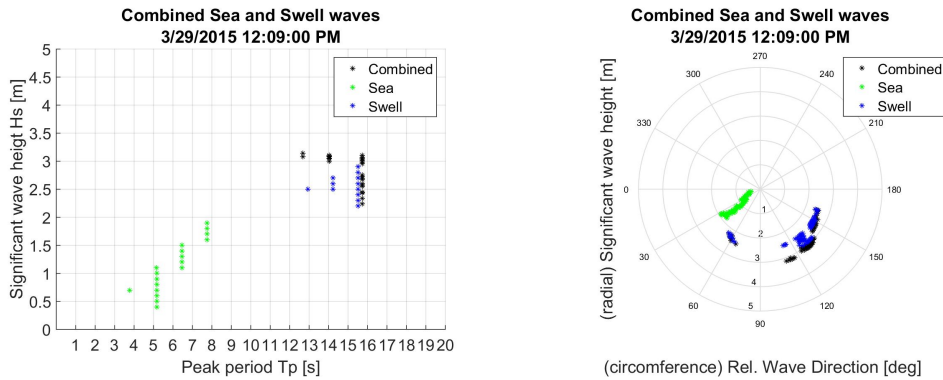


Figure 4.3: One Day Wave Data

A wave direction of $\mu = 0[deg]$ means aft incoming waves. Other than aft incoming wind, this wave direction does not lead to a decrease in resistance. The waves still induce vessel motions which lead to resistance. Figure 4.1 therefore only shows positive values.

Uncertainties

The parameter that have the most significant influence is the wave height, as this is quadratically related to the wave loading. However the uncertainty of this parameter is relatively low with respect to the wave direction $U_{H_{windwave}} = 7.5\%$ and $U_{H_{swellwave}} = 4\%$. While a 15 degree change in wave direction can lead to a factor 4 difference in wave loading.

As mentioned in Section 1.8, the uncertainty of swell wave characteristics are lower than for wind waves. This is beneficial as swell waves provide a larger contribution to the total wave loading than wind waves.

Validation

The wave resistance alone can not be validated separately from the other resistance components. The sum of wave and wind resistance can be validated as this should be equal to the difference

in total resistance minus the calm water resistance. This is done in the next chapter.

4.4 Conclusions and recommendations

(from conclusions total research) The added resistance due to waves is calculated using the SPAWAVE method. This method includes wave radiation and wave refraction in all relative wave directions, which is the result of ship motions and waves reflecting on the hull respectively. Swell waves show the largest contribution in the added resistance due to waves as this contributes the most to wave radiation. The uncertainty of wave radiation is determined by the uncertainty in wave conditions and in the motion response of the ship, due to the large changes in weight distribution for heavy lift vessels.

Recommendations

The SPAWAVE method does not include the influence of the loading condition on wave radiation, As mentioned in Section 1.5. For many ship types the radius of gyration is equal to $0.25 \cdot L_{pp}$, Grin [2014]. It is expected that for heavy lift vessels this can change significantly in between voyages. It is recommended to further investigate the influence of loading condition on the radius of gyration. If this is significant, the influence on radiated waves can be determined using the method of Jinkine and Ferdinande [1974].

Chapter 5

Total Resistance and Fuel Consumption

The total resistance is calculated by the sum of the calm water resistance, the added resistance due to waves and the added resistance due to wind. The results are translated to consumed fuel and validated with noon report data. The used methodology lead to a mean under estimation daily fuel consumption.

5.1 Calculation procedure

1. The total resistance is the sum of the individual components
2. The resistance is translated to break power
3. The break power is translated to consumed fuel

5.2 Calculations and results

Total resistance

Figure 5.1 shows a time series of the total resistance including the noon reported values for that day. The figure shows the no-cargo conditions(green line) and cargo conditions(blue line) separated. The vertical lines indicate the end of a voyage.

Translation to break power

The weather data provides information about the weather and ship conditions every fifteen minutes. Uncertainties are introduced if these resistance values are averaged over one day, since data regression never fully represents the actual value. A better method is to calculate the total fuel consumed over one day and compare that with the daily fuel consumption from the noon-reports. The total resistance is calculated over fifteen minutes, this value is translated to break power in [kWh]. The break power is then averaged over one day, $(\overline{P_B})$. Equation 5.1 shows this method. The resulting fuel consumption is calculated with the regression curve presented earlier in Figure 1.11.

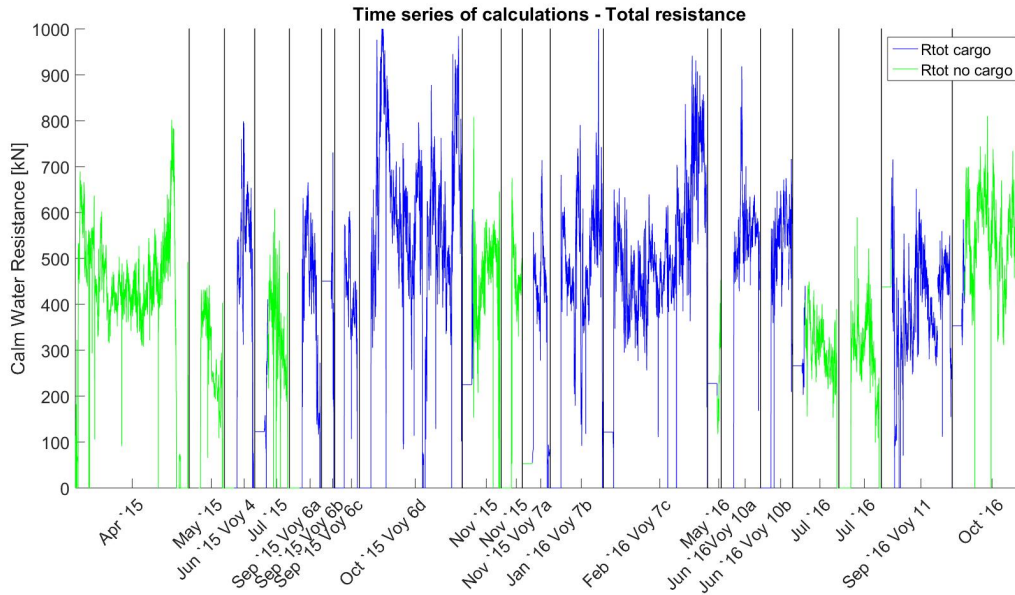


Figure 5.1: Time series of the calculated total resistance

$$\overline{P_B} = \left(\sum_{i=1}^N \frac{R_i \cdot V_i}{\eta_d \cdot \eta_s \cdot \eta_{gb}} \right) \cdot \frac{N \cdot 0.25}{24} \quad (5.1)$$

Where N is the total number of i data points in one day

Translation to consumed fuel

The translation of break power to fuel consumption is explained in Section 1.7. The average break power from the previous section is translated to the daily fuel consumption and compared to the noon reported values. Figure 5.2 shows this comparison for cargo conditions and Figure 5.3 for no-cargo conditions. If all the dots in this cross-plot would be on the diagonal of the figure, the calculation model would provide a perfect fit. A calculated value is considered an outlier when it differs a factor 2.5 with the reported value. Outliers are removed from the data set.

5.3 Discussion

The draft changes in draft as shown in Figure 5.5 and Figure 5.4 for no-cargo and cargo conditions respectively. At 7.5[m] the bulbous bow submerges and at 8.0[m] draft the transom submerges. Both phenomena have significant effect on the resistance. As mentioned in Chapter 2 the Admiralty function is therefore disregarded. The changes between cargo and no-cargo conditions are relatively small, this is due to the relatively voluminous rather than heavy cargoes. The dotted line indicates the uncertainty limit of the calculated fuel consumption as determined in Appendix E.

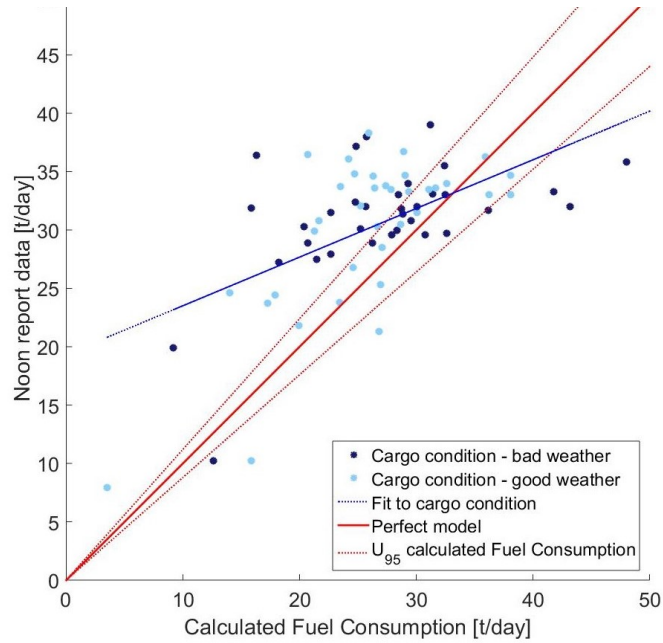


Figure 5.2: Calculated fuel consumption versus reported fuel consumption, cargo condition

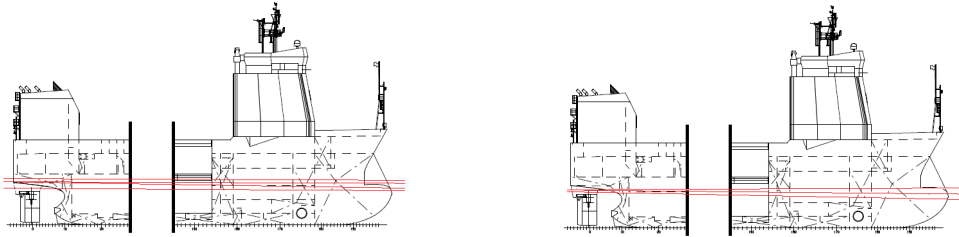


Figure 5.4: Trim conditions, no-cargo voyages

Figure 5.5: Trim conditions, cargo voyages

Table 5.1 shows the typical values for total resistance in good/bad weather and cargo/no-cargo conditions. A scaling factor K is determined using Equation 5.2 in combination with the least square method. The K value that shows the best fit with the data indicates the typical contribution of that resistance component with respect to the calm water resistance.

$$f(R_{calm}) = K \cdot (p_1 \cdot V_s^3 + p_2 \cdot V_s^2 + p_1 \cdot V_s) \quad (5.2)$$

Roughly the same method is applied to determine the relative contributions of the individual components to the total resistance, presented in Table 5.2. The contributions of the several resistance components do not always add up to a 100% since K is determined by the best fit to the individual resistance components.

Verification

The verification of the individual components are already discussed in the previous chapters and

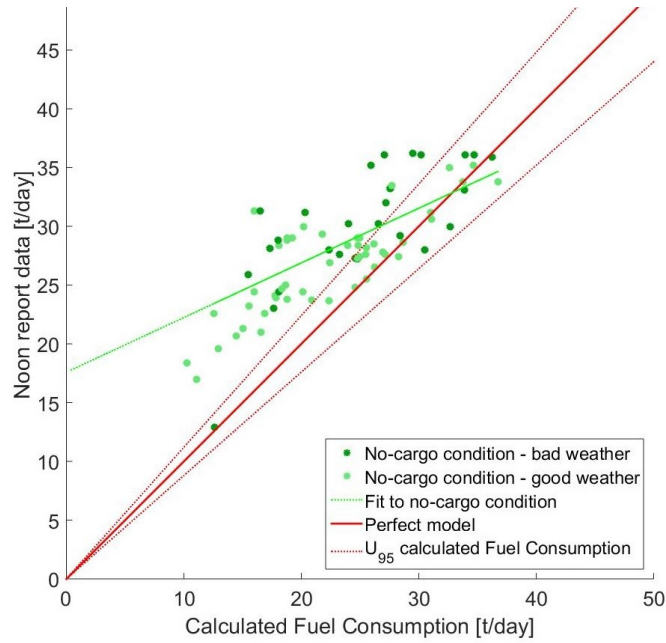


Figure 5.3: Calculated fuel consumption versus reported fuel consumption, no cargo condition

Sailing condition		Typical value	R^2	MAPE	Prediction error
No-cargo	Good weather	0.98	61%	31%	60%
	Bad weather	1.14	55%	25%	54%
	All		63%	11%	58%
Cargo	Good weather	1.15	50%	27%	56%
	Bad weather	1.49	22%	29%	60%
	All		32%	28%	55%

Table 5.1: Characteristics of fuel consumption prediction

will not be discussed any further.

Validation

The uncertainty limit for the fuel consumption is $U_{95FC} = 3.60[t/day]$ applied to the nominal daily fuel consumption of 30 [t/day] and results in a relative uncertainty of $U_{95FC} = 12\%$. The uncertainty of the reported fuel consumption, $U_{noon} = 1.5[t/day]$, as mentioned in Section 1.8 is included in the calculations of the error percentage, but it is not visualized in the figures.

The goodness of the fit including uncertainties is expressed by the correlation coefficient R^2 . Table 5.1 shows these values for no-cargo, cargo and all voyages together. The table also shows the goodness of the fit (R^2), the mean average percentage error (MAPE) and prediction error in cargo/no-cargo and good/bad weather conditions. A high R^2 indicates a low amount of scatter. The MAPE is calculated using Equation 5.3 and indicates the bias error. The prediction error is determined by the number of failures divided by the total number of measurements. A failure is a measurement that lies outside the uncertainty limit.

Sailing condition		$\frac{FC_{calm}}{FC_{tot}}$	$\frac{FC_{windwave}}{FC_{tot}}$	$\frac{FC_{swellwave}}{FC_{tot}}$	$\frac{FC_{wind}}{FC_{tot}}$
No-cargo	Good weather	101%	1%	2%	-4%
	Bad weather	87%	6%	7%	6%
Cargo	Good weather	86%	1%	3%	16%
	Bad weather	67%	5%	4%	32%

Table 5.2: Contributions of the resistance components to the total resistance

$$MAPE = \frac{100}{n} \sum_{i=1}^i \left[\frac{Noon_i - Calc_i}{Noon_i} \right] \quad (5.3)$$

Several other cross-plots are made in order to find a source of the scatter in the calculations. A criterion is used to determine the color of the dots. Several results are presented;

- Section 1.6 mentioned the added resistant due to a leeway drift angle, which is a result of asymmetric wind and wave loading. Figures 5.6 and 5.6. A clear trend is not visible.

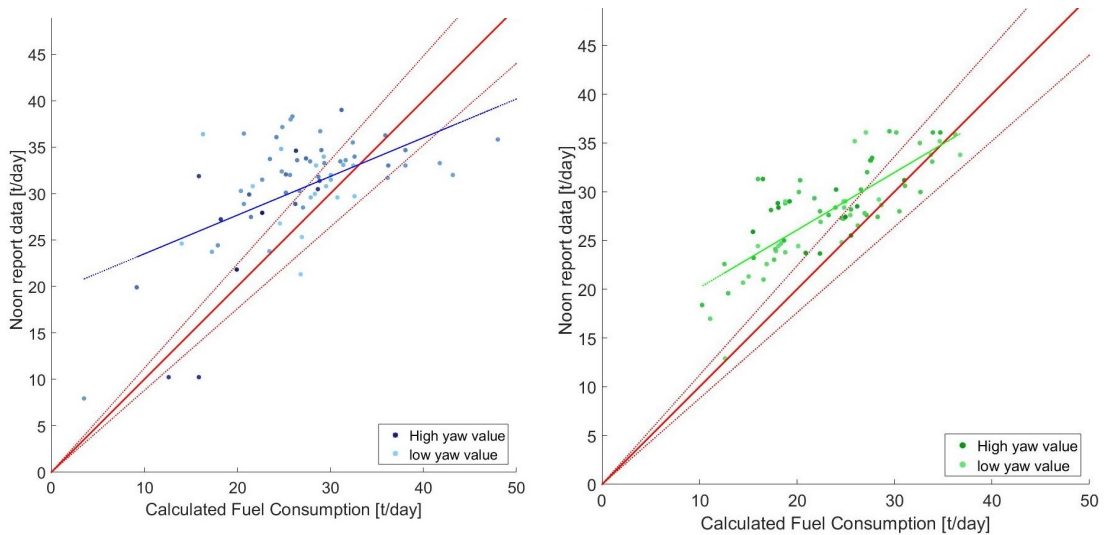


Figure 5.6: Calculated vs. reported fuel consumption and the influence of yaw moment, no-cargo condition

Figure 5.7: Calculated vs. reported fuel consumption and the influence of yaw moment, cargo condition

- Figure 5.8 shows the cross-plot using the level of calm water resistance as a criterion. The trend shows that high values for calm water resistance is associated with high daily fuel consumption. This confirms the calm water resistance as the most dominant contributor to the total resistance.
- Figure 5.9 shows that the largest over predictions are made for high levels of wind resistance. This may indicate a too large estimate of wind resistance. It is however contradictory that the lower wind resistance values are associated with an under prediction of daily fuel consumption.

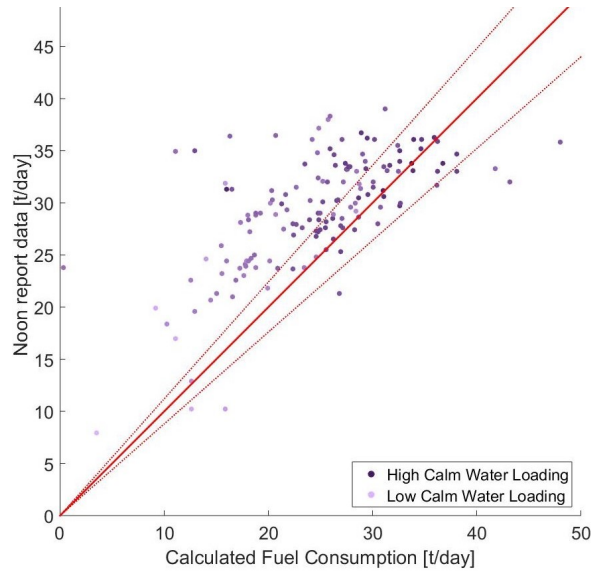


Figure 5.8: Calculated vs. reported fuel consumption and the influence of calm water resistance

- Figure 5.10 shows that the outliers of the predictions are related to the same voyage. The cargo configurations of these voyages are presented next to the graph. Both voyages feature an overhanging (voy. 6) or high cargo (voy. 7). Overhanging cargo is cargo that is wider than the width of the hull.
- Figure 5.11 shows the voyages which are less related to scatter in the data. These cargoes are smaller and probably lighter. The cargo that does reach above the accommodation is related to the highest scatter in this data set.

Figures 5.13 and 5.12 show the $FC - V_s$ relation based on the typical values as determined using Equation eq:polyfit_k. The currently used $FC - V_s$ as presented in Table B is repeated below and also plotted in the figure. If the same confidence interval U_{95FC} is applied to this relation, the prediction error is 79% for both no-cargo and cargo condition. The extended range of vessel speeds shows a better fit to the operational data than the currently used relation.

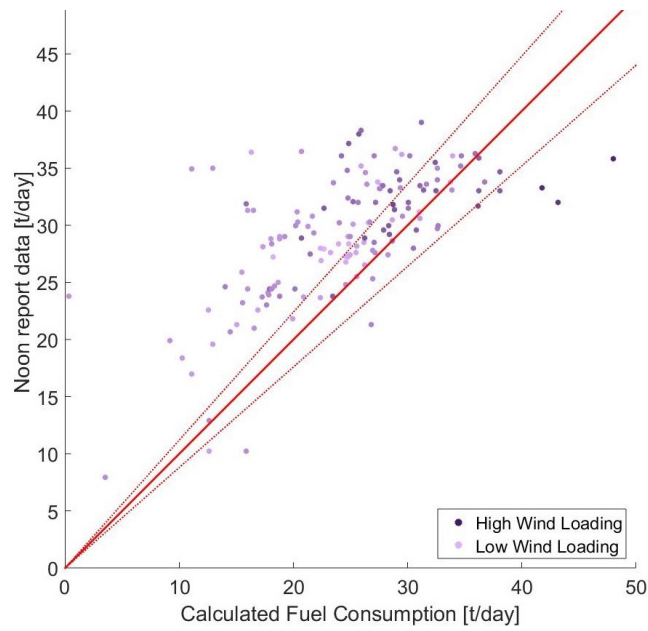


Figure 5.9: Calculated vs. reported fuel consumption and the influence of wind resistance

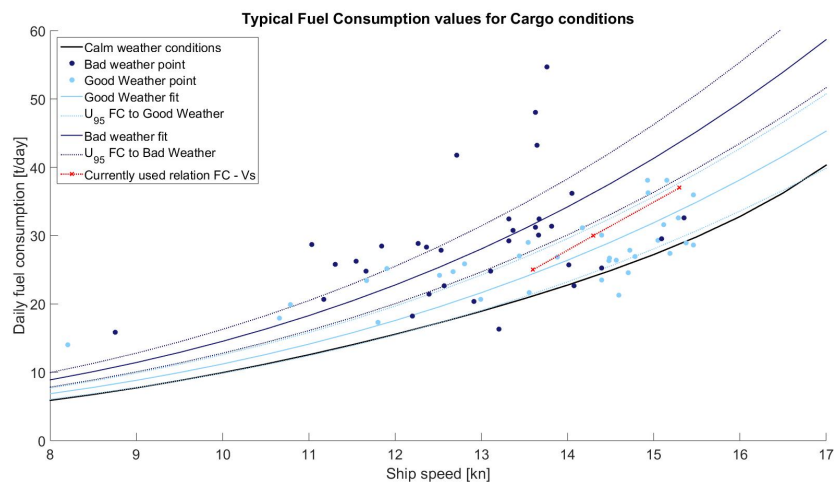


Figure 5.12: Calculated relation fuel consumption - ship speed relation, cargo conditions

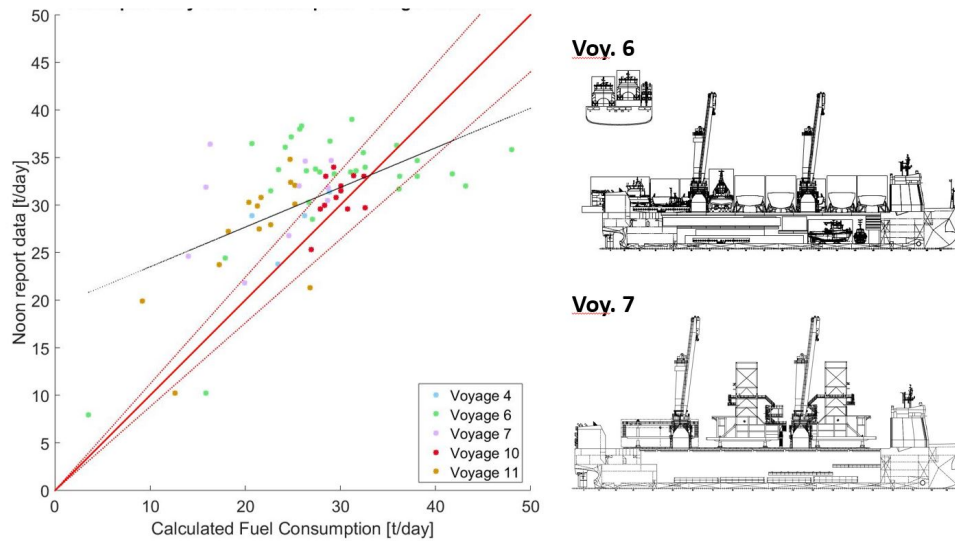


Figure 5.10: Calculated vs. reported fuel consumption visualized for separate cargo voyages

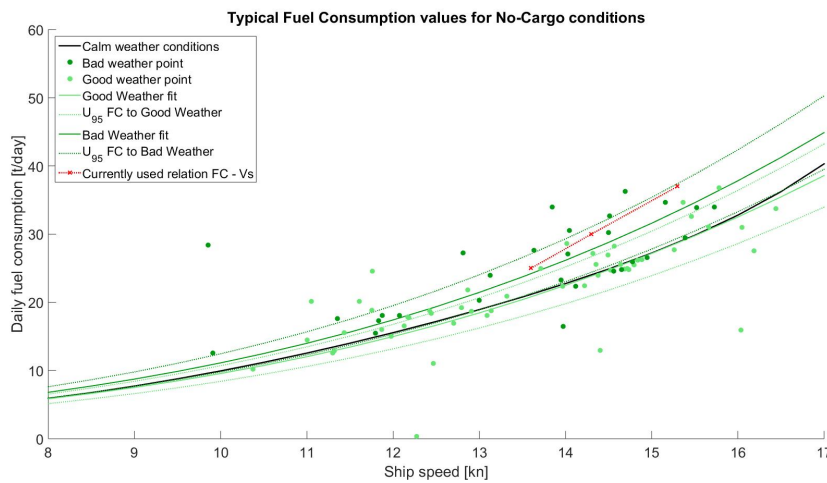


Figure 5.13: Calculated relation fuel consumption - ship speed relation, no cargo conditions

5.4 Sensitivity analysis

The sensitivity analysis is performed and reported in Appendix D to determine how dominant a variable is. Table 5.3 shows a summary of the most sensitive variables in the calculation of the total resistance. The uncertainty of these variables is shown in the last column of this table. A sensitive variable combined with a high uncertainty significantly influences the uncertainty of the total calculated resistance. The nominal values are calculated from one day data, Voyage004 Batam-Onslow, shown in Figure D.1. SF is the sensitivity factor, when a change in a variable leads to the same change in the total resistance, $SF = 1$.

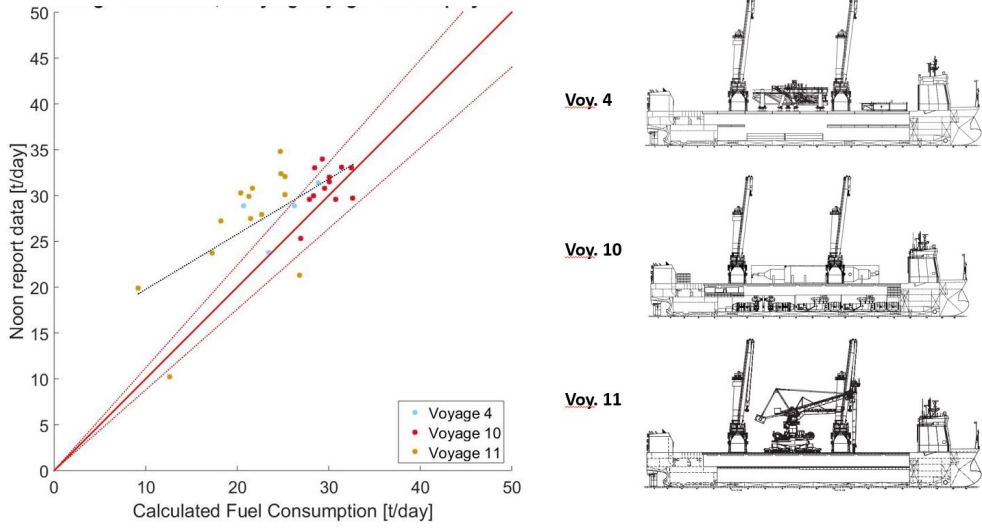


Figure 5.11: Calculated vs. reported fuel consumption for cargo voyages with a good fit

The table shows that V_{sog} has a non-linear sensitivity as the SF increases for higher speeds. The speed is not doubled since this speed is above the maximum vessel speed and therefore not included in the calculations. The sensitivity $\Theta_{truewind}$ is calculated for the best and the worst condition, $0[deg]$ and $180[deg]$ respectively. The SF is non-linear since the resistance is calculated with the apparent wind for which the speed is exponentially related to the wind resistance. The sensitivity of Cx_{cargo} is linear as the SF remain equal for half and double the nominal value.

Variable	[-]		$R_{tot}[kN]$	% diff	SF
	Nominal		639		
V_{sog}	12.5[kn]	50%	326	51%	0.98
		120%	802	126%	1.28
$\Theta_{truewind}$	95 [deg]	0[deg]	429	67%	0.33
		180[deg]	952	149%	0.49
Cx_{cargo}	-4.8[-]	50%	516	81%	0.38
		200%	885	138%	0.38
Hs_{swell}	2.4[m]	50%	593	93%	0.14
		200%	822	129%	0.29
V_{wind}	7.3 [m/s]	50%	585	92%	0.17
		200%	729	114%	0.14
AHR	300 [μm]	50%	550	86%	0.28
		200%	754	118%	0.18

Table 5.3: Most sensitive variables and their sensitivity, summary of Appendix D

5.5 Conclusion and recommendations

- Table 5.1 indicates the amount of scatter, the bias error and the error percentage of the calculations. Although the prediction error of no-cargo and cargo is quite the same, 58% and 55% respectively, the difference in goodness of fit(R^2) is significant, 55% and 22% respectively in bad weather conditions
- Table 5.2 indicates the typical contributions of the separate resistance components total resistance. It is shown that after calm water resistance, the wind resistance has the largest contribution to the total resistance in all sailing conditions
- It is shown that over sized cargo, in width and height, leads to a high scatter in the daily fuel consumption.

Recommendations

- BigLift should consider to perform more extensive research on the wind resistance, in case of an over sized cargo
- A recommendation to BigLift would be to study the possibility of sail with the jibs down in no-cargo condition. The tip of the jib is around 60 meter above the waterline at which the wind blows 40% harder than at the reference height of 10 meter, according to the log-law. An calculated 20% decrease on wind loading coefficient when the jibs are down, can results in 1-2% decrease on the total resistance

Chapter 6

Conclusion and Recommendations

The current ship speed prediction at a given fuel consumption shows large differences with the actual operational values. The ship speed prediction at a given fuel consumption currently used does not suffice for the wide range of operational conditions. Simulations on fuel consumption calculations were performed. From the results it seems justified to conclude that;

1. The separation of cargo/no-cargo conditions and good/bad weather gives an improved estimation the relation between vessel speed and daily fuel consumption, as expressed by the prediction error;
 - For no-cargo condition from 79% to 60%/55% in good/bad weather respectively
 - For cargo condition from 79% to 56%/60% in good/bad weather respectively
2. The goodness of the fit for no-cargo conditions is 63% while this is 32% for cargo conditions. This difference results from overhanging and high deck cargoes.
3. Wind resistance is the dominant resistance component after calm water resistance in all sailing conditions. In cargo condition during bad weather this contribution gets up to 32% of the total resistance comparing to 9% for wave resistance.
4. Following from the previous statement, the most important calculation parameters including highest uncertainty are the true wind angle, the wind load coefficient and true wind speed.

Recommendations

- BigLift should consider to perform more extensive research on the wind resistance, in case of an over sized cargo.
- The used methodology allows BigLift to calculate the fuel consumption ship speed relation for other vessels in the fleet.
- Monitoring of the following parameters would decrease the uncertainty in the calculations for fuel consumption;
 - PTO enabled and how many power produced
 - Combinator or fixed shaft frequency mode enabled
 - A flow meter for the main engine only
 - Automated measurements of shaft and break power
 - The actual power setting provided by the captain

List of Figures

1	Sign convention used throughout the report, BigLift [2017]	vii
2	Illustration of error types , H.W. Coleman [2009]	viii
1.1	Route as planned	11
1.2	Actual route	11
1.3	Approach to calculate the total resistance	13
1.4	Townsin and HSVA method to determine the increase in friction coefficient	16
1.5	Most probable Hs-Tp combinations for 3 Beaufort in the Chinese sea	17
1.6	Comparison of wind coefficients by BigLift, Blendermann and WINDOS	19
1.7	Windsensor on top of the wheelhouse - Happy star	20
1.8	Parameters that influence SPAWAVE , Grin [2014]	21
1.9	System diagram of the engine configuration	24
1.10	Calculation process of resistance to fuel, based on H. Klein Woud [2002]	25
1.11	Relation of fuel consumption against break power	26
2.1	7.0 and 7.5 [m] draft visualized	31
2.2	Comparison of scaled model tests including the corrected curve	32
2.3	Sea Trial Power Take Off correction	33
2.4	Sea Trial corrections	34
2.5	Polynomial fit to known delivered efficiency values	34
2.6	Sea Trial results translated to resistance and corrected for fouling and cranes	35
2.7	Fuel Consumption in calm weather conditions including operational data points	36
3.1	Happy Star and the simplified model in WINDOS	38
3.2	Cargo voyage 7 as in the shipping manual and the simplified model in WINDOS	38
3.3	Time series of the wind resistance over several voyages	40
3.4	Comparison of C_x by three different methods	41
4.1	Time series of the calculated added resistance resistance due to waves	43
4.2	One Day Time series of the Wave Resistance - 29 March 2015	44
4.3	One Day Wave Data	44
5.1	Time series of the calculated total resistance	47
5.2	Calculated fuel consumption versus reported fuel consumption, cargo condition	48
5.4	Trim conditions, no-cargo voyages	48
5.5	Trim conditions, cargo voyages	48
5.3	Calculated fuel consumption versus reported fuel consumption, no cargo condition	49
5.6	Calculated vs. reported fuel consumption and the influence of yaw moment, cargo condition	50

5.7	Calculated vs. reported fuel consumption and the influence of yaw moment, no-cargo condition	50
5.8	Calculated vs. reported fuel consumption and the influence of calm water resistance	51
5.9	Calculated vs. reported fuel consumption and the influence of wind resistance	52
5.12	Calculated relation fuel consumption - ship speed relation, cargo conditions	52
5.10	Calculated vs. reported fuel consumption visualized for separate cargo voyages	53
5.13	Calculated relation fuel consumption - ship speed relation, no cargo conditions	53
5.11	Calculated vs. reported fuel consumption for cargo voyages with a good fit	54
B.1	Schematic representation of the cargo booking process	64
D.1	Resistance components of one day data	79
E.1	Representation of Monte Carlo results, single sample	85

List of Tables

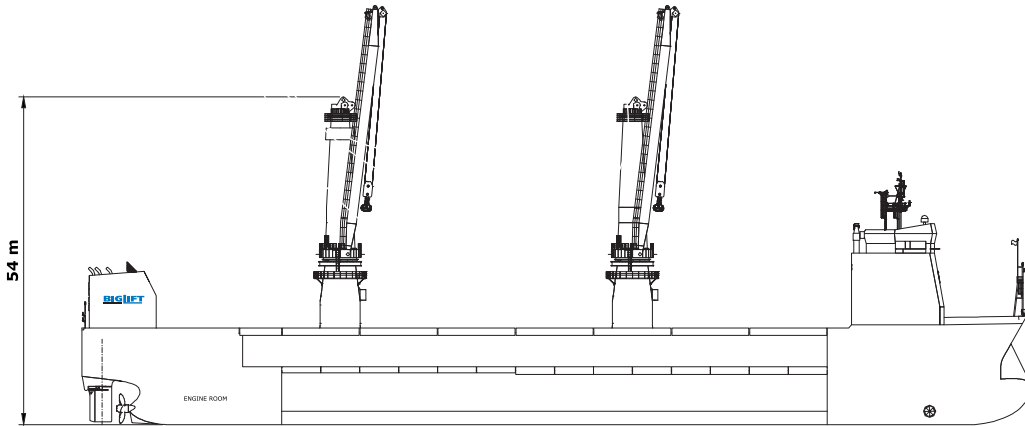
- 1 Used symbols and abbreviations viii
- 1.1 Currently used speed prediction at given fuel consumption 10
- 1.2 Summary of voyages used for validation C 23
- 2.1 Model test specifications 30
- 5.1 Characteristics of fuel consumption prediction 49
- 5.2 Contributions of the resistance components to the total resistance 50
- 5.3 Most sensitive variables and their sensitivity, summary of Appendix D 54
- D.1 Variables and their sensitivity 80
- E.1 Monte Carlo input parameters 84

Appendices

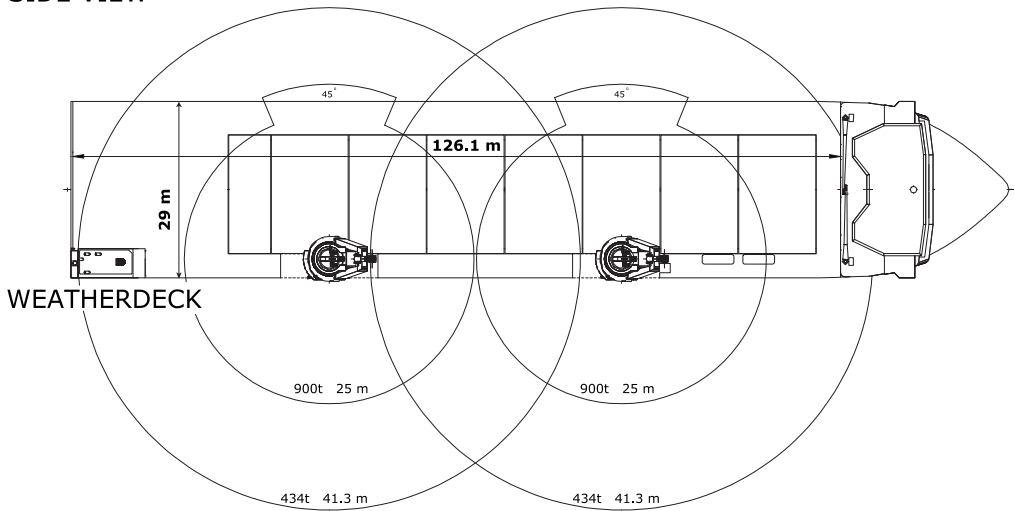
Appendix A

Specifications Happy Star

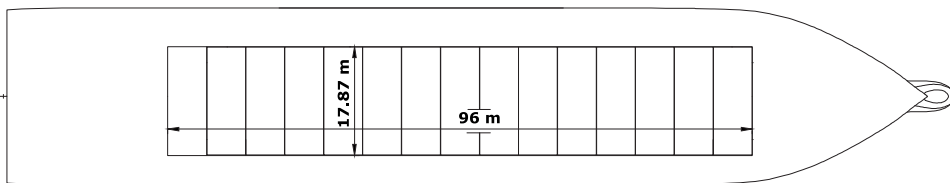
HAPPY STAR



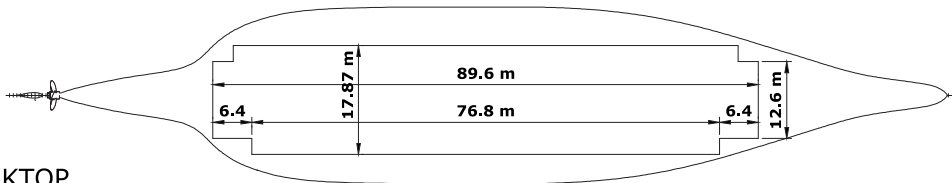
SIDE VIEW



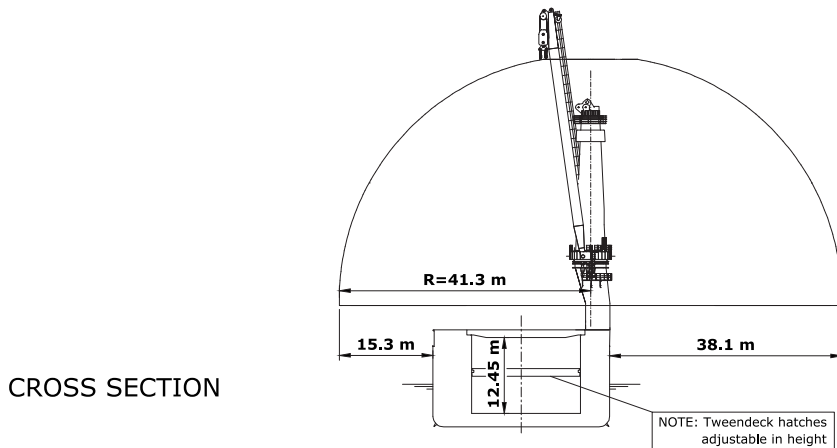
WEATHERDECK



TWEENDECK



TANKTOP



CROSS SECTION

HAPPY STAR

CLASS		LRS ✕ 100 A1, Ice class 1A (Finnish) strengthened for heavy cargoes		
Principal Dimensions	Length overall	155.97	m	
	Length p.p.	147.60	m	
	Breadth moulded	29.00	m	
	Scantling draft	9.50	m	
	Draft "open sailing"	7.50	m	
Deadweight	Scantling	18,374	mton	inc. tween deck hatch covers
Capacity	Grain = bale	20,535	m ³	if tween deck installed, 18,677 m ³
Floor space	Weather deck	3,280	m ²	
	Tween deck	1,716	m ²	
	Tank top	1,624	m ²	
Hatch openings	Weather deck	96.0 x 17.87	m	sailing with open hatches possible
	Tween deck	89.6 x 17.87	m	
Heights	Heights adjustable in steps of 50 cm	12.50	m	with no tween deck
	Minimum height	2.60	m	maximum 8.100 m
Allowable loads	Weather deck	15.0	t/m ²	
	Tween deck hatch covers	15.0	t/m ²	
	Tank top	20.0	t/m ²	
Cranes	Combinable	1800	mt	SWL
	Situated on starboard side	2 x 900	mt	SWL
	Fitted with trolley	37.5	mt	SWL
Main engine	Wärtsilä 8L46	8775	kW	
	Bowthruster	1000	kW	
	Speed	16	kn	

HAPPY STAR

Happy Star Amsterdam The Netherlands 2014

These particulars are believed to be correct, but without guarantee, and they must not be used as basis for Charter Parties or contracts without Owners' explicit written authority.



Radarweg 36	:	P.O. Box 2599	:	t. +31 (0) 20 - 448 83 00	:	info@bigliftshipping.com
1042 AA Amsterdam	:	1000 CN Amsterdam	:	f. +31 (0) 20 - 448 83 33	:	www.bigliftshipping.com

Appendix B

BigLift way of working

This section will explain the work flow of a project within BigLift Shipping and indicates that a better prediction of the fuel consumption and ship speed is most beneficial in the early stage of the project process. Figure B.1 shows a simplified way how a cargo is booked within BigLift Shipping.

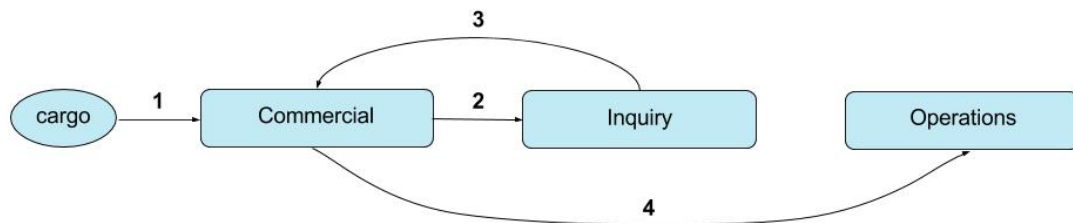


Figure B.1: Schematic representation of the cargo booking process

1. A request for a cargo shipment is received by the commercial department, consisting of basic technical details and a time frame
2. The commercial department looks into the vessels suitable for that cargo specifications. Even vessels that are not available for that time frame are considered as it leads to a higher profitability
3. the inquiry department performs some basic calculations and returns a technical proposal for each considered vessel back to the commercial department. A technical proposal includes the most safe and suitable configuration of the cargo on the ship and indicates the lifting gear required. The most profitable ship that fits in the sailing schedule is most suitable for the project. In general, the smallest vessel available for that cargo is the most profitable
4. Upon contract agreement, the cargo is booked and the operations department becomes responsible for the complete project including: engineering, stowage, rigging, lifting, stability, port arrangements, quality health safety and environment and planning

The process above includes day-to-day communication between the shipping company and the customer, quick calculations in the order of minutes are therefore required. After the cargo is booked the vessel coordination team takes care of the voyage planning:

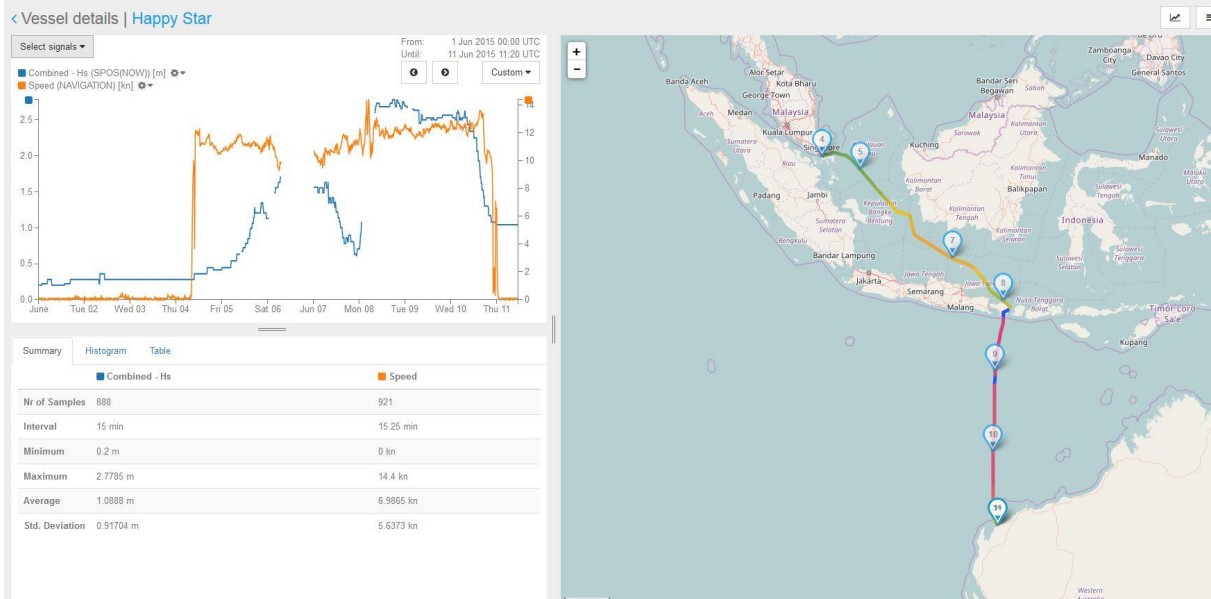
1. The distance and route between ports or other loading/discharge locations are calculated using the great circle distance between known waypoints
2. A sailing mode follows from the cost calculation. Table B shows the three sailing modes defined based on the expected fuel consumption. The default sailing mode is 'Eco'
3. For calm weather a sailing mode corresponds to a ship speed. The coordinator usually adjusts this speed based on experience with the weather that time of year and the loading conditions
4. The manually chosen ship speed is used to calculate the sailing time and the total fuel consumption. A buffer is included to account for delay in loading, discharging, weather rerouting or speed reduction

Sailing mode name	Ship speed [kn]	Fuel consumption [T/day]
Slow	13.6	25
Eco	14.3	30
Speed	15.3	37

Appendix C

Voyage data - Cargo conditions

Voy. 4, Batam - Onlsow



VOYAGE SPECIFICS

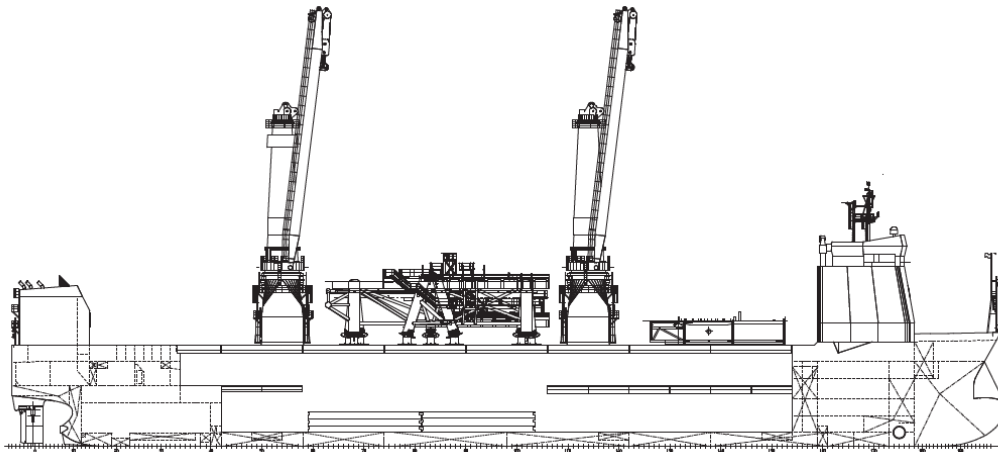
	EXPECTED	ACTUAL
DEPARTURE		23 / 06 / 2015
ARRIVAL		01 / 07 / 2015
DURATION	[hr] 138	192
DISTANCE	[nm] 1745	2056
TOTAL FUEL CONSUMED	[t] 172	194
DAILY FUEL CONSUMPTION	[t/day] 30	24.3

LOADING CONDITIONS

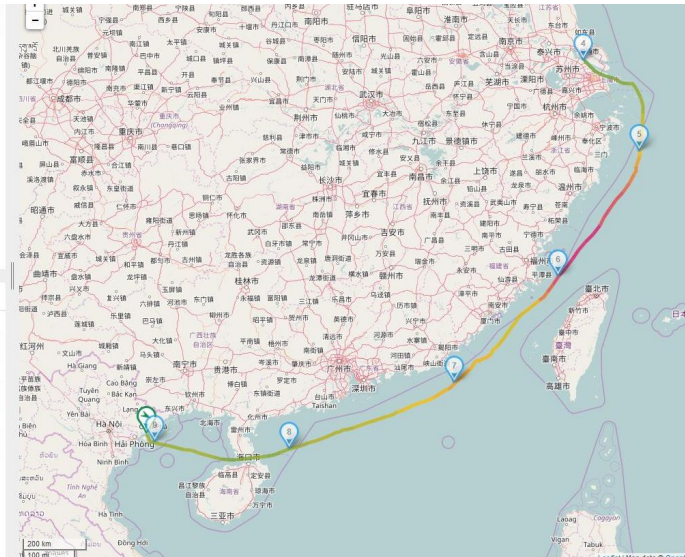
DRAFT AFT	[m]	7.2
DRAFT BOW	[m]	6.6
DISPLACEMENT	[T]	18777

WEATHER CONDITIONS

WIND WAVES	[m]	< 1.5
SWELL WAVES	[m]	< 2.1
APPARENT WIND SPEED	[m/s]	< 11.8



Voy. 6a, Shanghai - Haiphong



VOYAGE SPECIFICS

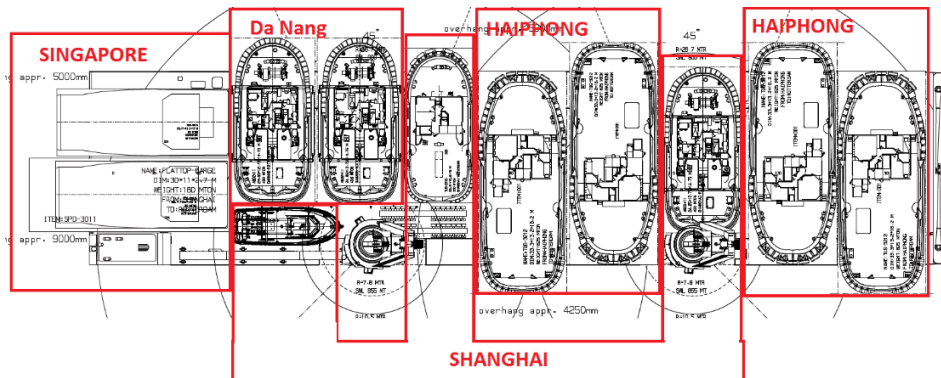
	EXPECTED	ACTUAL
DEPARTURE		04 / 09 / 2015
ARRIVAL		09 / 09 / 2015
DURATION	[hr] 126	141
DISTANCE	[nm] 1304	1344
TOTAL FUEL CONSUMED	[t] 157	161
DAILY FUEL CONSUMPTION	[t/day] 30	27.5

LOADING CONDITIONS

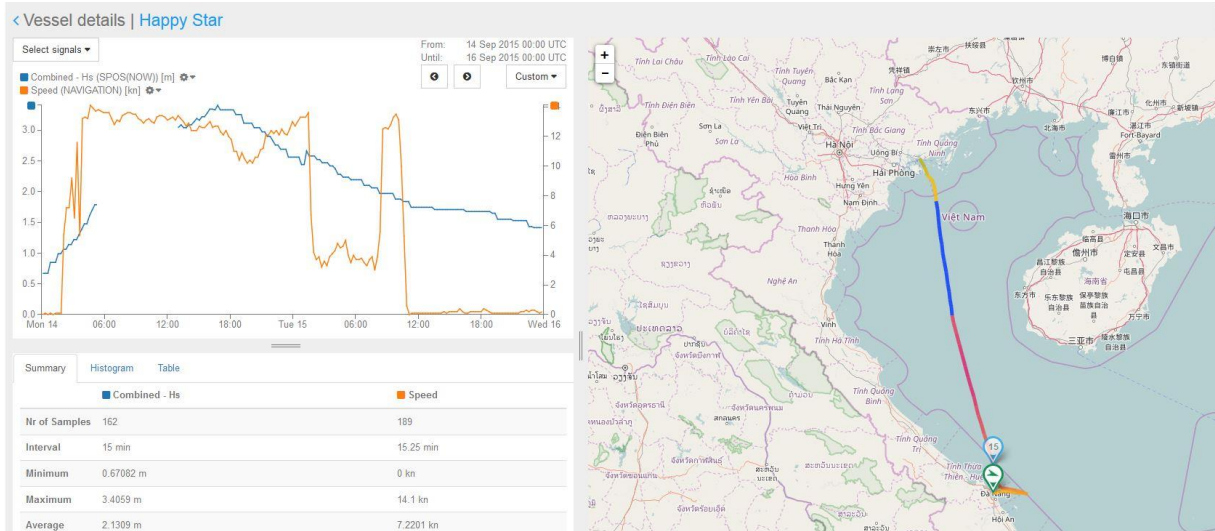
DRAFT AFT	[m]	?
DRAFT BOW	[m]	?
DISPLACEMENT	[T]	?

WEATHER CONDITIONS

WIND WAVES	[m]	< 1.4
SWELL WAVES	[m]	< 0.9
WIND SPEED	[m/s]	< 16.8



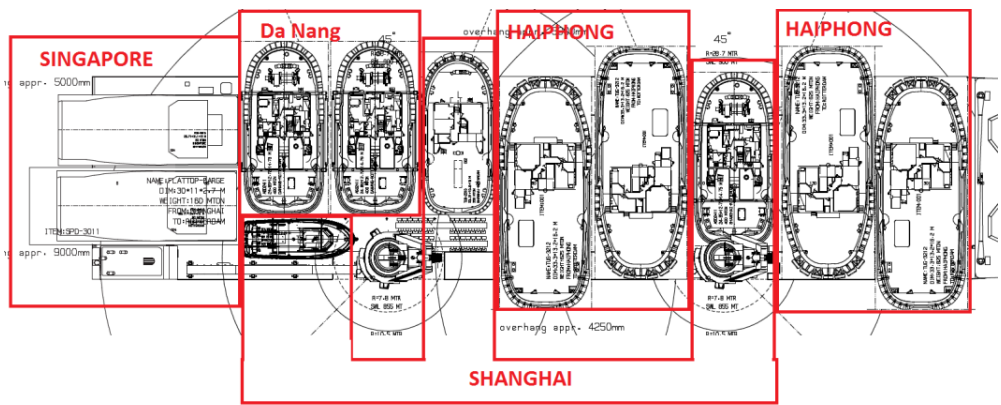
Voy. 6b, Haiphong – Da Nang



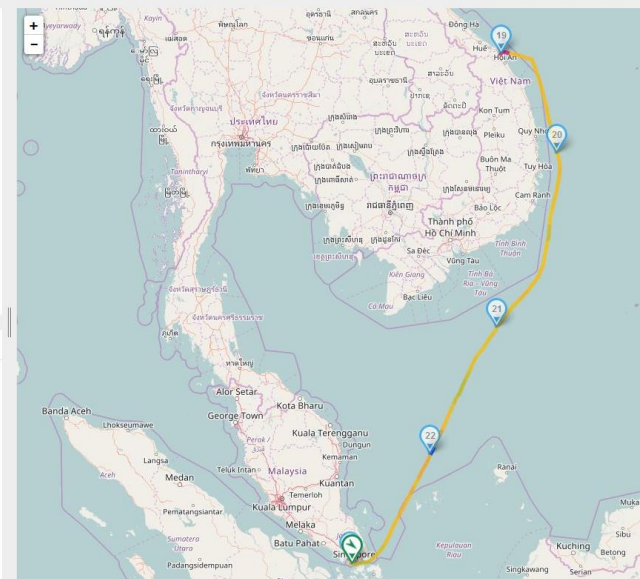
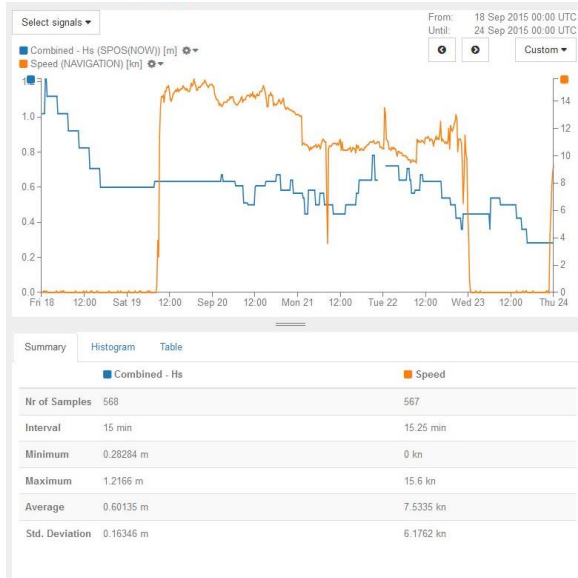
VOYAGE SPECIFICS	EXPECTED	ACTUAL
DEPARTURE		14 / 09 / 2015
ARRIVAL		15 / 09 / 2015
DURATION	[hr]	34
DISTANCE	[nm]	308
TOTAL FUEL CONSUMED	[t]	42
DAILY FUEL CONSUMPTION	[t/day]	30

LOADING CONDITIONS		
DRAFT AFT	[m]	?
DRAFT BOW	[m]	?
DISPLACEMENT	[T]	?

WEATHER CONDITIONS		
WIND WAVES	[m]	< 2.8
SWELL WAVES	[m]	< 2.2
WIND SPEED	[m/s]	< 15



Voy. 6c, Da Nang - Singapore



VOYAGE SPECIFICS

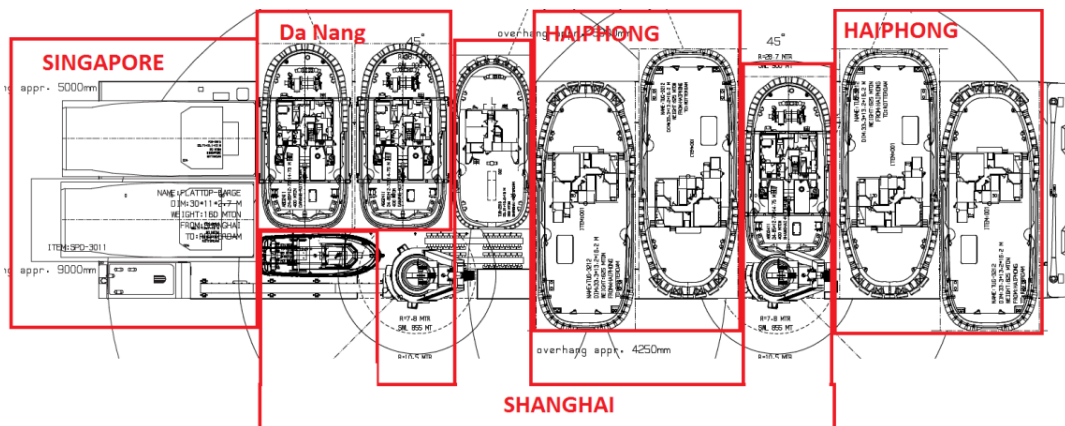
		EXPECTED	ACTUAL
DEPARTURE			19 / 09 / 2015
ARRIVAL			23 / 09 / 2015
DURATION	[hr]	103	92
DISTANCE	[nm]	1024	1052
TOTAL FUEL CONSUMED	[t]	128	109
DAILY FUEL CONSUMPTION	[t/day]	30	28.3

LOADING CONDITIONS

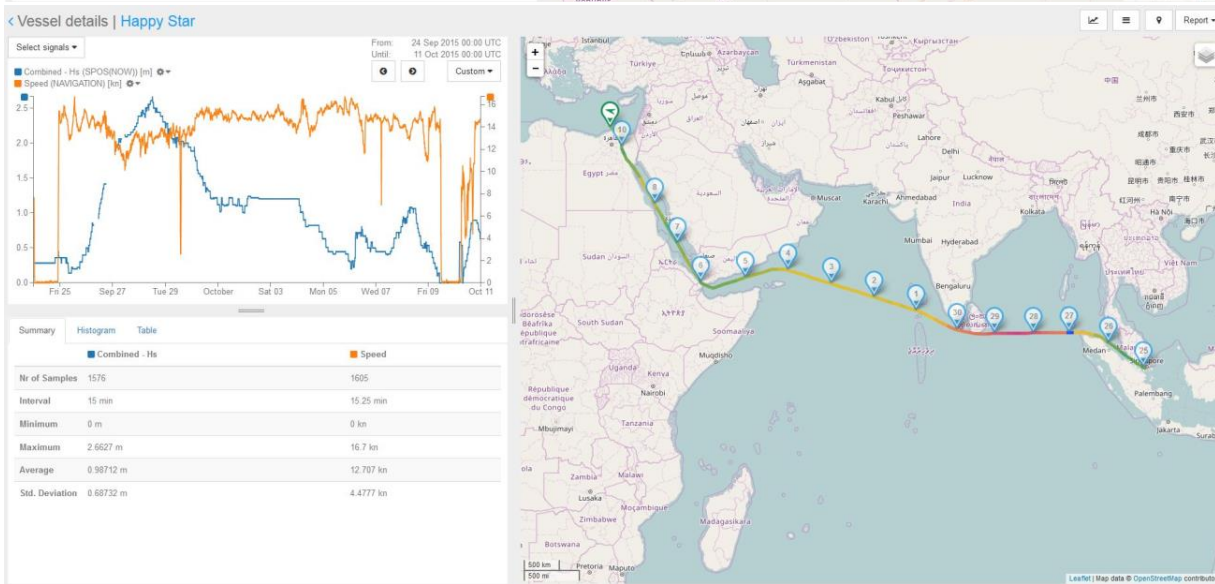
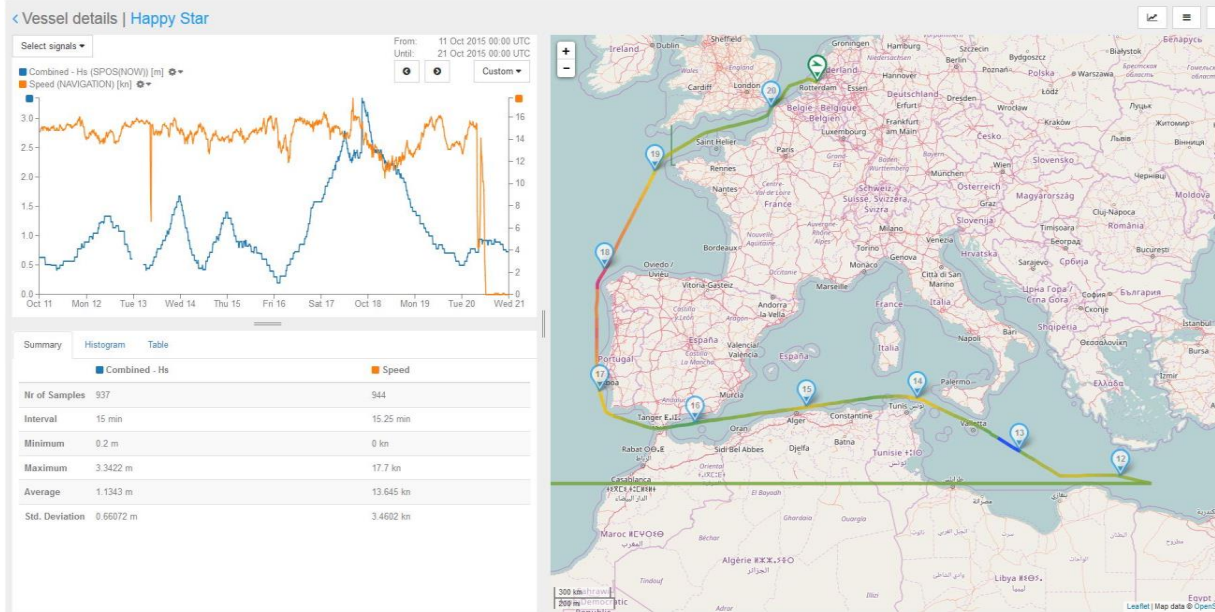
DRAFT AFT	[m]	?
DRAFT BOW	[m]	?
DISPLACEMENT	[T]	?

WEATHER CONDITIONS

WIND WAVES	[m]	< 0.5
SWELL WAVES	[m]	< 0.6
WIND SPEED	[m/s]	< 12.1



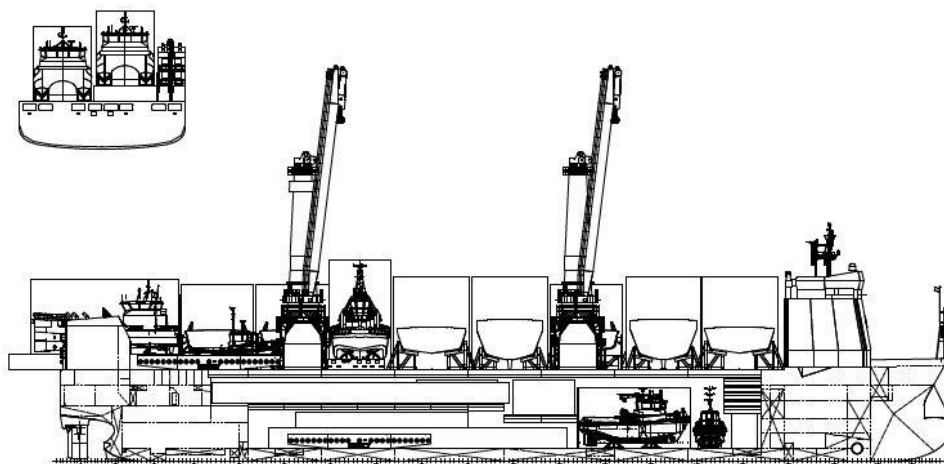
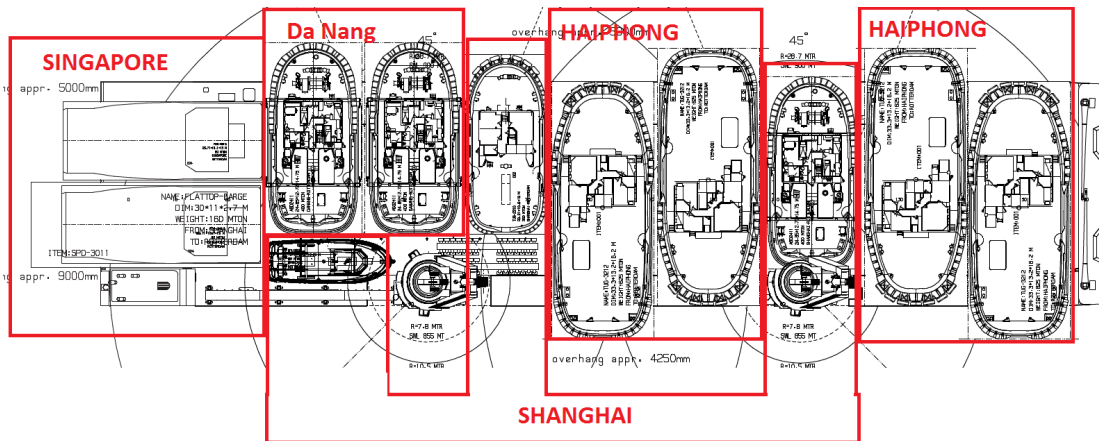
Voy. 6d, Singapore - Rotterdam



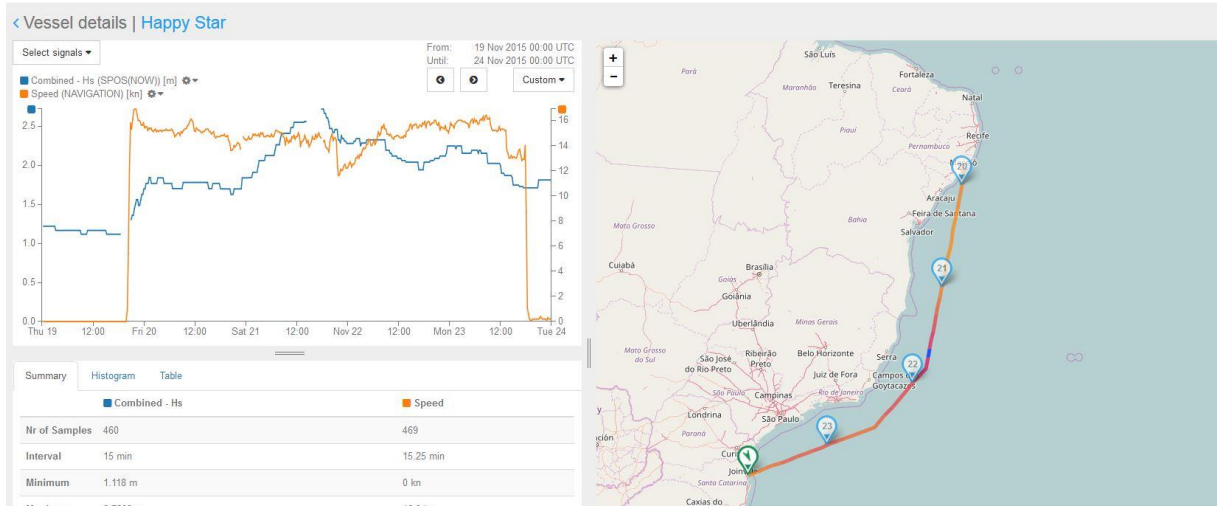
VOYAGE SPECIFICS		EXPECTED	ACTUAL
DEPARTURE			24 / 09 / 2015
ARRIVAL			20 / 10 / 2015
DURATION	[hr]	657	621
DISTANCE	[nm]	8471	8176
TOTAL FUEL CONSUMED	[t]	822	833
DAILY FUEL CONSUMPTION	[t/day]	30	32.2

LOADING CONDITIONS			
DRAFT AFT	[m]		8.6
DRAFT BOW	[m]		8.3
DISPLACEMENT	[T]		24184

WEATHER CONDITIONS			
WIND WAVES	[m]		< 2.4
SWELL WAVES	[m]		< 2.9
WIND SPEED	[m/s]		< 16.1



Voy. 7a, Maceio – Itajai (aft module only)



VOYAGE SPECIFICS

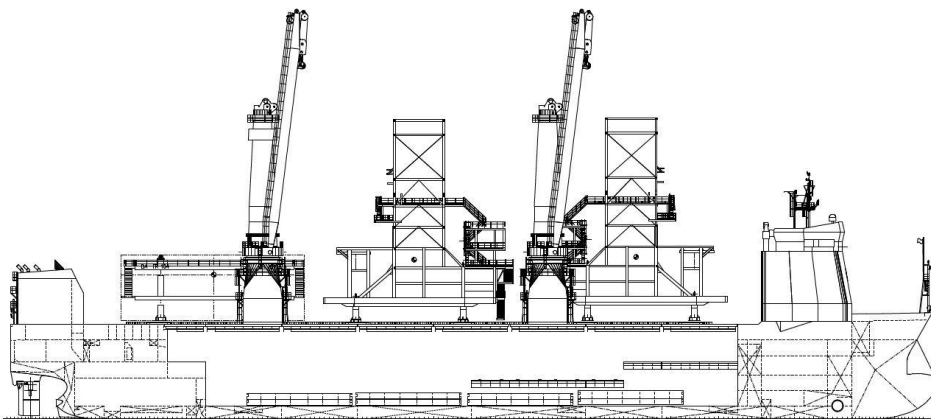
	EXPECTED	ACTUAL
DEPARTURE		19 / 11 / 2015
ARRIVAL		23 / 11 / 2015
DURATION	[hr] 104	117
DISTANCE	[nm] 1314	1347
TOTAL FUEL CONSUMED	[t] 131	174
DAILY FUEL CONSUMPTION	[t/day] 30	35.9

LOADING CONDITIONS

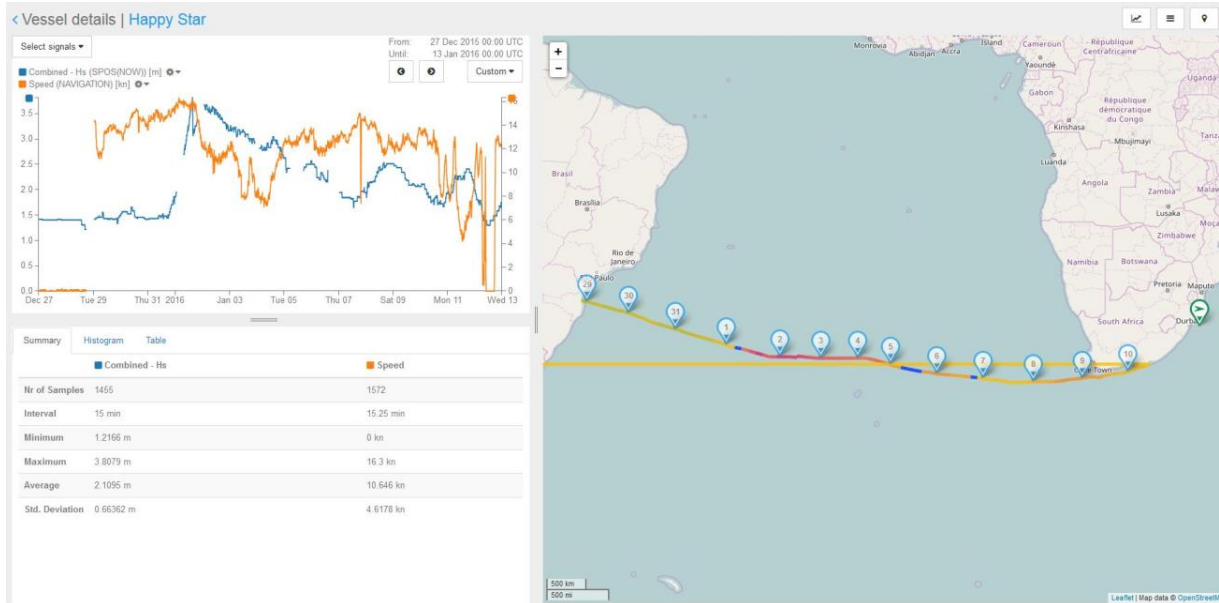
DRAFT AFT	[m]	6.9
DRAFT BOW	[m]	6.7
DISPLACEMENT	[T]	18410

WEATHER CONDITIONS

WIND WAVES	[m]	< 1.7
SWELL WAVES	[m]	< 2.2
WIND SPEED	[m/s]	< 14.1



Voy 7b, Itajai - Durban



VOYAGE SPECIFICS

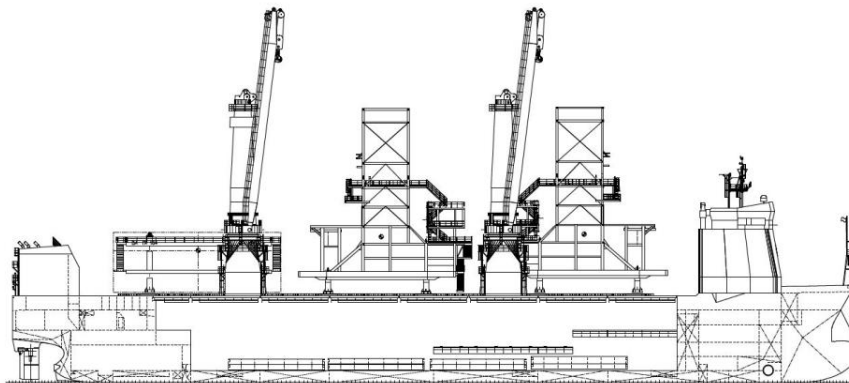
	EXPECTED	ACTUAL
DEPARTURE		29 / 12 / 2015
ARRIVAL		12 / 11 / 2016
DURATION	[hr] 360	357
DISTANCE	[nm] 4176	3708
TOTAL FUEL CONSUMED	[t] 450	530
DAILY FUEL CONSUMPTION	[t/day] 30	35.7

LOADING CONDITIONS

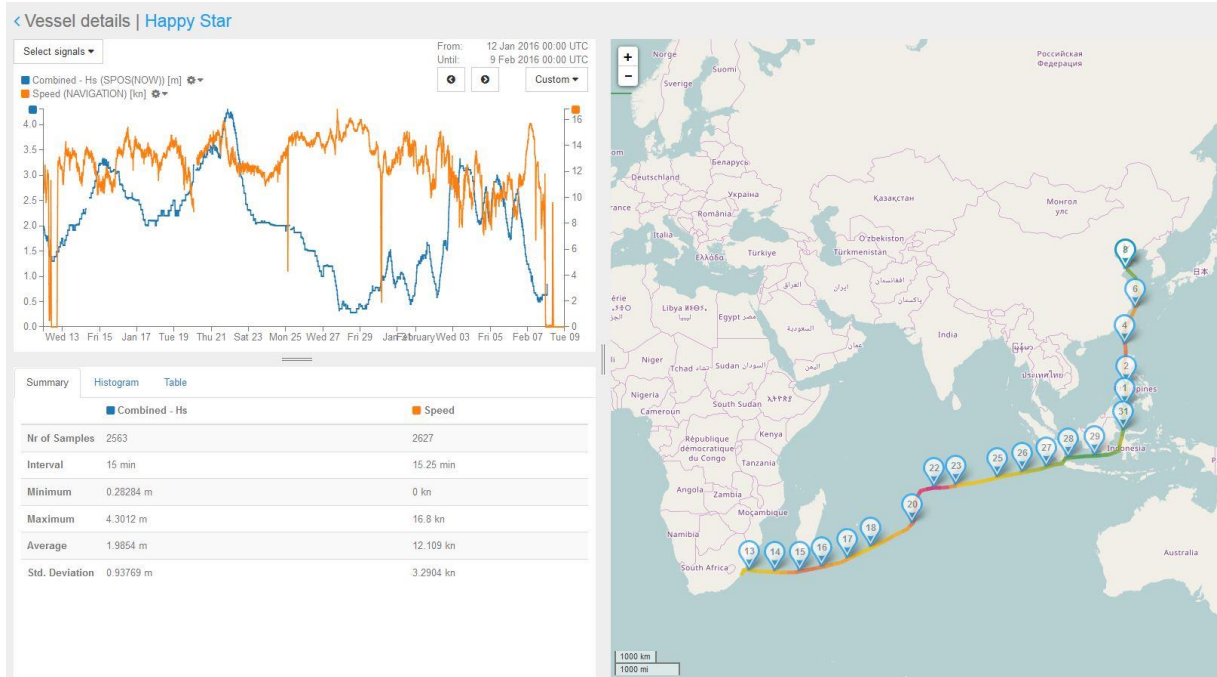
DRAFT AFT	[m]	8.1
DRAFT BOW	[m]	7.4
DISPLACEMENT	[T]	21740

WEATHER CONDITIONS

WIND WAVES	[m]	< 3.5
SWELL WAVES	[m]	< 3.5
WIND SPEED	[m/s]	< 16.1



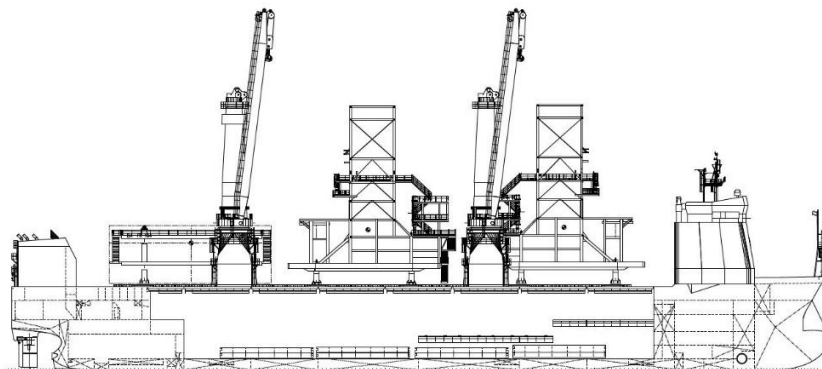
Voy. 7c, Durban - Qingdao



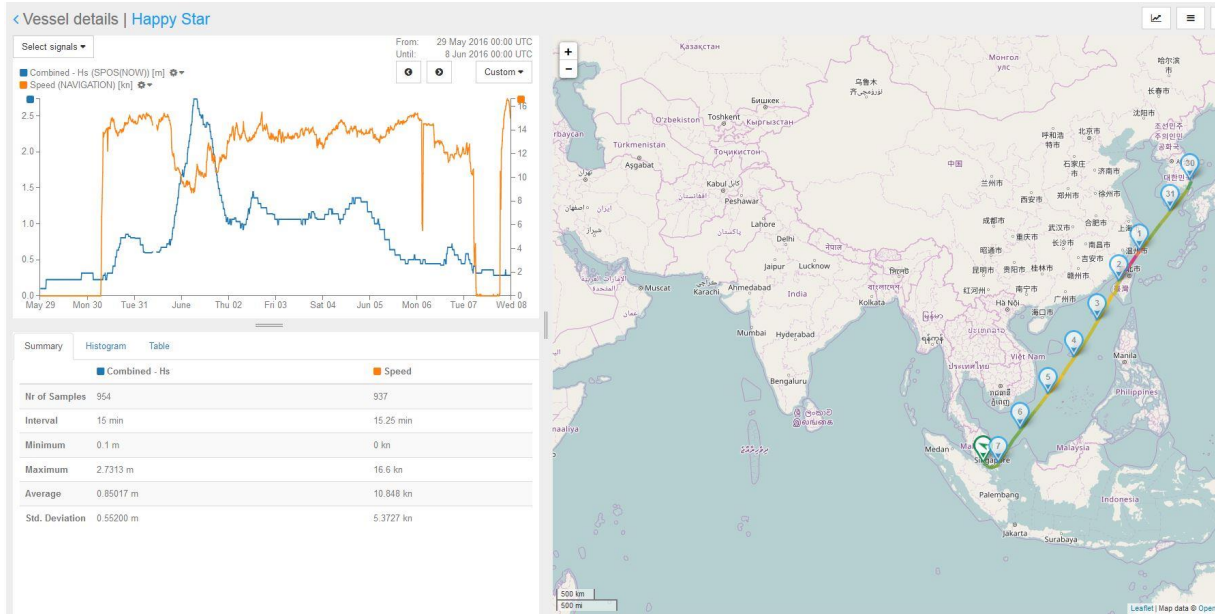
VOYAGE SPECIFICS	EXPECTED	ACTUAL
DEPARTURE		12 / 01 / 2016
ARRIVAL		08 / 02 / 2016
DURATION	[hr] 719	639
DISTANCE	[nm] 7291	7937
TOTAL FUEL CONSUMED	[t] 899	900
DAILY FUEL CONSUMPTION	[t/day] 30	33.8

LOADING CONDITIONS		
DRAFT AFT	[m]	8.1
DRAFT BOW	[m]	8.1
DISPLACEMENT	[T]	22724

WEATHER CONDITIONS		
WIND WAVES	[m]	< 3.5
SWELL WAVES	[m]	< 3.3
WIND SPEED	[m/s]	< 19.1



Voy. 10a, Ulsan – Singapore



VOYAGE SPECIFICS

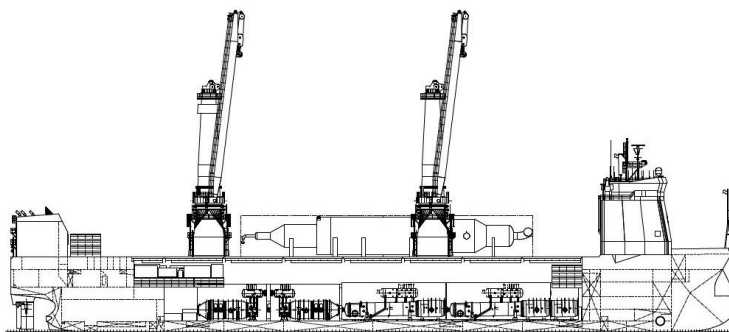
	EXPECTED	ACTUAL
DEPARTURE		30 / 05 / 2016
ARRIVAL		07 / 06 / 2016
DURATION	[hr] 192	216
DISTANCE	[nm] 2514	2506
TOTAL FUEL CONSUMED	[t] 240	227
DAILY FUEL CONSUMPTION	[t/day] 30	25.2

LOADING CONDITIONS

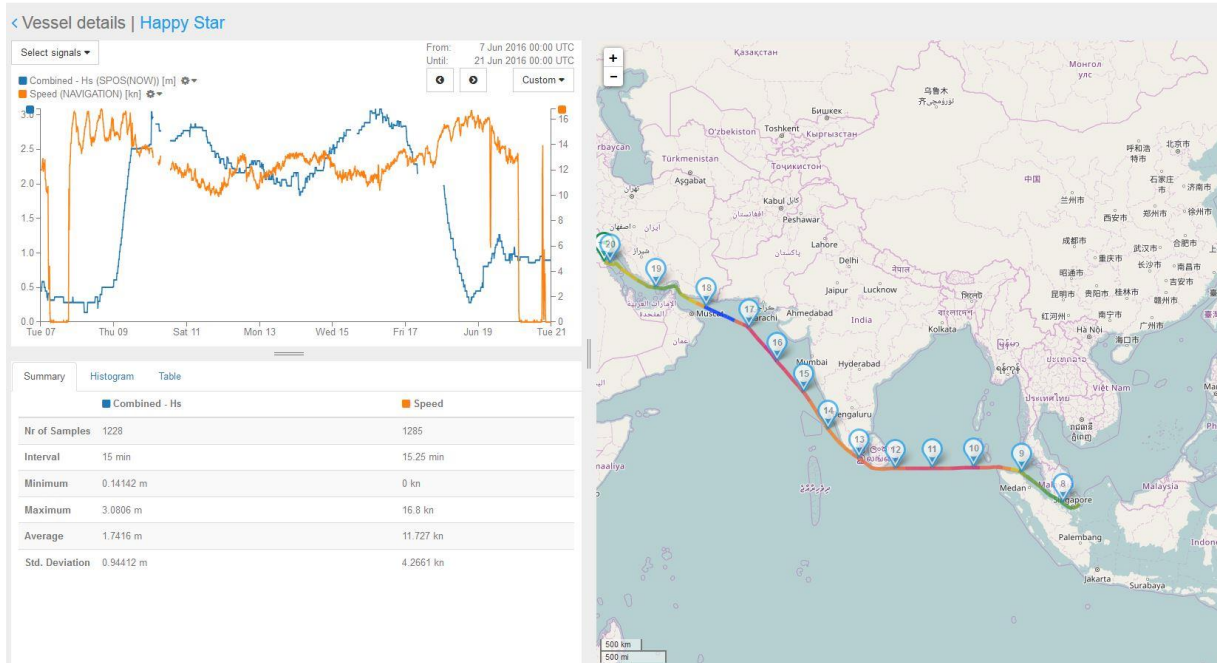
DRAFT AFT	[m]	?
DRAFT BOW	[m]	?
DISPLACEMENT	[T]	?

WEATHER CONDITIONS

WIND WAVES	[m]	< 2.5
SWELL WAVES	[m]	< 1.2
WIND SPEED	[m/s]	< 19.9



Voy. 10b, Singapore – Shuaiba



VOYAGE SPECIFICS

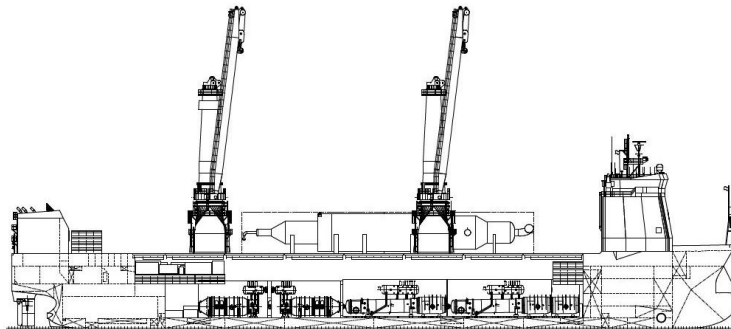
	EXPECTED	ACTUAL
DEPARTURE		07 / 06 / 2016
ARRIVAL		20 / 06 / 2016
DURATION	[hr] 307	312
DISTANCE	[nm] 3817	3502
TOTAL FUEL CONSUMED	[t] 384	368
DAILY FUEL CONSUMPTION	[t/day] 30	28.3

LOADING CONDITIONS

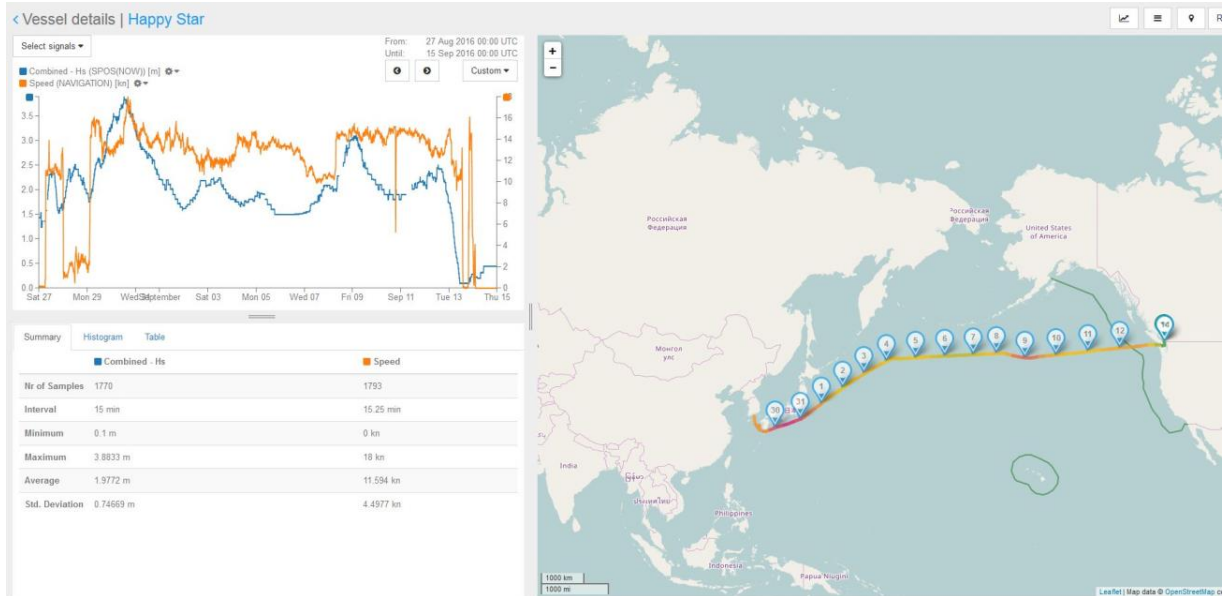
DRAFT AFT	[m]	6.8
DRAFT BOW	[m]	7.4
DISPLACEMENT	[T]	19353

WEATHER CONDITIONS

WIND WAVES	[m]	< 1.4
SWELL WAVES	[m]	< 2.5
WIND SPEED	[m/s]	< 16.5



Voy. 11, Nantong - Vancouver



VOYAGE SPECIFICS

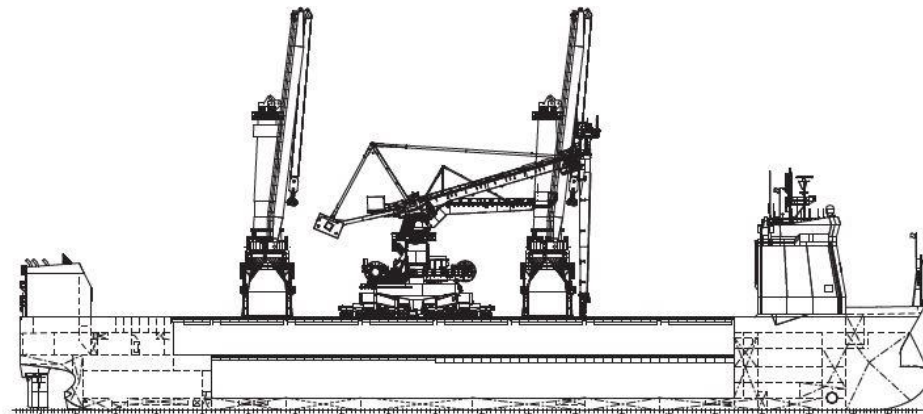
	EXPECTED	ACTUAL
DEPARTURE		25 / 08 / 2016
ARRIVAL		14 / 09 / 2016
DURATION	[hr]	
DISTANCE	[nm]	
TOTAL FUEL CONSUMED	[t]	
DAILY FUEL CONSUMPTION	[t/day]	

LOADING CONDITIONS

DRAFT AFT	[m]	6.7
DRAFT BOW	[m]	6.2
DISPLACEMENT	[T]	17278

WEATHER CONDITIONS

WIND WAVES	[m]	< 3.2
SWELL WAVES	[m]	< 2.6
WIND SPEED	[m/s]	< 16.1



Appendix D

Sensitivity Analysis

The sensitivity analysis is performed to determine how dominant a variable is. The One-at-a-time(OAT) is used which changes one variable at the time while keeping the other variables the same value. After calculation the changed variable is returned to it's nominal value. This method does not take into account interactions between variables. The calculated resistance with the changed variable is divided by the resistance at nominal value. This calculation is performed for half the nominal value and double the nominal value, this should indicate if a variable has non-linear influence. The table below shows the sensitivity of the variables used. The sensitivity is calculated for the individual resistance components as well as for the total resistance.

Figure D.1 shows day 45, Batam-Onslow for which the data is used to determine the nominal values. This is a representative voyage with cargo and quite heavy weather, see Figure D.1.

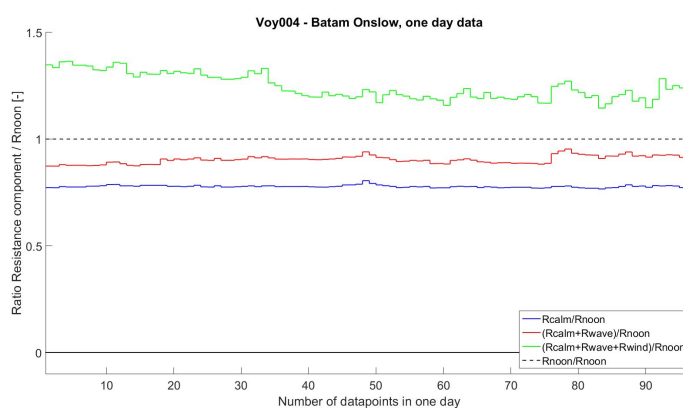


Figure D.1: Resistance components of one day data

Variable	[-]		R_{calm}	% diff	SF	R_{wave}	% diff	SF	R_{wind}	% diff	SF	R_{tot}	% diff	SF
nominal			354			77			209			639		
V_{sog}	12.5[kn]	50%	175	49%	1.01	53	69%	0.62	98	47%	1.06	326	51%	0.9
		120%	468	132%	1.61	88	114%	0.71	245	117%	0.86	802	126%	1.5
V_{cur}	0.4[m/s]	50%	356	101%	-0.01	77	100%	0.00	209	100%	0.00	642	100%	0.0
		200%	349	99%	-0.01	76	99%	-0.06	209	100%	0.00	634	99%	-0.0
μ_{cur}	155[deg]	0[deg]	348	49%		77	99%		209	100%		634	99%	
		180[deg]	371	49%		79	103%		209	100%		659	103%	
V_{wind}	7.3[m/s]	50%	354	100%	0.00	77	100%	0.00	155	74%	0.52	585	92%	0.3
		200%	354	100%	0.00	77	100%	0.00	298	143%	0.43	729	114%	0.3
μ_{wind}	95[deg]	0[deg]	354	100%		77	100%		-1	0%		429	67%	
		180[deg]	354	100%		77	100%		521	249%		952	149%	
β	135[deg]	0[deg]	354	100%		77	100%		-407.3	-195%		33.8	5%	
		180[deg]	354	100%		77	100%		268	128%		698	109%	
A_f	1000[m ²]	50%	354	100%	0.00	77	100%	0.00	104	50%	1.00	534	84%	0.3
		200%	354	100%	0.00	77	100%	0.00	417	200%	1.00	848	133%	0.3
Cx_{cargo}	-4.8[-]	50%	354	100%	0.00	77	100%	0.00	86	41%	1.18	516	81%	0.3
		200%	354	100%	0.00	77	100%	0.00	454	217%	1.17	885	138%	0.3
Cx_{ship}	-1.5[-]	50%	336	49%	1.01	77	100%	0.00	227	109%	-0.17	640	100%	0.0
		200%	391	49%	1.01	77	100%	0.00	171	82%	-0.18	639	100%	0.0
AHR	160[-]	50%	264	49%	1.01	77	100%	0.00	209	100%	0.00	550	86%	0.3
		200%	468	49%	1.01	77	100%	0.00	209	100%	0.00	754	118%	0.3
Hs_{sea}	0.8[m]	50%	354	100%	0.00	64	83%	0.34	209	100%	0.00	627	98%	0.0
		200%	354	100%	0.00	125	162%	0.62	209	100%	0.00	687	108%	0.0
Tp_{sea}	5[s]	50%	354	100%	0.00	68	88%	0.23	209	100%	0.00	631	99%	0.0
		200%	354	100%	0.00	63	82%	-0.18	209	100%	0.00	625	98%	-0.0
μ_{sea}	265[deg]	0[deg]	354	100%		65	84%		209	100%		627	98%	
		150[deg]	354	100%		77	100%		209	100%		639	100%	
Hs_{swell}	2.4[m]	50%	354	100%	0.00	31	40%	1.19	209	100%	0.00	593	93%	0.3
		200%	354	100%	0.00	260	338%	2.38	209	100%	0.00	822	129%	0.3
Tp_{swell}	14.2	50%	354	100%	0.00	153	199%	-1.97	209	100%	0.00	715	112%	-0.3
		141%	354	100%	0.00	34	44%	-1.37	209	100%	0.00	596	93%	-0.3
μ_{swell}	173	0[deg]	354	100%		23	30%		209	100%		585	92%	
		150[deg]	354	100%		73	95%		209	100%		636	100%	

Table D.1: Variables and their sensitivity

Appendix E

Uncertainty Analysis

The goal of uncertainty analysis is to find a bandwidth in between which the calculated values lie from the true value, for a certain level of confidence, H.W. Coleman [2009]. This appendix explains the theory and calculation methods used for uncertainty analysis in the next chapters. Uncertainties of individual variables are based in educated guesses or calculations. The uncertainty of calculated results is the result of a propagation of errors.

E.1 Calculation Procedure

The procedure explained below is inspired by the course notes of 'Advanced Course in Resistance and Propulsion' lectured by van Terwisga Methodology uncertainty analysis proposed by W.C. Lin [1990]

1. Identify all error sources
2. Determine the individual precision (statistical) and bias errors (judgement) for each source from 1
3. Determine the sensitivity of each error source to the end result
4. Create the total precision uncertainty interval from steps 2 and 3.
5. Create the total bias uncertainty interval from 2 and 3.
6. Combine the total precision and bias uncertainty intervals from 4 and 5.

Step 1

The first step is performed in Section 1.8.

Step 2

The second step is to determine the precision error and if possible the bias error. The precision error is expressed by the precision index S and is calculated using Equation E.1a. x_i Should be from the same sample, this is challenging in this research as the environmental input parameters change every 15 minutes. This results in a small sample size N , according to W.C. Lin [1990] this leads to a high uncertainty of S_i . The precision error of an average value is calculated using Equation E.1b and is always lower than

$$S_i = \text{sqrt}\left(\sum_{j=1}^N \frac{(x_{ij} - \overline{x_i})^2}{(N-1)}\right) \quad (\text{E.1a})$$

$$S_{\bar{X}_i} = \frac{S_i}{\sqrt{N}} \quad (\text{E.1b})$$

A bias error is the mean offset of the experimental data with respect to the actual data. The bias error is often related to a calibration error in measurements or a standard over prediction in the calculation method used. A bias error is mainly quantified based on engineering judgement.

Step 3

Once the precision and the bias errors are determined for the separate error sources, the sensitivity (Θ_i) of these sources with respect to the final answer is calculated. The sensitivity is required in the propagation of errors, since some error sources are more dominant than others. Equation E.2 is used to calculate the precision index including the sensitivity of the final result. This is the propagation of errors.

$$S_{result} = \sqrt{\sum_{j=1}^k (\Theta_j S_j)^2} \quad (\text{E.2})$$

Appendix D explains the calculation method to determine the sensitivity of the input parameters.

Step 4 and 5

The uncertainty interval is associated with a certain level of confidence. 95% Confidence (U_{95}) indicates that in 95% of the time the calculated value lies within the uncertainty interval around the true value, see Equation E.3a. The uncertainty interval is calculated using Equation E.4. H.W. Coleman [2009] stated that for many engineering applications $t_{95} = 2$ is justified to use when the number of observations is large enough, > 30 samples. The bias uncertainty interval is which is indicated with B_R .

$$R_{best} - S_R \leq R_{true} \leq R_{best} + S_R \quad (\text{E.3a})$$

$$S_R = \frac{+}{-} t_{95} \frac{S_{result}}{\sqrt{M}} \quad (\text{E.3b})$$

where M is the number of times the test is repeated

Step 6

Total uncertainty combines the uncertainty interval of the precision and bias error. Equation E.4 is used to determine the uncertainty interval at a 95% confidence level.

$$U_R = \sqrt{B_R^2 + (t_{95} S_R)^2} \quad (\text{E.4})$$

Uncertainty of a regression line

An explanation is made how to determine the uncertainty of a linear regression line. This is used to determine the regression error in the relation of break power and fuel consumption in Section 1.7.

A curve fitted to measured values can be used to predict values, this curve can be determined using a data regression method. The most used data regression method is the Least Squares

method and uses the mean of the squared differences. Equations E.5a to E.5e show this method for a linear curve. The differences between the measured, Y_i and the true or most probable value, Y_0 is squared. When the partial derivative equals zero, Equation E.5c and Equation E.5d, the differences between the measured values and the regression line is zero. The method is used throughout the report.

The measured data is visible as a scatter around the fitted curve, this is the standard error of regression. The standard error of regression is calculated using Equation E.5e and is only valid when the X input is true. The in the case of the relation between break power and fuel consumption the actual error is therefore even larger.

$$Y = m \cdot X + c \quad (\text{E.5a})$$

$$\eta = \sum_{i=1}^N (Y_i - Y_0)^2 \quad (\text{E.5b})$$

$$\frac{\partial \eta}{\partial m} = 0 \quad (\text{E.5c})$$

$$\frac{\partial \eta}{\partial c} = 0 \quad (\text{E.5d})$$

$$s_Y = \left[\frac{\sum_{i=1}^N (Y_i - m \cdot X_i - c)^2}{N - 2} \right]^{1/2} \quad (\text{E.5e})$$

E.2 Calculation and results

The calculation procedure is performed for the translation of resistance to fuel consumption. No uncertainty is considered for the resistance input, this results in a non-conservative estimate of the total resistance of daily fuel consumption. It does give the reader insight in the uncertainty that is accompanied with this translation.

The two most widely used methods are the Taylor Series Method (TSM) and Monte Carlo Method(MCM). The TSM method is quick and robust analysis which can be used for equations. The MCM can be used for a combination of equations and allows for different probability distribution functions. The MCM best suitable for the relation of resistance with daily fuel consumption also includes a regression curve fit, this is challenging to include in the TSM.

As explained in Section 1.8, there are three types of uncertainties: input, method and model uncertainty. Equations E.6a, E.6b and E.6c show how the values are calculated in order to determine U_{95} . The calculation procedure from the previous section is followed. A sample is considered as a constant power setting over one day. The power setting is assumed constant as the change in vessel speed is less than $0.25[kn]$. The parameters are assumed independent for the sake of this exercise.

$$E = S - D \quad (\text{E.6a})$$

The error(E) is the difference between the noon reported(S) and calculated(D) value

$$std(E) = \sqrt{u_{method}^2 + u_{input}^2} \quad (E.6b)$$

$$S_{result} = \sqrt{std_E^2 + u_{method}^2} \quad (E.6c)$$

$$FC = f(R_{tot}, V_{stw}, \eta_d, \eta_s, \eta_{gb}) \quad (E.7)$$

1. Equation E.7 shows the parameters involved
2. Table E.1 shows the precision errors of the parameters involved. The Monte Carlo analysis is performed. The precision error of V_{stw} is half the uncertainty as defined in Section 1.8, which is valid for Normal distributions.

The precision errors are used to determine the distribution of the input parameters.

A random sample is taken from the input parameters

Equation E.7 is solved with the input parameter from the previous step

The calculations are repeated for $M = 10.000$ times.

A random sample of the noon reported fuel consumption is taken.

The standard deviation of the error indicates the calculation and input uncertainty.

See Equation E.6b

3. The sensitivity analysis is not necessary as all parameters involved have sensitivity one.
4. The precision and bias error of the result is determined

This is the regression uncertainty resulting from the trend line fit, see Section 1.7
5. The bias is estimated by the mean difference between the calculated and reported fuel consumption. $B_R = 3.0[t/day]$
6. The uncertainty interval at 95% confidence is calculated using Equation E.4. The number of samples(49) is larger than 30, so it is justified to use $t_{95} = 2$. The mean uncertainty interval is $U_{95} = 3.6[t/day]$.

Parameter	μ	S_i	distribution
η_s	0.99	0.0025	Normal
η_{gb}	0.97	0.01	Normal
FC_{noon}	var	1.5	Normal
V_{stw}	μ_{Vi}	$\frac{1}{2}0.05$	Normal
R_{tot}	μ_{Ri}	0	Normal
η_d	$\mu_{\eta_{di}}$	$\sigma_{\eta_{di}}$	Normal

Table E.1: Monte Carlo input parameters

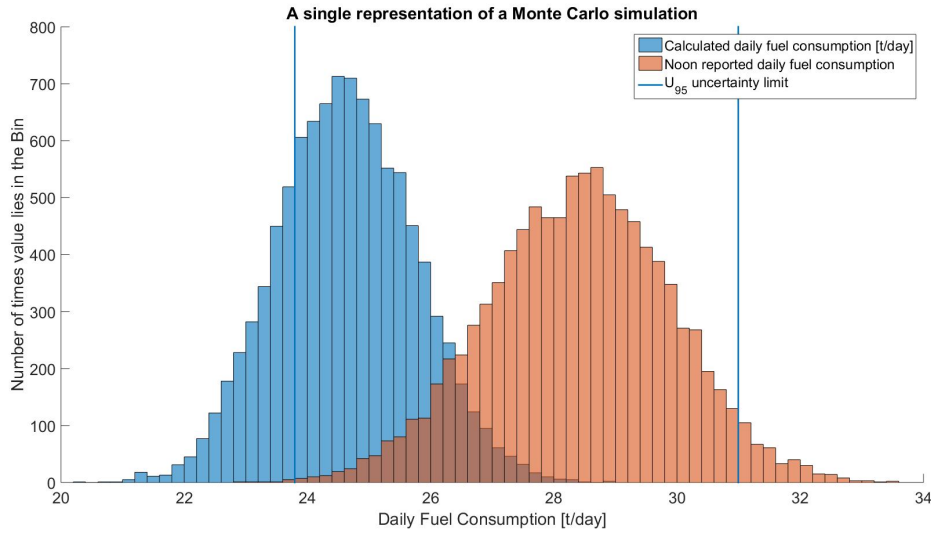


Figure E.1: Representation of Monte Carlo results, single sample

E.3 Discussion

An uncertainty analysis is performed for the translation of fuel consumption, an important assumption is this calculation is the zero precision error of the input parameter R_{tot} . This is not correct as the uncertainty propagation of the calculations to determine R_{tot} definitely does not lead to zero. However, the goal of this chapter is to give insight in the uncertainty propagation of the translation of resistance to fuel consumption alone.

Another important remark is the assumption of independent parameters. It is shown in the report that the individual resistance components are related to the speed of the vessel. Correlation effects are introduced when this dependency is taken into account, this increases the complexity of the calculations. It is expected that this also increases the uncertainty interval.

The uncertainties are speed independent, while for example the uncertainty of η_{ad} increases for lower speeds due to the extrapolation error, as mentioned in Section 2.2.1. This is also simplified in followed calculation procedure, the actual uncertainty should be speed dependent.

Bibliography

- BigLift Shipping. Biglift company profile. *Energy Fuels*, 2008. URL <http://pubs.acs.org/doi/suppl/10.1021/ef800539g>.
- BigLift. Shipping manual template. 2017.
- et al W.C. Lin. Report of the panel on validation procedures. *19th ITTC, Madrid*, 1990.
- W.G Steele H.W. Coleman. Experimentation, validation, and uncertainty analysis for engineers. Third edition:H1, H2, H3, H7, 2009.
- DNV. Environmental conditions and loads. 2007.
- C. Ciortan K. Hassan, M.F. White. Effect of container stack arrangements of the power optimization of a container ship. *Journal of ship production and design*, 28, 2015. URL <http://www.ingentaconnect.com/content/sname/jspd/2012/00000028/00000001/art00002>.
- D. Murdey. Evolution of ittc technical committees. 2014. URL <http://ittc.info/downloads/Generel%20files/ITTC%20history%202.pdf>.
- SNAME. Guide for sea trials. *SNAME technical and research bulleting*, 3-47:Chap 4., 2015.
- F. Mennen H. van den Boom, H. Huisman. New guidelines for speed/power trials. 2013.
- V. Jinkine and V. Ferdinande. A method for predicting the added resistance of fast cargo ships in head waves. *Int. Shipbuilding Progress*, 1974.
- H. Fuji and T. Takahashi. Experimental study on the resistance increase of a ship in regular oblique waves. *Proceedings of the 14th ITTC*, 4, 1975.
- R. Grin. On the prediction of wave added resistance with empirical methods. *Sea Trial Analysis JIP*, 2014.
- ITTC. Testing and extrapolation methods, propulsion, performance, predicting powering margins. *Proceedings of the 25th ITTC*, 2008.
- R.L. Townsin. Ship design for fuel economy, bottom condition and fuel conservation. 1983.
- G. Lund G. Swain. Dry dock inspection: Methods for improved fouling control coating performance. *Journal of Ship production and Design*, 2016.
- DNV. Rules for classification of ships in operation. 2003.
- T.W.F. Hasselaar. Speed through water measurement on ships in service. *Marin Report*, 2014.

- O.M. Faltinsen. Sea loads on ships and offshore structures. 1990.
- W. Blendermann. Wind loading of ships, collected data from wind tunnel tests in uniform flow. *Institut fr Schiffbau der Universitt Hamburg*, 574, 1996.
- E. Simiu and R. H. Scanlan. Wind effects on structures : An introduction to wind engineering. 1978.
- Meteogroup. Ship performance and optimization system. 2015. URL www.spos.eu.
- T.W.F. Hasselaar. Effect of a drift angle on propulsion performance. *Marin Report*, 2016.
- D. Stapersma H. Klein Woud. Design of propulsion and electric power generation systems. pages chap. 3, chap. 7, chap. 10, 2002.
- A. Malmendal et al. K.E. Nielsen, J. Dittmer. Quantitative analysis of constituents in heavy fuel oil by nmr spectroscopy and multivariate data analysis. *Energy Fuels*, 22, 2008. URL <http://pubs.acs.org/doi/suppl/10.1021/ef800539g>.
- K. van Zijl D. Wouters. Accuracy of spos. *Minor study report*, 2016.
- F. Walree. Windos - assessment of wind loads on ships and offshore structures. *MARIN leaflet*, 2010.
- J. de Wilde. Wind load jip. *Manoeuvring and Nautical Study Forum*, 2016.
- T.C.J. van Terwisga. Uncertainty analysis, an introduction. *Course notes MT1419*.